AgRISTARS

SR-K1-04214

A Joint Program for Agriculture and Resources Inventory Surveys Through Aerospace Remote Sensing

Supporting Research

December 1981

COHERENT OPTICAL DETERMINATION OF THE LEAF ANGLE DISTRIBUTION OF CORN

Michael Pihlman, Fawwaz T. Ulaby

University of Kansas Center for Research, Inc.
Remote Sensing Laboratory
Campus West
Lawrence, Kansas 66045

Lyndon B. Johnson Space Center
Houston, Texas 77058

1. Report No. RSL TR-360-15; SR-K1-04124	2. Government Accession No.	3. Recipient's Catalog No.
4. Title and Subtitle COHERENT OPTICAL DETERMINATION OF THE LEAF ANGLE DISTRIBUTION OF CORN		5. Report Date December 1981 6. Performing Organization Code RSL TR-360-15
7. Author(s) Michael Pihlman and Fawwaz T. Ulaby		8. Performing Organization Report No. 10. Work Unit No.
9. Performing Organization Name and Address Remote Sensing Laboratory University of Kansas Center for Research, Inc. 2291 Irving Hill Drive - Campus West Lawrence, Kansas 66045		11. Contract or Grant No. NAS 9-15421
12. Sponsoring Agency Name and Address NASA/Johnson Space Center Houston, Texas 77058 Technical Monitor: Jack F. Paris		13. Type of Report and Period Covered Technical Report 14. Sponsoring Agency Code
15. Supplementary Notes		

16. Abstract

A coherent optical technique for the diffraction analysis of an image is presented. Recent developments in radar remote sensing have shown a need to understand plant geometry and its relationship to plant moisture, soil moisture, and the radar backscattering coefficient σ^{o}. A corn plant changes its leaf-angle distribution (LAD), as a function of time, from a uniform distribution to one that is strongly vertical. It is shown that plant- and soil-moisture may have an effect on plant geometry.

17. Key Words (Suggested by Author(s)) Leaf Angle Distribution, Optical Processing, Earth Resources, Crops	18. Distribution Statement		
19. Security Classif. (of this report) Unclassified	20. Security Classif. (of this page) Unclassified	21. No. of Pages 137	22. Price*

*For sale by the National Technical Information Service, Springfield, Virginia 22161

RSL Remote Sensing Laboratory

The University of Kansas Center for Research, Inc.
2291 Irving Hill Drive-Campus West, Lawrence, Kansas 66045

Telephone: (913) 864-4832

COHERENT OPTICAL DETERMINATION OF THE LEAF ANGLE DISTRIBUTION OF CORN

Remote Sensing Laboratory
RSL Technical Report 360-15

Michael Pihlman
Fawwaz T. Ulaby

December 1981

Fawwaz T. Ulaby, Principal Investigator

Supported by:
NATIONAL AERONAUTICS AND SPACE ADMINISTRATION
Lyndon B. Johnson Space Center
Houston, Texas 77058
CONTRACT NAS 9-15421

ACKNOWLEDGMENT

This research was supported by the National Aeronautics and Space Administration, Lyndon B. Johnson Space Center, Houston, Texas, under Contract NAS 9-15421

TABLE OF CONTENTS

LIST OF SYMBOLS AND ABBREVIATIONS

LAD	Leaf-angle distribution
SM	Soil moisture
PM	Plant moisture
σ^o	Radar backscatter coefficient
ω_o	Radian frequency
π	3.14
k	Propagation factor
λ	Wavelength
ϕ_k	Phase
PSD	Power spectral density
f_o	Fundamental frequency
τ	Time, pulse-width notation
x(t)	Complex time signal
X(f)	Fourier transform of x(t)
$I_o(x_o y_o)$	Intensity at observation plane
$\vec{U}_o(x_o y_o)$	Electric field at observation plane
$\vec{U}(x_i y_i)$	Electric field at input (image) plane
$\lvert\ \rvert$	Absolute value
S	Spatial frequency
Å	Angstroms, 1×10^{-10}m
RSI	Recognition Systems, Inc.
RVAL	Real value of intensity
NVAL	Normalized intensity
CUMVAL	Cumula intensity value
VAL	Value of intensity from digital display

AMB	Value of intensity from digital display in the dark
ΣRVAL	Total wedge power
LBL	Label
STO	Store in memory
IND	Indirect
OP	Operation
R/S	Run stop
RCL	Recall from memory
GTO	Go to

LIST OF FIGURES

LIST OF TABLES

COHERENT OPTICAL DETERMINATION OF THE LEAF ANGLE DISTRIBUTION OF CORN

Michael Pihlman and Fawwaz T. Ulaby
Remote Sensing Laboratory
University of Kansas Center for Research, Inc.
Lawrence, Kansas 66044

ABSTRACT

A coherent optical technique for the diffraction analysis of an image is presented. Recent developments in radar remote sensing have shown a need to understand plant geometry and its relationship to plant moisture, soil moisture, and the radar backscattering coefficient σ^{o}. A corn plant changes its leaf angle distribution (LAD), as a function of time, from a uniform distribution to one that is strongly vertical. It is shown that plant moisture decreases with maturity and that plant- and soil-moisture may have an effect on plant geometry.

1.0 INTRODUCTION

Radar can be used to identify crop type, crop maturity, and crop health [25-30] by analyzing radar response to a vegetation canopy. To describe the way in which the radar return power is affected by the canopy, a description of the crop's geometry as a whole is needed, as are the individual plant geometries. This report will emphasize the latter aspect.

Individual plant geometry has been studied as it relates to photosynthesis and crop yield [17,22,23,32,34]. Several methods have been developed to measure the leaf-angle distribution (LAD) for this purpose. The use of a protractor, with a weighted string attached to its base, is one common method of measurement [17,32,34]. In addition, several photographic techniques exist wherein a manual calculation of an angle is made from the photograph, or integral relationships are drawn between gap frequency, look angle, and LAD [23]. These methods, although acceptable for photosynthetic research, lack the accuracy needed for radar remote sensing purposes since they measure only a portion of the leaf and tend to ignore other plant parts.

Every part of the plant plays a role in the scattering of radar energy. The angle at which a plant part is oriented will, in turn, help to determine the strength of the returned radar power. It is, therefore, desirable to have a complete angular description of the plant so that an accurate model for radar scattering by the plant can be developed.

An optical method of determining LAD was introduced by Smith in 1979 [22]. This method uses the well-known techniques of Fourier optics [12] to obtain the angular distribution of the entire plant by analyzing its Fourier transform. The geometry of a complete, single plant can thus be described as a function of angle and can be classified as a planophile, erectophile, plagiophile, or extremophile structure [23]. By taking an average using several plants, it may be possible to correlate mean LAD and radar backscattering data.

This report will attempt to tie together some of the aspects of the LAD of corn that have been neglected heretofore. Therefore, we propose to:

1. Describe the change in LAD as the corn matures.
2. Develop a family of LAD graphs for the entire plant, including the stalk and fruit.
3. Compare LAD to plant- and soil-moisture histories.

In summary, this report will apply a new optical technique to the determination of the LAD of corn and will present the LAD as it changes with corn maturity. It will also show how the LAD of corn relates to ground-truth data, e.g., plant- and soil-moisture. An argument will be presented supporting the contention that only one photograph of the corn plant is needed to accurately describe its LAD.

Chapter 2 will present a brief tutorial on Fourier optics. Chapter 3 will explain the optical bench used for this experiment and will outline the data-collection procedures employed. Chapter 4 will present the models used to test the system. Chapter 5 contains

the results of the experiment. The appendices contain a literature review for each of the three main topics of this research: LAD, radar response to vegetation, and optics.

2.0 FOURIER OPTICS

The development of the Fourier transform using coherent optical techniques will be discussed in this chapter. The coherent source is a laser and the transform is analyzed using a photodiode array. Examples of transforms will be shown and discussed. The development of the Fourier-transform relationship will also be discussed.

2.1 Fourier Series and Transforms

A complex periodic signal can be shown to be the sum of simple sine and cosine functions:

$$x(t) = C_o + \sum_{k=1}^{\infty} A_k \cos k\omega_o t + \sum_{k=1}^{\infty} B_k \sin k\omega_o t \qquad (2\text{-}1)$$

where:

$$C_o = \frac{1}{T} \int_{t_o}^{t_o + T} x(t)\, dt \qquad (2\text{-}2)$$

$$A_k = \frac{2}{T} \int_{t_o}^{t_o + T} x(t) \cos k\omega_o t\, dt \qquad (2\text{-}3)$$

$$B_k = \frac{2}{T} \int_{t_o}^{t_o + T} x(t) \sin k\omega_o t\, dt \qquad (2\text{-}4)$$

where C_o, A_k and B_k are all constants.

Using Euler's identities, a more general form for x(t) can

be described as:

$$x(t) = \sum_{n=-\infty}^{\infty} C(kf_o)\, e^{jk2\pi f_o t} \quad , \omega_o = 2\pi f_o . \tag{2-5}$$

$C(kf_o)$ is the Fourier series coefficient constant and is defined as:

$$C(kf_o) = \frac{1}{T_o} \int_{-T_o/2}^{T_o/2} x(t)\, e^{-j2\pi k f_o t} \, dt , \tag{2-6}$$

$C(kf_o)$ can also be found from A_k and B_k (Eq. 2-3, 2-4)

$$C(kf_o) = \frac{\sqrt{A_k^2 + B_k^2}}{2} e^{-j\phi_k} \qquad k = 1,2,3 \ldots \tag{2-7}$$

where

$$\phi_k = \tan^{-1}\left(\frac{B_k}{A_k}\right). \tag{2-8}$$

The distribution of power as a function of frequency, the power spectral density (PSD), can be found as:

$$PSD = \sum_{n=-\infty}^{\infty} |C(kf_o)|^2 . \tag{2-9}$$

This will be important in optical diffraction analysis as the detected intensity will take this form.

The Fourier representation of a periodic signal results in a line spectrum in the frequency domain (Fig. 2.1).

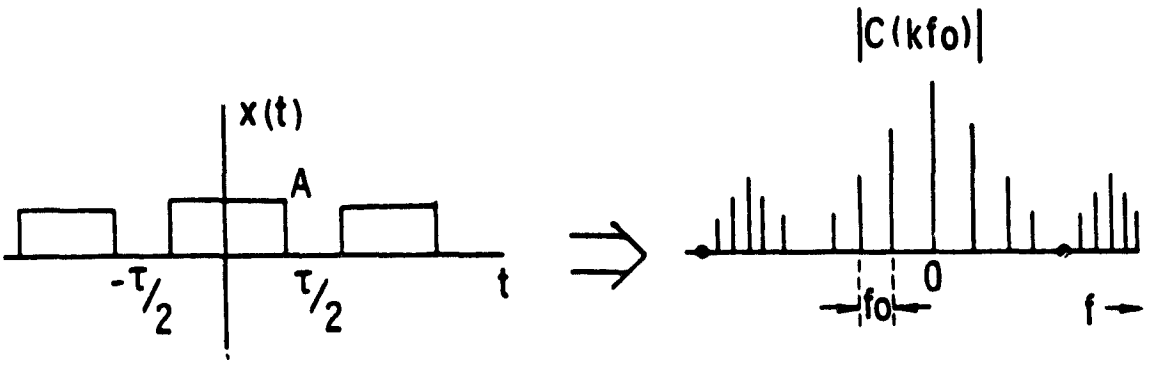

Figure 2.1. A periodic signal is shown along with its Fourier transform. It can be seen that the transform is a line spectrum showing discrete frequencies used to define the function, x(t).

However, most signals, and this is true of a corn plant, are <u>not</u> periodic in nature, so a Fourier transform relationship is derived to represent these nonperiodic functions.

$$X(f) = \int_{-\infty}^{\infty} x(t)\, e^{-j2\pi ft}\, dt \qquad (2\text{-}10)$$

where X(f) is the Fourier transform of x(t).

This transformation results in a continuous spectral representation of a nonperiodic function (Fig. 2.2).

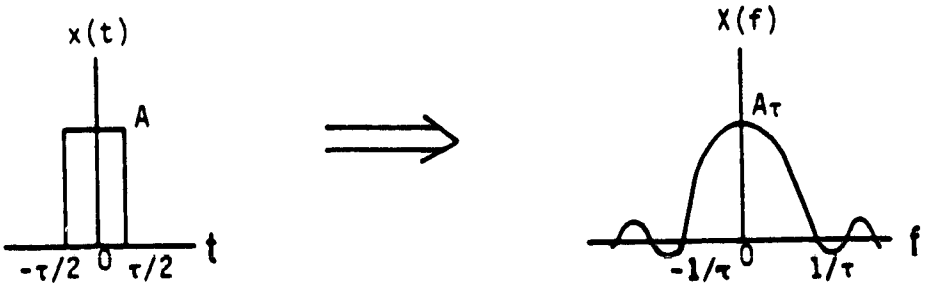

Figure 2.2. The Fourier transform of x(t) is shown to be a continuous spectrum in the frequency domain if x(t) is an aperiodic signal.

Note that the width of the spectral response is proportional to $1/\tau$. If the rectangular pulse gets very small, then the frequency components needed to produce this small pulse approaches infinity, (Fig. 2.3).

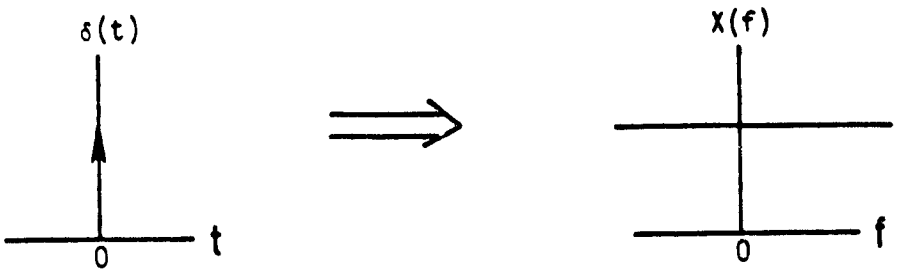

Figure 2.3. As the pulse width decreases, more frequency components are needed to properly describe the pulse. The limiting case is shown where a delta function transforms to an infinite number of frequency components.

and vice versa in Fig. 2.4.

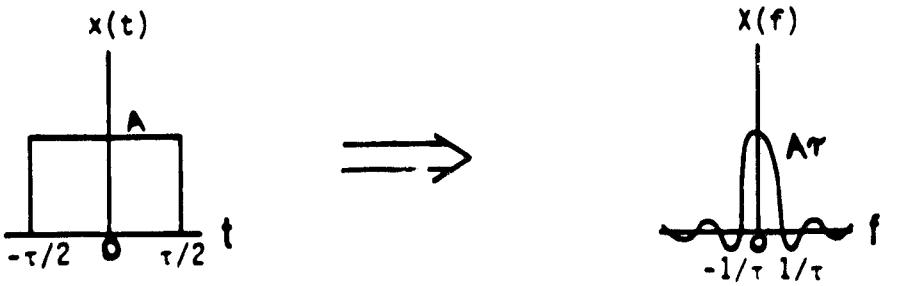

Figure 2.4. The number of frequency components needed to describe a wider pulse width decreases as pulse width approaches infinity.

This section has discussed basic Fourier series and transform relationships. The progression from periodic to nonperiodic waveforms was discussed and the time-bandwidth relationships shown. The next section will extend this theory to the spatial domain (rather than the time domain) and also will extend it to two dimensions (x and y). The Fourier transform relationships will be shown for the general case of a spatially modulated coherent beam.

2.2 Fresnel and Fraunhofer Approximations

Given the aperture (Σ) shown in Fig. 2.5, and observing the electric field at the observation point, the equation defining the electric field can be written [12],

$$\vec{u}(x_0 y_0) = \iint_{\Sigma} \vec{u}(x_1 y_1) \underbrace{\frac{\exp[jk\, r_{01}]}{j\lambda r_{01}} \cos\theta_1}_{\vec{h}(x_0 y_0,\, x_1 y_1)} dx_1 dy_1 \qquad (2\text{-}11)$$

where

$\vec{u}(x_1 y_1)$ is the electric field distribution at the aperture,

$\vec{h}(x_0 y_0, x_1 y_1)$ is the spherical propagation factor,

r_{01} is the distance from the incremental area to $(x_0 y_0)$.

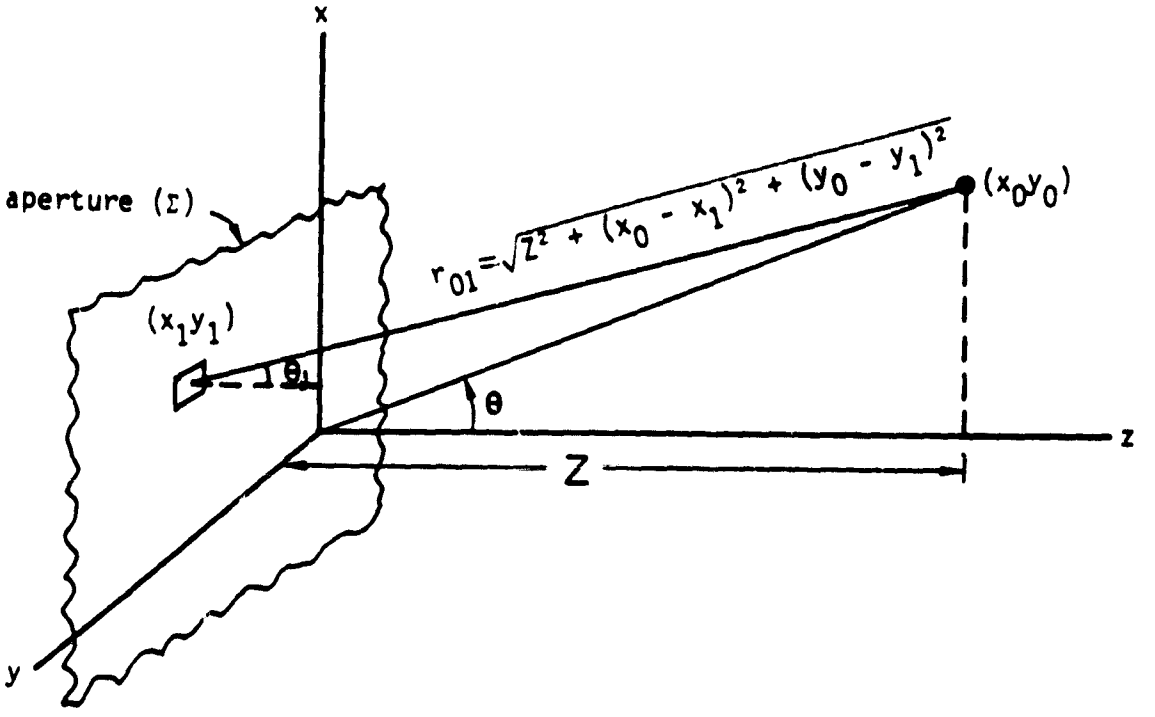

Figure 2.5. Geometry used to determine the Fresnel and Fraunhofer approximations at an observation point at distance Z from the image plane.

θ_1 is the angle between normal and r_{01}, and

k is the propagation factor = $2\pi/\lambda$;

see Ulaby, Moore and Fung [35].

From the geometry shown in Fig. 2.5, certain assumptions can be made:

1. Assuming that z is very much greater than the maximum linear dimension of the aperture,
   then: $\theta_1 = \theta$.
2. If we observe the field only in the vicinity of the z-axis, then:
   $\cos\theta_1 = \cos\theta \approx 1$,
   $z \approx r_{01}$ (in the denominator of the exponential term, not <u>in</u> the exponential).

with these assumptions made, and applying the binomial expansion approximation:

$$r_{01} = z\left[1 + \frac{1}{2}\left(\frac{x_0 - x_1}{z}\right)^2 + \frac{1}{2}\left(\frac{y_0 - y_1}{z}\right)^2\right] \qquad (2\text{-}12)$$

and substituting r_{01} in $\vec{h}(x_0y_0, x_1y_1)$, Eq. 2-11:

$$\vec{h}(x_0y_0, x_1y_1) = \frac{e^{[jkz]}}{j\lambda z}\exp\left[\frac{jk}{2z}\left[(x_0 - x_1)^2 + (y_0 - y_1)^2\right]\right] \qquad (2\text{-}13)$$

substituting $\vec{h}(x_0y_0, x_1,y_1)$ into Eq. 2-11 and simplifying, we get the Fresnel approximation:

$$\vec{u}(x_0y_0) = \frac{\exp(jkz)}{j\lambda z} \exp\left[j \frac{k}{2z} (x_0^2 + y_0^2)\right] \cdot$$

$$\iint_{-\infty}^{\infty} \vec{u}(x_1y_1) \underbrace{\exp\left[j \frac{k}{2z} (x_1^2 + y_1^2)\right]}_{\text{quadratic phase factor}} \exp\left[\frac{-j2\pi}{\lambda z} (x_0x_1 + y_0y_1)\right] dx_1dy_1 \qquad (2\text{-}14)$$

for details, see Goodman [12] or Ulaby et al. [35].

The Fraunhofer approximation can simplify this equation slightly if:

$$z >> \frac{(x_1^2 + y_1^2)}{2} k \qquad (2\text{-}15)$$

so that the quadratic phase factor approaches 1 then

$$\vec{u}(x_0y_0) = \frac{\exp(jkz)\exp\left[j \frac{k}{2z} (x_0^2 + y_0^2)\right]}{j\lambda z} \cdot$$

$$\iint_{-\infty}^{\infty} \vec{u}(x_1y_1) \exp\left[-j \frac{2\pi}{\lambda z} (x_0x_1 + y_0y_1)\right] dx_1dy_1. \qquad (2\text{-}16)$$

The distance required for z to make the Fraunhofer approximation valid is very large. For example, $z > 2.03 \times 10^3$ meters for a red light (6328Å = 6×10^{-7} meter wavelength) and a 1-inch (2.54 cm) aperture using $r > 2D^2/\lambda$. However, one need not set up a mile-long optical bench to analyze image transforms. The double convex lens can bring the transform plane (that point at which the Fraunhofer approximation is valid and where the Fourier transform of the image occurs) within the confines of a small laboratory.

? 3 Optical Transforms

Using the configuration shown in Fig. 2.6, the electric field at the transform plane can be determined as the Fourier transform of the spatially modulated electric field at the image plane.

$$\vec{u}_0(x_0y_0) = \frac{A \exp\left|j \frac{k}{2f} \left(1 - \frac{d_1}{f}\right) (x_0^2 + y_0^2)\right|}{j\lambda f} \cdot \int_{-\infty}^{+\infty}\int \vec{u}(x_1y_1)\, P(xy) \exp\left[-\frac{j2\pi}{\lambda f} (x_1x_0 + y_1y_0)\right] dx_1dy_1 \tag{2-17}$$

where

$\vec{u}_0(x_0y_0)$ is the Fourier transform of the input electric field $\vec{u}(x_1y_1)$

$P(xy)$ is the pupil function of the lens:

= 1 inside aperture

= 0 outside aperture

f = focal length of FT lens

A = amplitude of the coherent light source = 1.

As discussed previously (Eq. 2-9) the detected intensity will have the form:

$$I_0(y_0x_0) = |\vec{u}_0(x_0y_0)|^2. \tag{2-18}$$

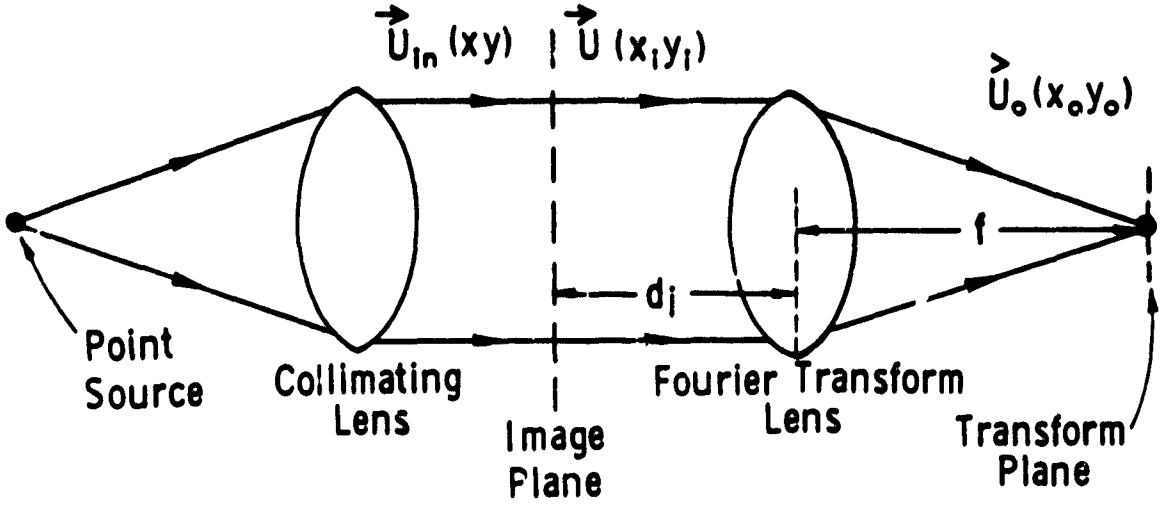

Figure 2.6. The point source emits a diverging beam of coherent light. The collimating lens produces a plane wave from this beam. The image, placed in the image plane, spatially modulates the plane wave, $\vec{U}(x_i y_i)$, which is focused at point $(x_o y_o)$ by the Fourier transform lens. The point $(x_o y_o)$ is referred to as the Fourier transform plane and $\vec{U}_o(x_o y_o)$ is the Fourier transform of the image.

or,

$$I_o(x_o y_o) = \frac{A^2}{\lambda^2 f^2}\left|\int_{-\infty}^{\infty}\vec{u}(x_i y_i)\exp\left[-j\frac{2\pi}{\lambda f}(x_i x_o + y_i y_o)\right]dx_i dy_i\right|^2. \tag{2-19}$$

The Fourier transform of the image is then related to intensity and the spatial frequency and angular information, contained in the transform, can be detected and analyzed.

The spatial frequency, s, is included in Eq. 2-19 and is defined as

$$s = \frac{x_o}{\lambda f} \text{ or } \frac{y_o}{\lambda f}. \tag{2-20}$$

where

x_o, y_o = the distances from the optical axis (DC) in the transform plane,

f = focal length of FT lens,

λ = wavelength of coherent light source (6328Å).

If f and λ are constant, and the spatial frequency at the image is changed, then the distances from the optical axis change directly with s.

An analogy may be drawn between aperture size in the spatial domain and pulse width in the time domain as discussed in Section 2.1, Fig. 2.7.

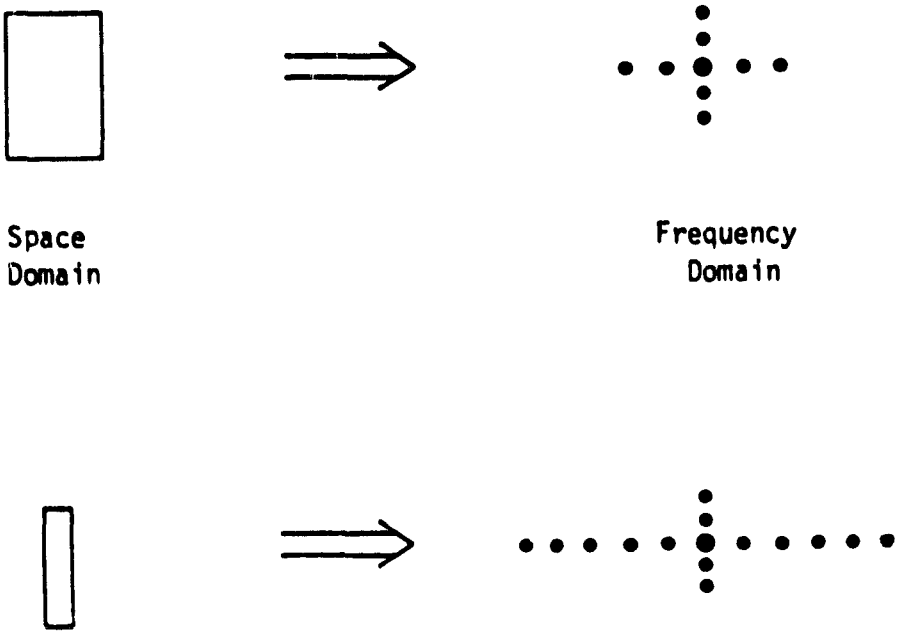

Figure 2.7. Two apertures, which are placed in the image plane, and their transforms are shown. The analogy with Figures 2.2, 2.3 and 2.4 is apparent. The larger aperture requires fewer frequency components than does the thinner aperture.

The "thinner" the aperture the "wider" the transform in the frequency domain. This is directly related to the pulse widths already discussed.

2.4 Examples of Transforms

The system used for this experiment is discussed in Chapter 3. Figure 3.4 shows the 32-wedge and 32-ring detector used to detect the intensity, $I_o(x_o y_o)$ (Eq 2-19). Figure 2.8 shows some "images" placed in the image plane and their resulting transforms. Note that the transforms are perpendicular to the image, and that a straight-line segment, in the image, will transform into a straight line. Similarly, a circular image will produce a circular transform. The transform is not dependent upon the spatial location of the image. Looking at the parallel-line image, Fig. 2.8, the transform of the right line is the same as that of the left line, assuming equal line dimensions.

2.5 Conclusions

This chapter has covered the theory underlying the process of detecting the leaf-angle distribution of corn. The Fourier series and transform were presented. Electric fields from an aperture were discussed and the Fresnel and Fraunhofer approximations were shown. The two sections were combined to show how an optical Fourier transform could be developed and detected. Two images were shown along with their transforms.

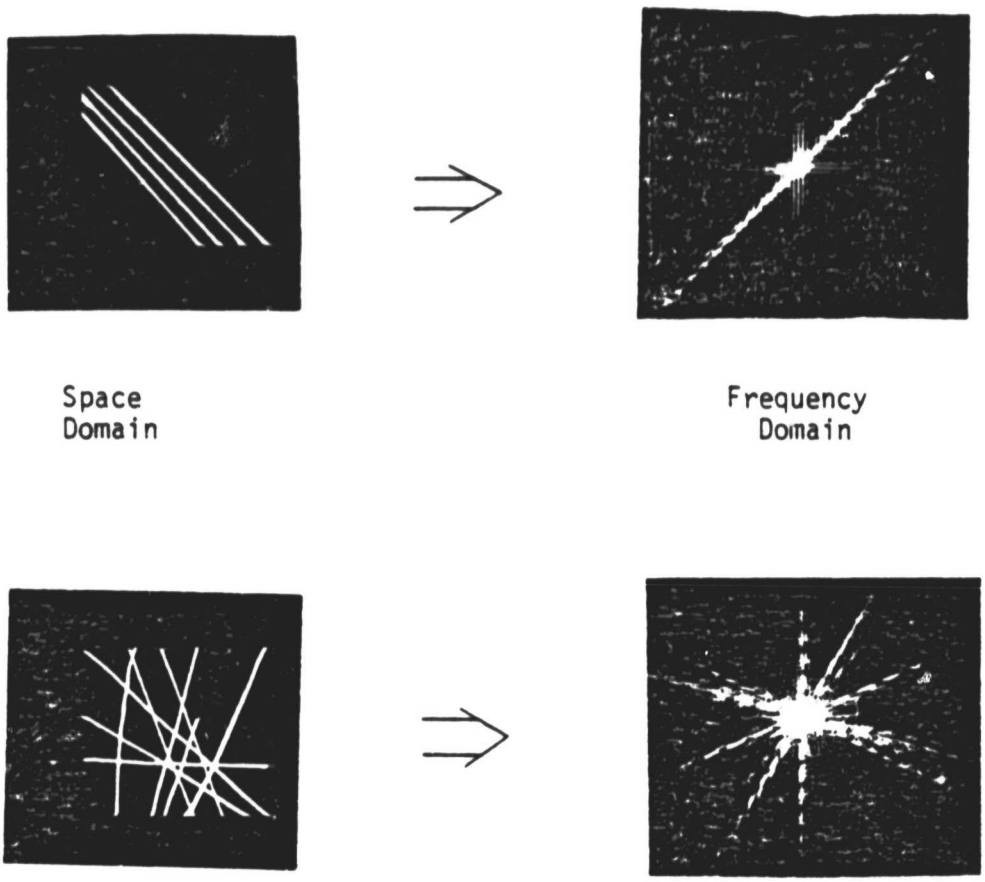

Figure 2.8. Examples of images and their transforms produced in the optical system used in this experiment. The transform is perpendicular to the image producing it, and can easily be detected using the 32-wedge, 32-ring detector explained in Chapter 4.

3.0 EXPERIMENTAL CONFIGURATION

This chapter will describe in detail both the field apparatus and the laboratory optical bench used during experimentation. Initial procedures for taking the data will be addressed; the detailed procedure will be included in the appendix.

3.1 Field

Radar data were taken by researchers from the Remote Sensing Laboratory during the summer of 1981 on 30 fields in North Lawrence, using a 10-GHz, truck-mounted system. There were 10 fields each of corn, wheat, and soybeans. Ground-truth data, which included plant- and soil-moistures and plant maturities, were taken also. A temporary shelter designed for the weighing and drying of ground-truth samples was erected at a central location. This shed also contained the photography station that was built for use in taking photographs of the plants for the leaf-angle distribution experiment (Fig. 3.1).

Two cornfields, C6 and C10, surrounded the shed site, and these fields were chosen as LAD experimental fields in order that greater control could be exercised with regard to breakage and wilting of the plant specimens. Three plants were cut from each field and placed, one by one, in front of a white background. The plant was first photographed at what was called the 0° look angle, which shows the projection of the plant's components in a plane orthogonal to the crop's row direction. This angle looks at the plant "broadside" (Fig. 3.2). The plant was rotated 45° and photographed; then rotated to 90° and photographed again. The 45° look angle proved to be the

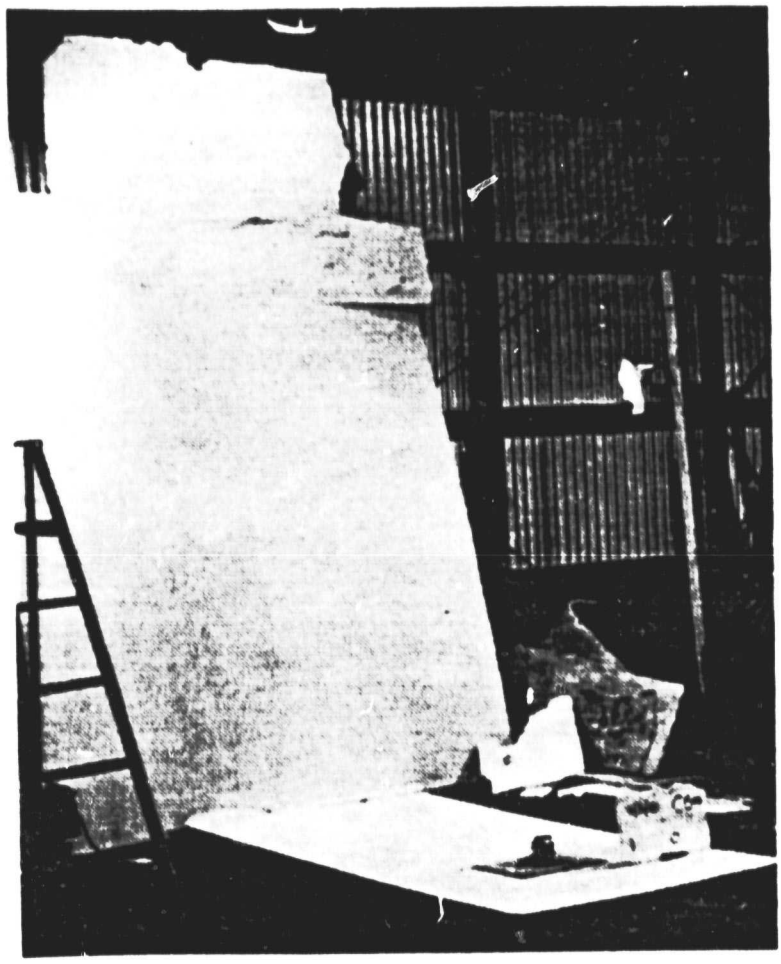

Figure 3.1. The photography station is shown. The corn plant was placed in the vise and photographed at the 0° look angle. Other angles were photographed by turning the base of the vise. The setup consisted of three sheets of plywood, three lights and styrofoam board.

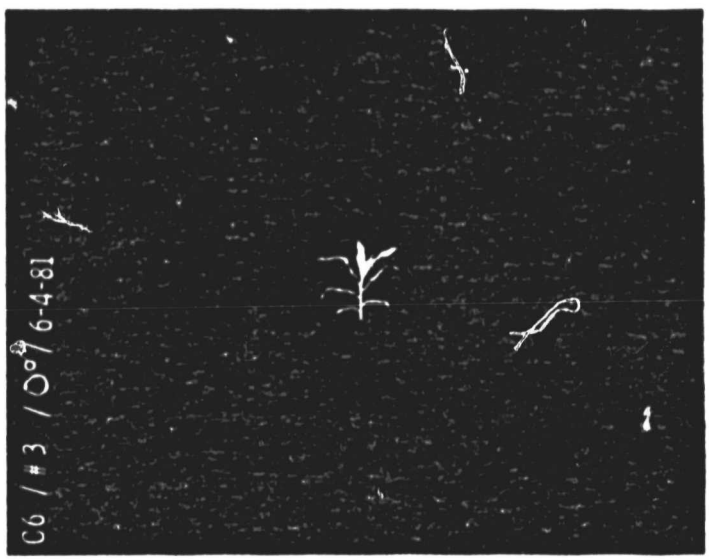

Figure 3.2. Shows a reduced version of the 4" x 5" binary image used in the optical system. It also shows the 0° look angle. Row direction is into the paper.

least productive angle for LAD information, while the 90° angle was useful in that, when compared to the 0° look angle, one could see the azimuthal orientation of the corn. Due to the bilateral nature of the corn plant, the 0° look angle is the one that contains most of the LAD information, thus it will be used to describe the results in Chapter 4.

The three plant photographs were then developed so that the plant appears to be transparent against an opaque background (Fig. 3.2). This "binary" photograph was then ready to be analyzed using the optical system to be described next. A full description of the photographic development procedure can be found in the appendix.

3.2 Laboratory Setup

The apparatus used is a basic optical system designed to perform a Fourier transformation on an image. It is this transform that can be analyzed to yield the image's angular information. This process was discussed in Chapter 2.

The bench consists of an HeNe 6328 Å red laser that illuminates a 25-micron pinhole, producing a diverging wave. The pinhole approximates the point source discussed in Chapter 2. The diverging coherent beam is passed through a double convex lens, which converges the beam into a plane wave. The plane wave is then spatially modulated by the image and made to converge again by the Fourier transform lens. The Fourier transform of the image is located at the back focal plane of this lens. It is here that the 32-wedge, 32-ring detector made by Recognition Systems, Inc. (RSI), is located. The entire system is shown in Fig. 3.3.

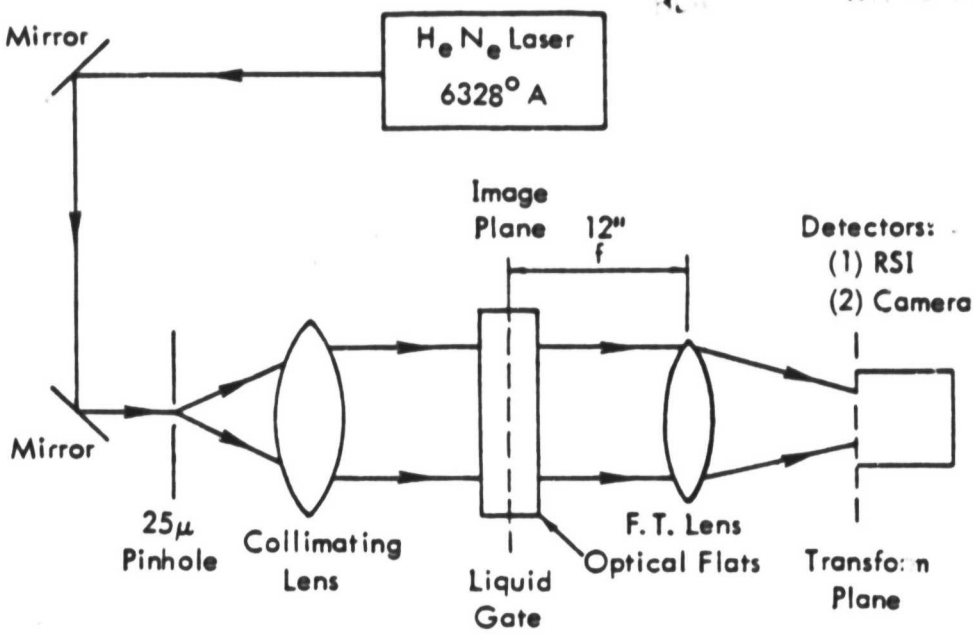

System Configuration

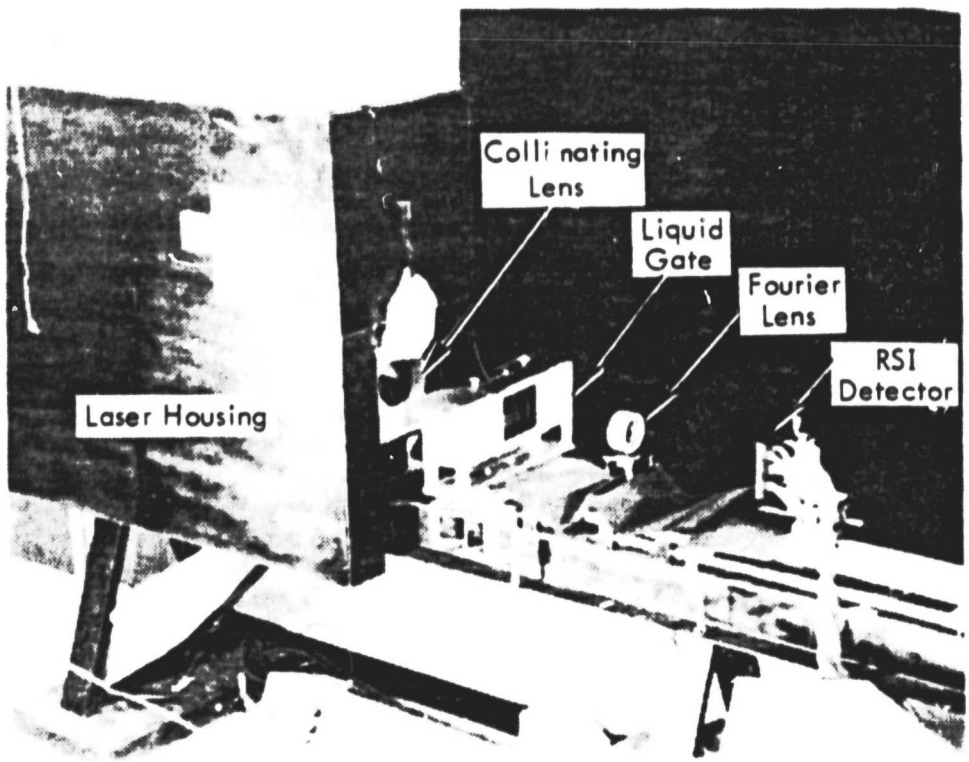

Figure 3.3. The optical system used for this experiment is shown both pictorially and schematically. A comparison with Figure 2.6 is instructive.

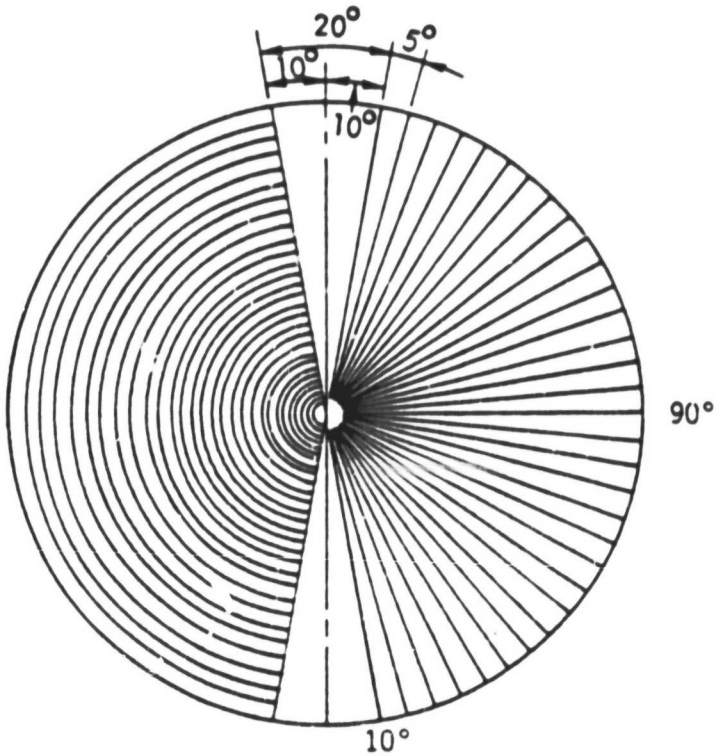

Figure 3.4. The detector is a 32-wedge, 32-ring photodiode array. Since the transforms are perpendicular to the image, the angles are defined as shown. One shortcoming to this device is the dead 10° area from 0° - 10° and 180° - 170°.

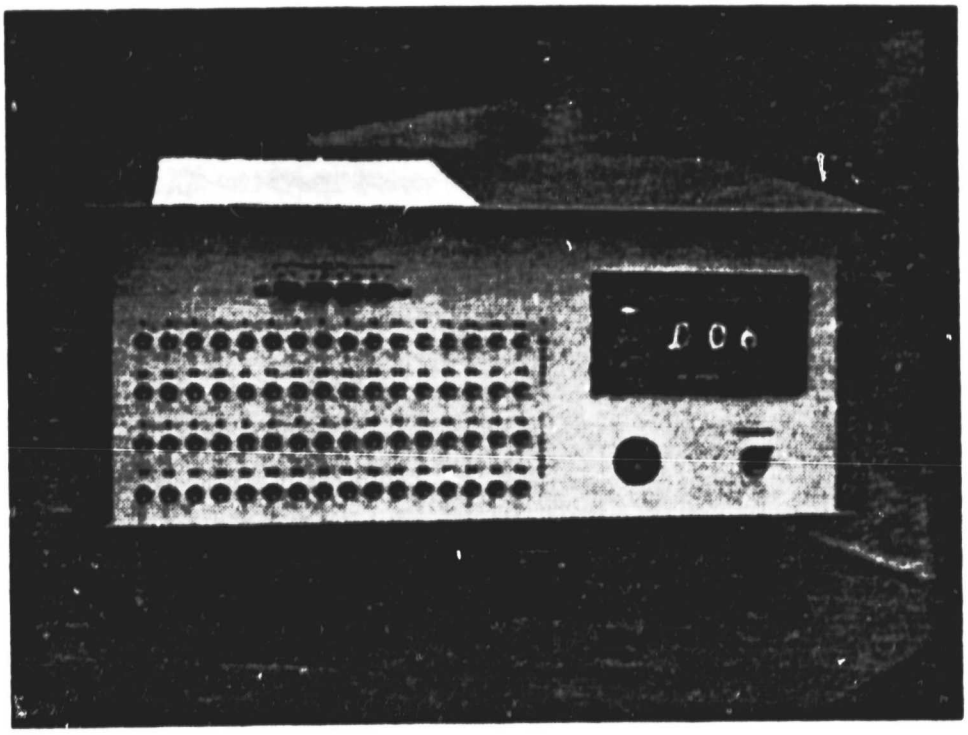

Figure 3.5. Recognition Systems, Inc. digital display and toggle switch array. Each wedge or ring can be selected by a toggle switch and the intensity read on the digital display.

This detector is a photodiode array sensitive to 6328 Å. The rings are used to measure spatial frequency while the wedges measure the angle. Each wedge or ring can be selected individually with a toggle switch and the intensity of light at that particular wedge or ring can be read out on the digital display (Figs. 3.4, 3.5). The image is placed in a liquid gate that matches the refractive indices of the film and glass (optical flats) so that the effects of any variations in film thickness are minimized. This matching process helps to reduce any phase errors that might occur due to film irregularities.

A detailed explanation of the data-taking procedure and the RSI device alignment is included in the appendix.

4.0 EXPERIMENTAL DATA

This chapter will cover the data obtained from several "models" especially designed for the purpose. These models were used to test the system and to "simulate" corn plants. Success with the modeling also added confidence to the accuracy of the corn data.

Models

One model used to test the system is shown in Fig. 4.1. This model was processed as explained in Chapter 3 and the appendix, and analyzed using the system shown in Fig. 3.3. The results of this analysis are shown in Fig. 4.1.

The Fourier transform of the "Vee" is seen in the top right corner, frequency domain. This intensity pattern is incident upon the 32-wedge, 32-ring detector where it is detected as a function of angle. The graph shows how intensity varies with angle. The peaks are in the 65° to 70° and 115° to 120° ranges corresponding to the angles 67.5° and 117° in the "Vee" image. Other models of a similar nature were studied but will not be shown here since the results are similar.

Corn leaves are not simple structures in the same way that rectangles or triangles are. As the leaf extends from the stalk, sinusoidal variations are visible in the photograph. These variations appear as thickness differences and will diffract coherent light to angles other than those actually occupied by the leaf. To test the system's ability to discern the "true" leaf angle in the presence of these nonuniformities, several models were constructed and tested.

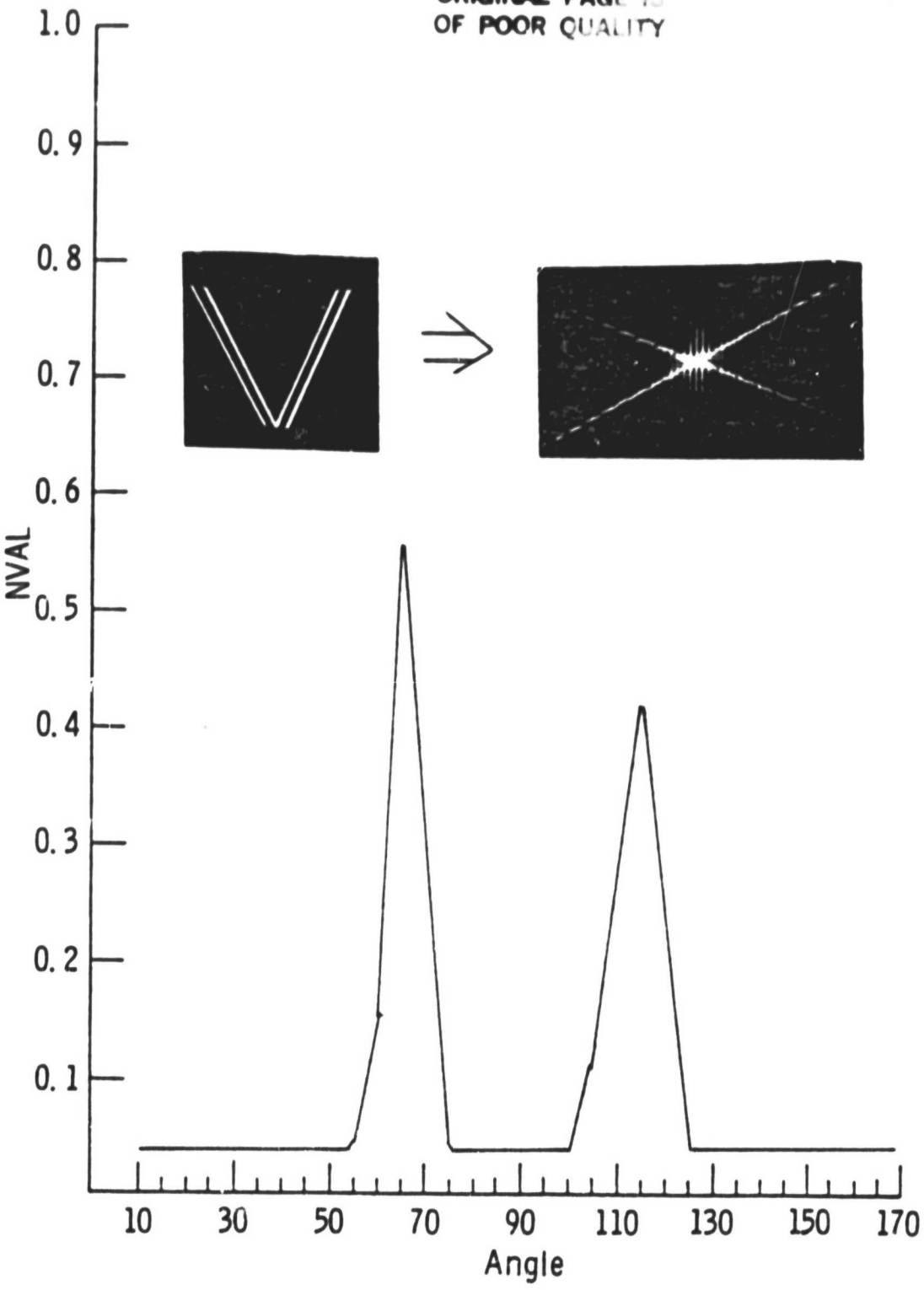

Figure 4.1. The "Vee" model and its transform are shown with a plot of normalized intensity vs. angle. It can be seen from the plot that the angular variations of the image (Vee model) are detected by the RSI device.

The first two models tested the system's ability to detect the varying thicknesses of leaves (Fig. 4.2).

The next model tested its ability to detect the general angular trend of a leaf corrupted by sinusoidal-type variations (Fig. 4.3).

The worst case will occur when the variations are represented by two half-circles. An Airy function will then appear in the transform. It is intuitively obvious that as the variations become less circular (i.e., elliptical), the transform will describe the angle more accurately.

The graphical analysis of Fig. 4.2a and b is shown in Figs. 4.4 and 4.5, respectively. These graphs are normalized to the peak at 40° to 45°. A comparison of the graphs shows that the 45° and 90° angles are indeed discernible. It can be seen that the thinner "leaf" reduces the overall DC component and therefore makes detection of the angle more accurate.

Several problems with the system can be seen from these models. First, note that the angular range near 90° for the thicker "leaf" is wider than that for the thinner "leaf." This occurs because the 32-wedge, 32-ring detector does not have the photodiodes at 90°, but has a "dead" line there. If the system were set up perfectly, the intensity would be split evenly between the 85° to 90° and the 90° to 95° ranges. However, a very small deviation on either side of this line will result in a higher reading in one wedge or the other. The accuracy, therefore, is ±5°, which is not very good.

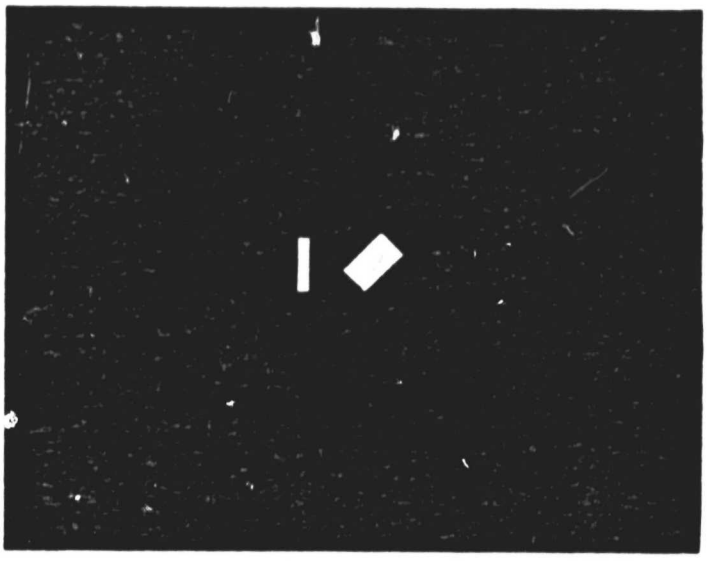

(a)

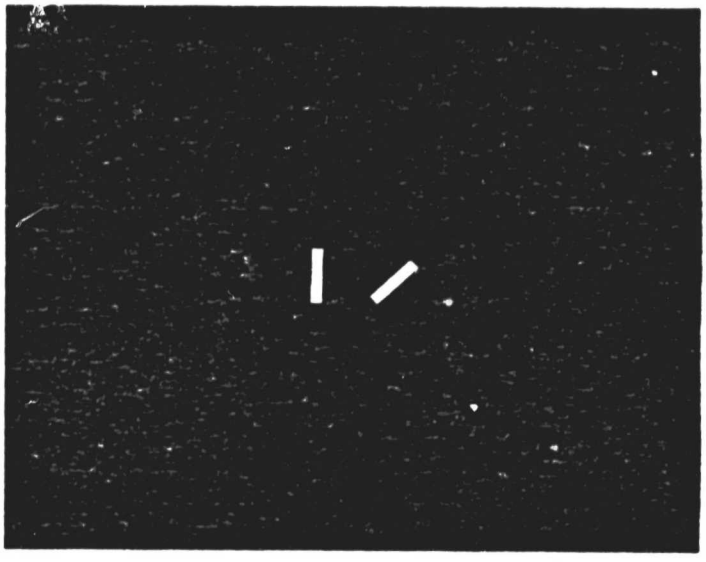

(b)

Figure 4.2 (a) and (b). Model images were developed to test the system's ability to distinguish thick and thin leaves.

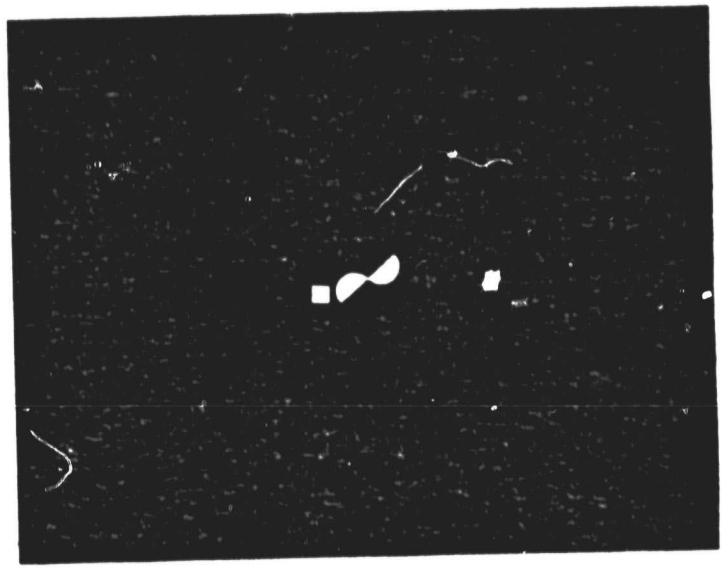

Figure 4.3. The complex variations of a corn leaf could cause erroneous angle determination. This model tested the system's ability to detect the leaf angle in the presence of worst-case variations.

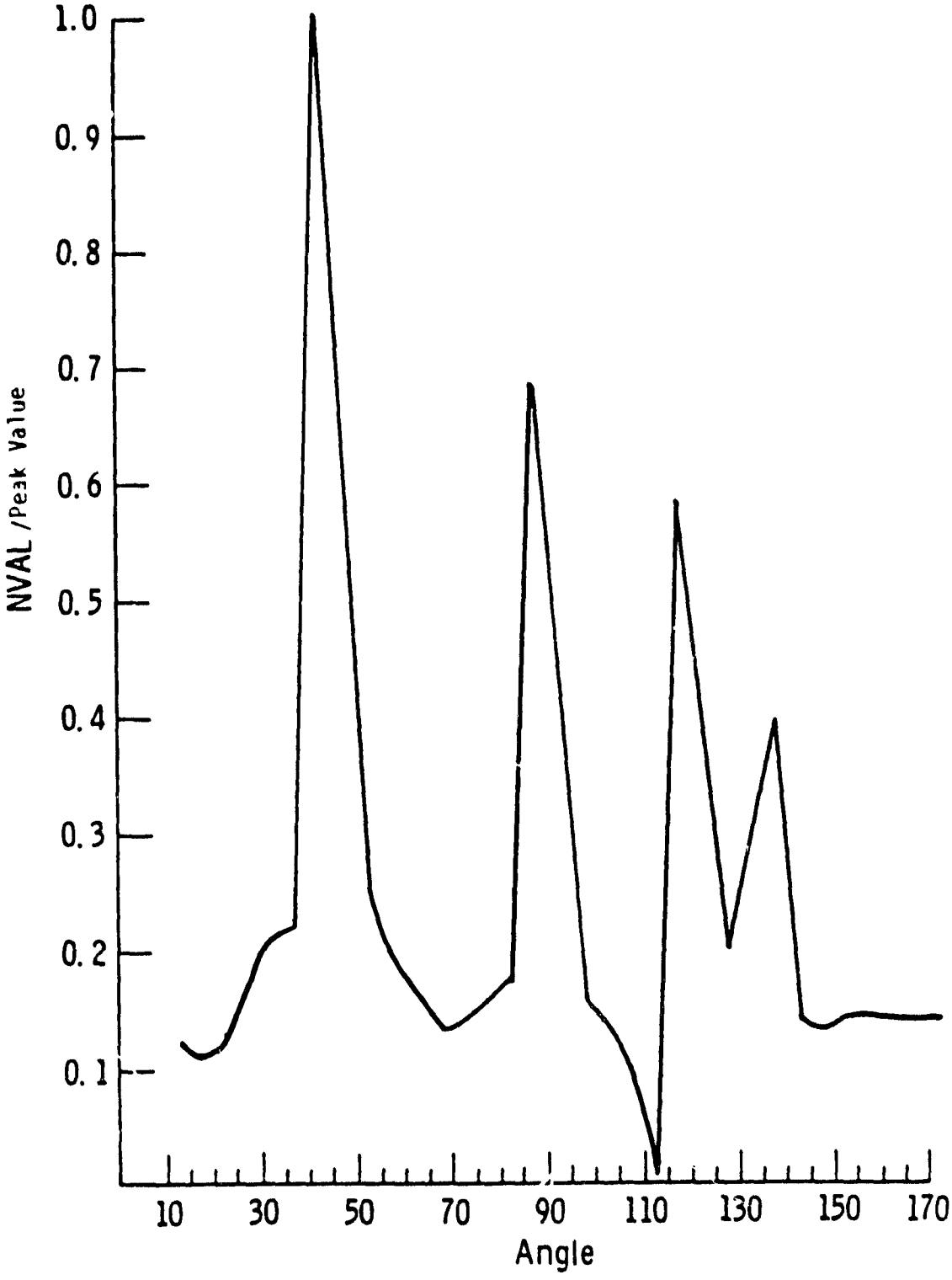

Figure 4.4. The analysis of the thick-leaf model shows the need for small components in the image plane so that the DC components and reflection are reduced.

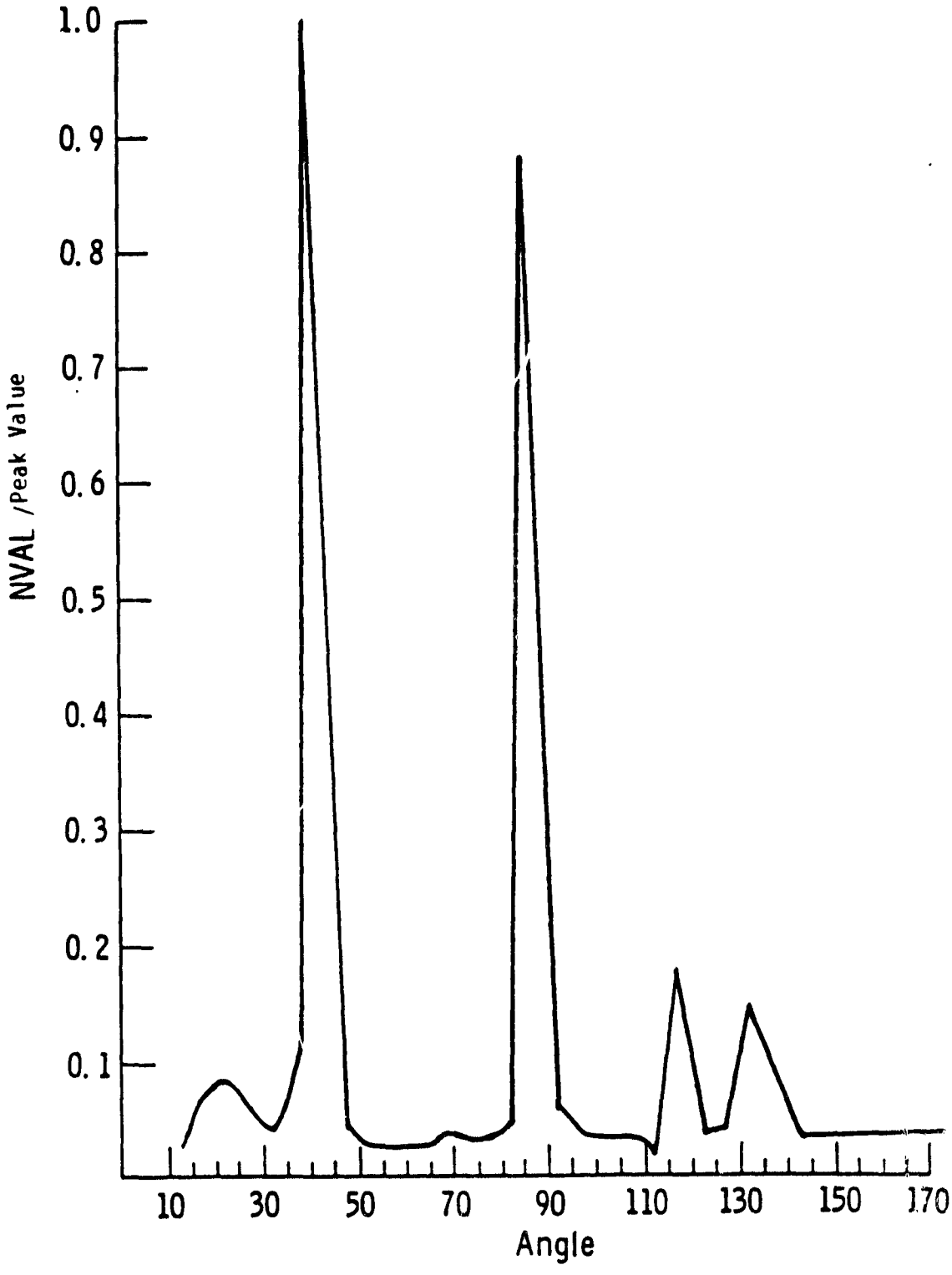

Figure 4.5. The thin-leaf analysis shows how well the leaf angle, 45°, and stalk, 90°, are detected.

The other problem is reflection. The model simulating the thicker "leaf" has a higher DC component, which reflects itself on the 115° to 120° wedge. It can be seen that when the thinner "leaf" is analyzed, this component is considerably reduced. The solution to this problem is to use smaller components to raise the spatial frequency (Eq. 2-20). Fortunately, the actual corn plant did not have the reflection problem.

The sinusoidal model graph is shown in Fig. 4.6. One can see that the 45° angle is indeed detected. The "stalk," although small, is also detected.

The next experiment performed involved removing the known-angle leaves from an actual corn plant (photo) and noting the difference in NVAL versus angle plot. Figure 4.7 shows C6 on 8/11/81. The solid line represents the whole plant; #1 shows what happens when a leaf measured at ≈45° is masked. The leaf also had other angle components and the percentage of change between 10° and 40° is as follows:

10° - 15°	17.24%
15° - 20°	20.00%
20° - 25°	15.03%
25° - 30°	19.00%
30° - 35°	6.00%
35° - 40°	29.00%
40° - 45°	23.24%
45° - 50°	9.00%

It is evident that the 35° to 40° and 40° to 45° ranges exhibit the greatest losses. There is also a strong component at 15° - 20°. A second corn leaf, #2, was masked at ≈145° (estimate) and the result

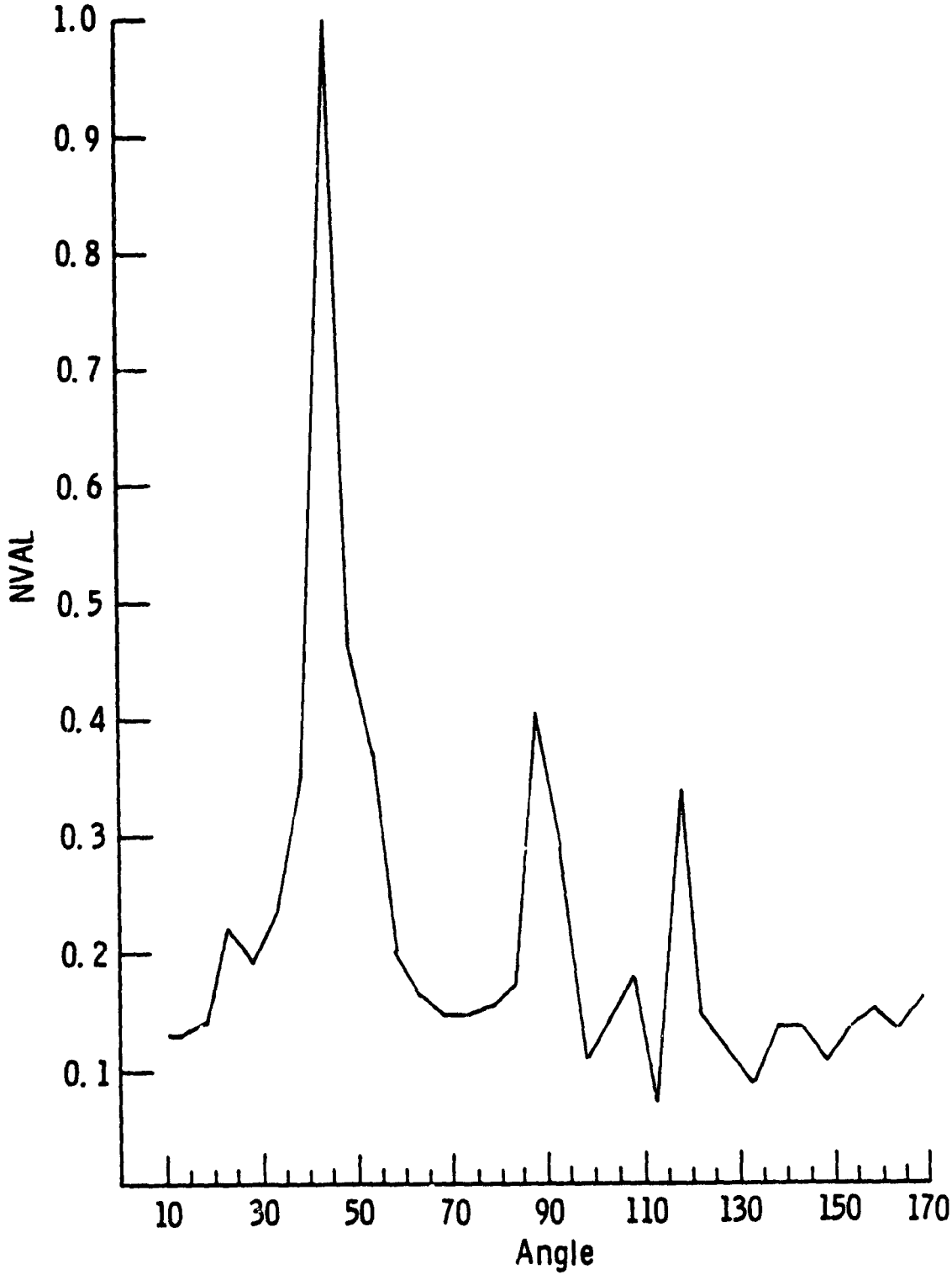

Figure 4.6. The sinusoidal model is analyzed and the 45° leaf angle is seen to be readily detected.

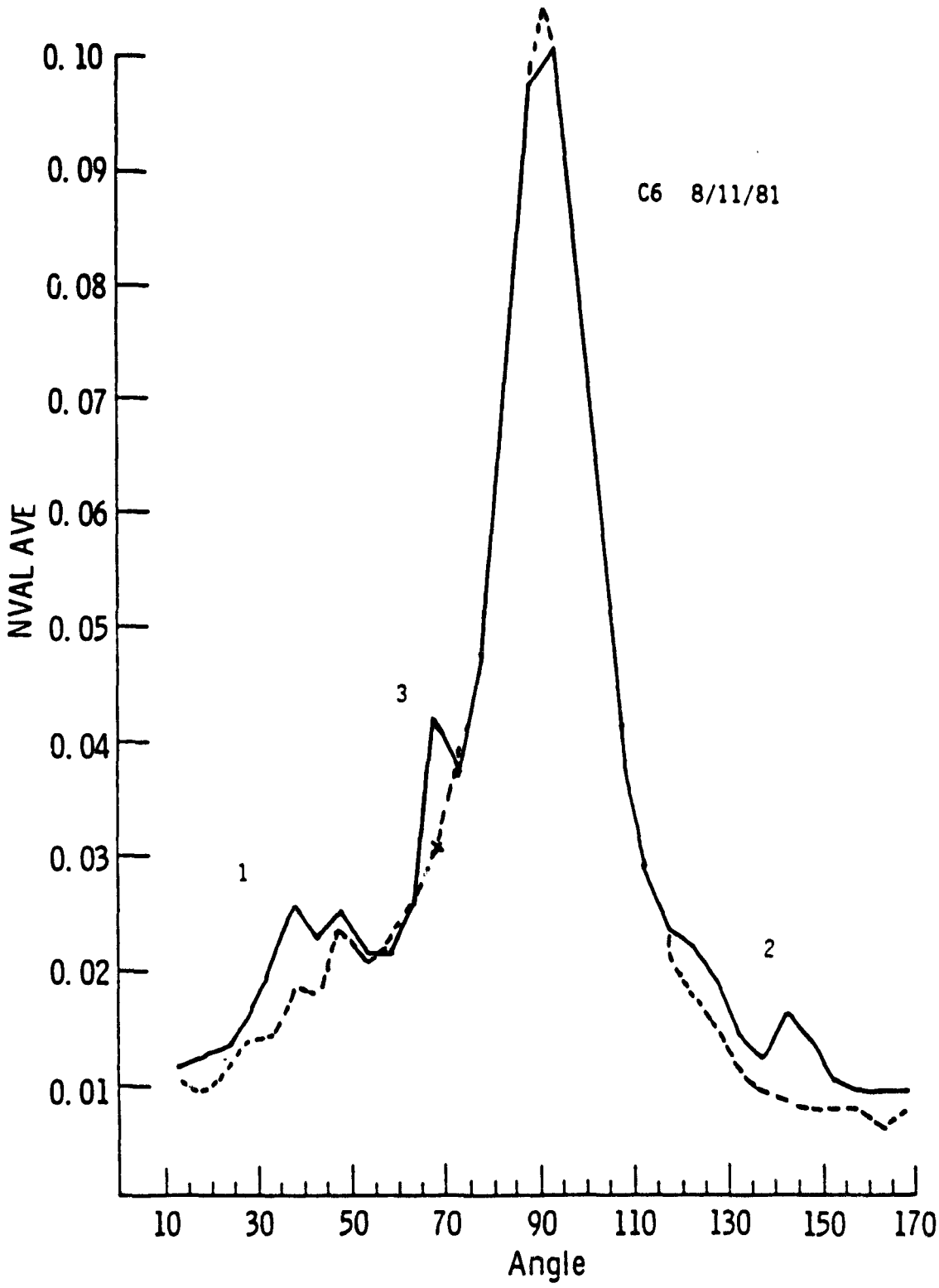

Figure 4.7. NVAL vs. angle of C6 8/11/81. Leaves were inked out of the image in steps and the resulting loss plotted.

shown. Here the maximum percentage of change occurred at 140° to 145° (31.92%) and 145° to 150° (?.86%). The reduction in NVAL at other angles can occur for two reasons:

1. The sinusoidal variations cause diffraction at angles other than those representing the general trend, and
2. parts of the other blocked-off leaf, as it bends, have a small effect.

Leaf #3 was blocked off at =65° and the corresponding loss is shown. The resulting loss (maximum) was in the 65° to 70° range and was 26.06%. Upon inspection, it is seen that the plant is becoming more erectophile in structure.

Figure 4.8 shows the effect of removing the stalk from the plant. The loss in NVAL corresponding to stalk-removal is 35%.

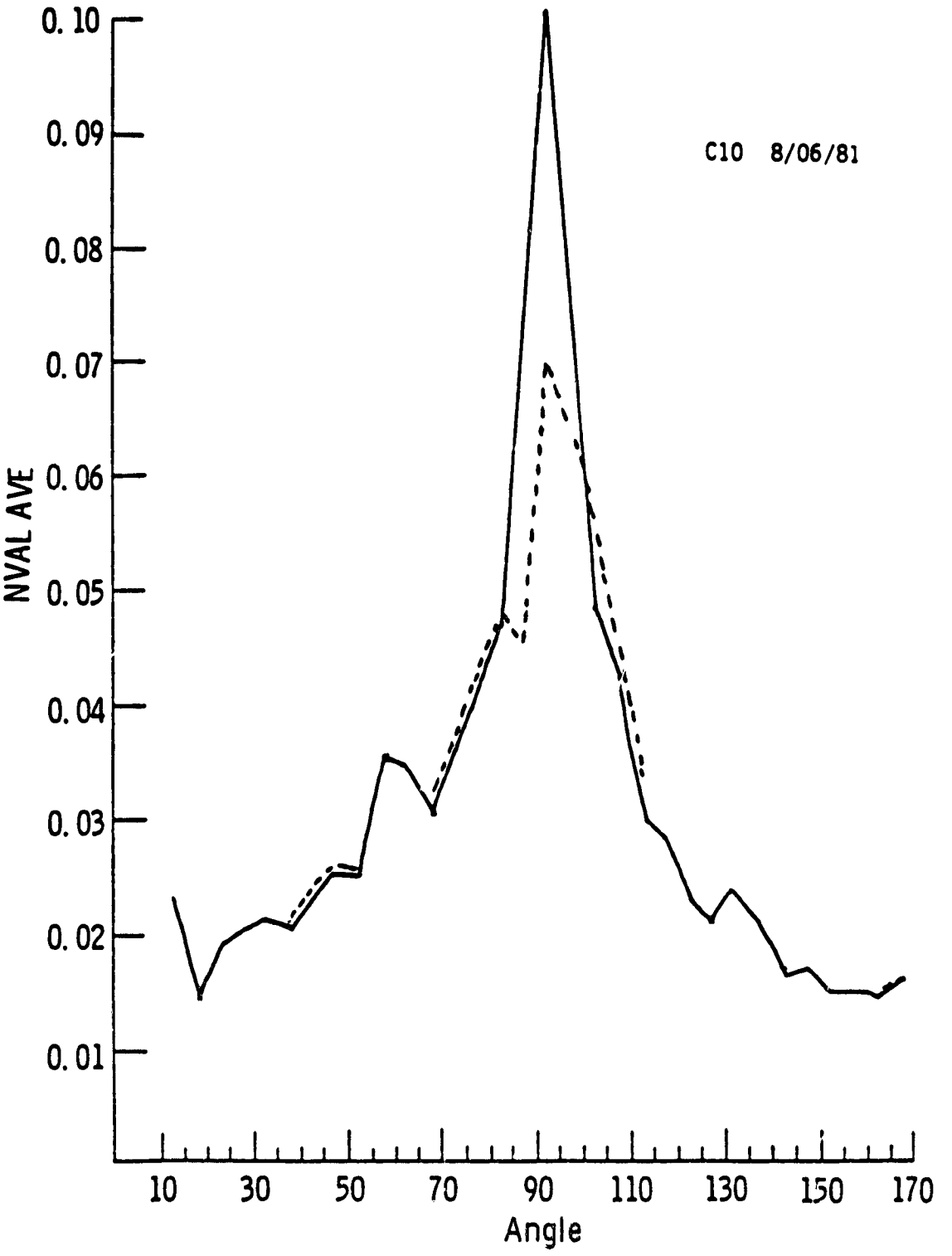

Figure 4.8. Stalk removal is indicated by a 35% decrease in the 90° component of C10, 8/6/81.

5.0 EXPERIMENTAL RESULTS

This chapter will detail the results of the LAD experiment. A comparison between σ°, LAD, plant moisture, and soil moisture will be shown. Results will be discussed and suggestions for further research made.

5.1 Leaf-Angle Distribution (LAD)

The geometry of a corn plant can be described by its leaf-angle distribution (LAD). The LAD refers to the manner in which the leaves of the plant occupy space, and to the angles they make with respect to the ground. Most of the work with LAD (see literature review) has dealt with photosynthetic research. Investigators have manually measured LAD at one point--the leaf-stalk interface--effectively ignoring the remaining portions of the leaf, stalk, and fruit, all of which can play a role in determining radar backscattering. The optical technique used here measures the entire plant from 10° to 170°, where 10° and 170° are the most horizontal and 90° is vertical.

Smith, Oliver and Berry [23] show a method of classifying plants according to their LAD (Fig. 5.1). The horizontal-leaf plants are classified as planophile. Those with mostly vertical orientation are erectophile, and those with leaves > 45° and < 45° are plagiophile and extremophile structures, respectively.

A new family of graphs showing cumulative frequency versus angle will be presented in this report. The angular range covered will be from 10° to 170°. It will be seen that at its least vertical

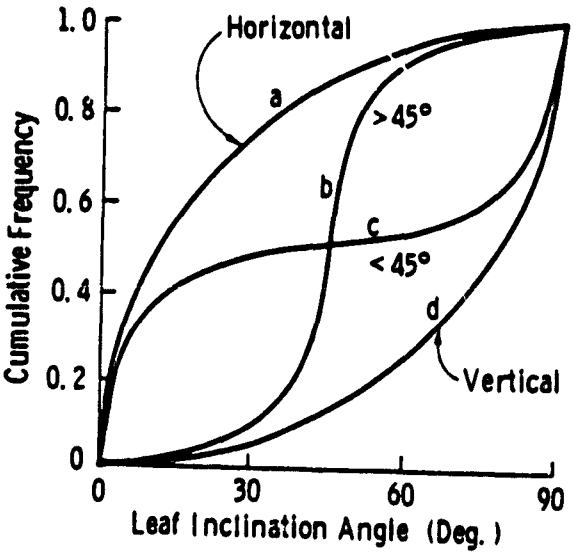

Figure 5.1 Shows the way in which plants are classified according to their geometry. Leaf angles are measured and a cumulative frequency of occurrence is obtained versus angle.

structure, the corn plant still contains 60 percent vertical components. This is due primarily to the stalk when the plant is young, but as the plant matures the leaves also become more vertical in nature.

5.2 Experimental Results

Along with the LAD-versus-maturity graphs showing the way in which a corn plant changes its geometry as it matures, this report will present several other items that have importance in the behavior of corn geometry and its effects on radar sensors:

1. This report will shown that a corn plant has a definite azimuthal orientation perpendicular to row structure.
2. It will be seen that plant moisture decreases with maturity after the growth stage (see Appendix H), and that the plant's ability to sustain a horizontal structure is directly related to its moisture content.
3. Near-surface soil moisture appears to play a role in plant geometry. The 1981 growing season was relatively wet.

It is known that if abundant water is available early in the life of the corn plant, its roots are less likely to penetrate deeply into the soil. The ready availability of soil moisture to the corn plants during the 1981 crop season made the development of deep roots unnecessary. Thus, the plants reacted quickly to the additional moisture provided by incident rainfall throughout the summer.

4. Graphical representation of changes in plant structure are shown by plotting the vertical and horizontal (90° and 10° plus 170°, respectively) plant components as a function of maturity in Fig. 5.2. Ignoring sampling- and measurement-error, the mean CUMVAL of the corn as a function of time is seen to be first more vertical, then less vertical, and finally, it exhibits a change toward the more vertical again. Since corn is an erectophile structure throughout its development, its structure must be defined as being "less vertical" or "more vertical" since it is always vertical.

The next several sections will describe these results.

5.2.1 LAD Versus Maturity

For any single azimuthal look angle, the 0° look angle (look direction is parallel to corn-row orientation) contains the maximum amount of information available on angular leaf distribution. The data for this report were based solely on this look angle except where comparisons are made to show azimuthal orientation.

It is seen from Figs. 5.2 and 5.3 that the plant has a fairly uniform distribution of angles when it is young but becomes strongly erectophile as it matures. The mean leaf angle from 10° to 90° (including the stalk) ranges from 55° to 61° (Table 5.1).

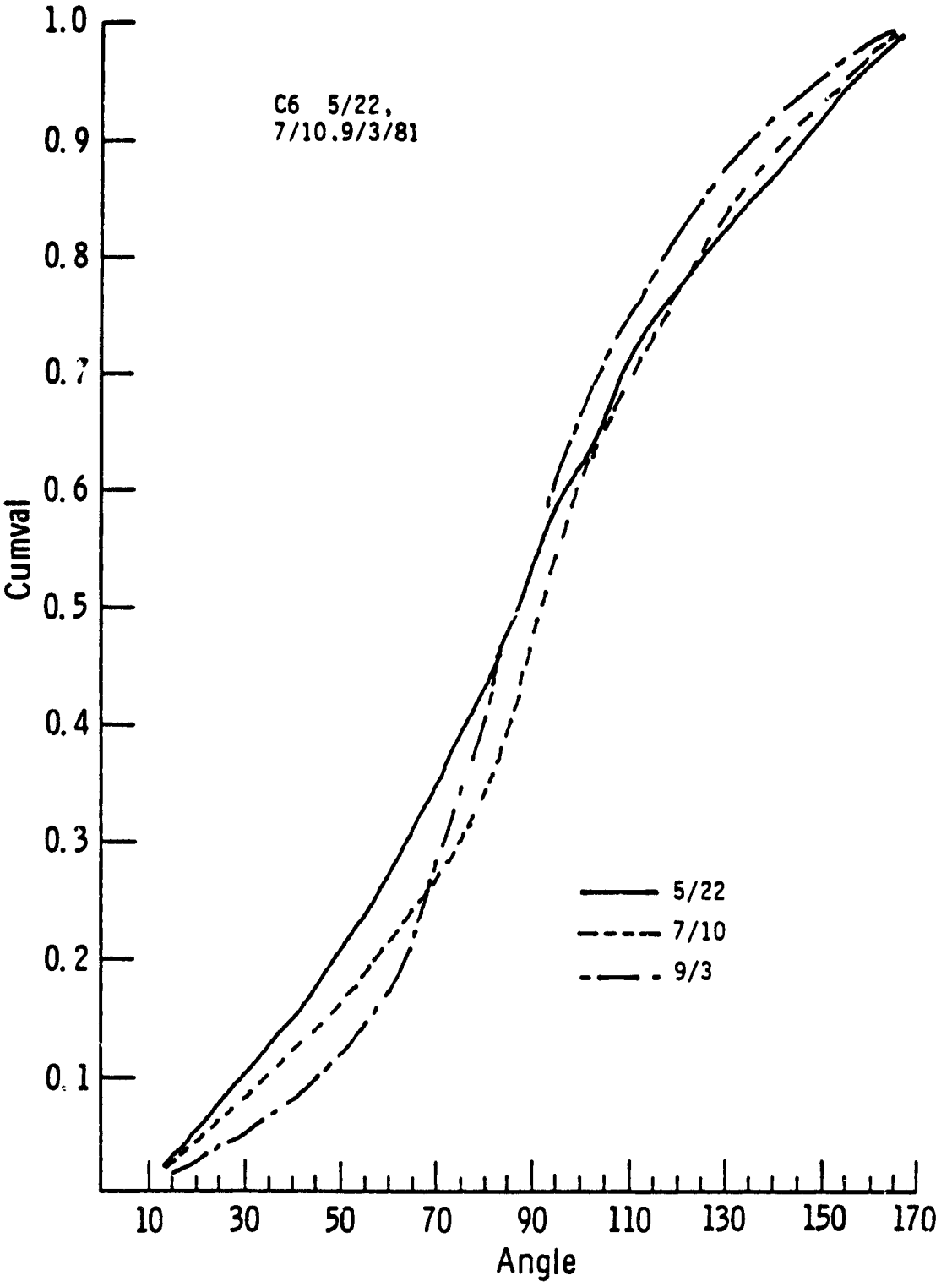

Figure 5.2. This graph shows how C6 matures. It is seen that the corn becomes more vertical (erectophile) in structure as it matures.

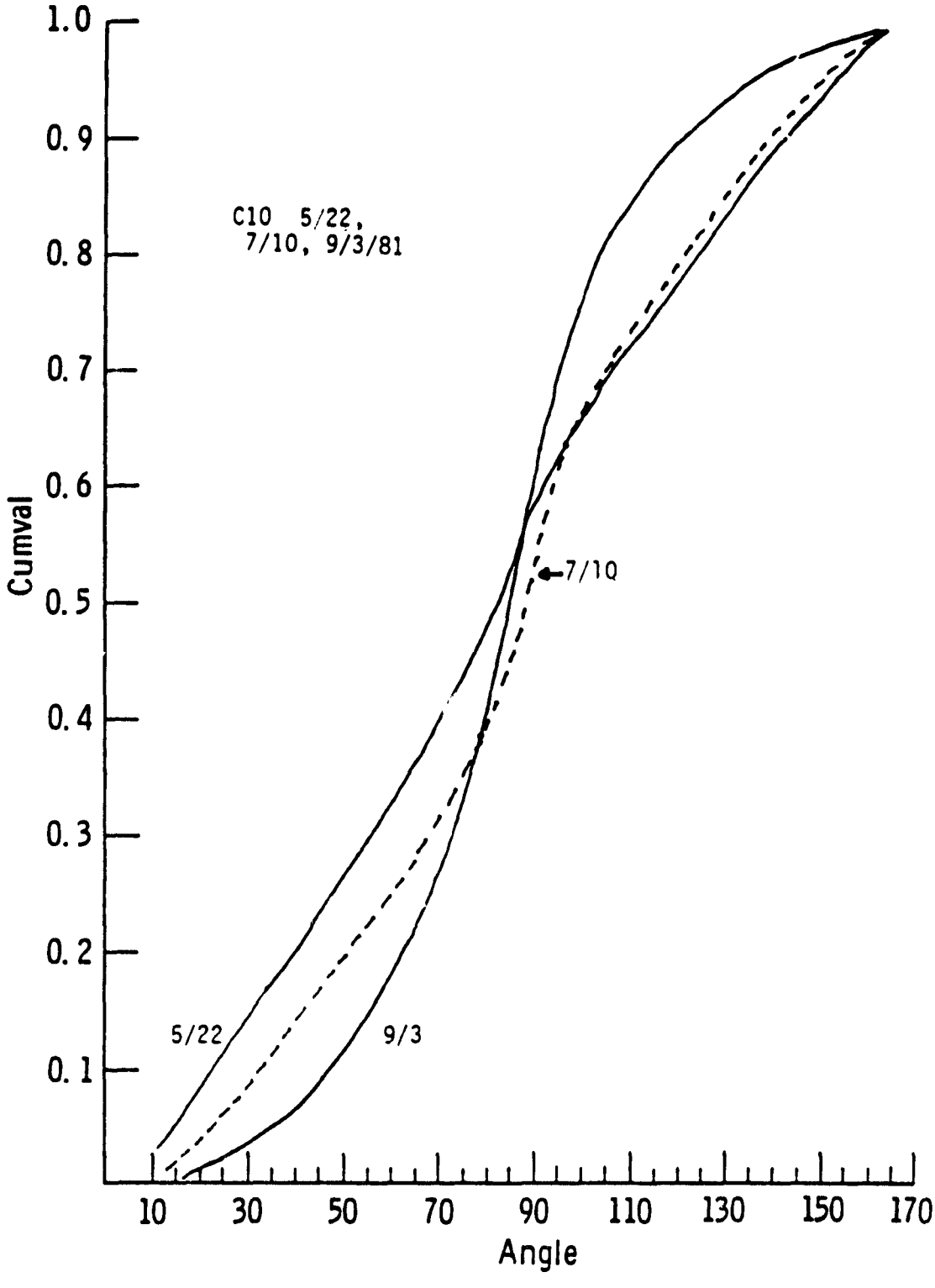

Figure 5.3. Shows how C10 becomes more erectophile as it matures.

TABLE 5.1

The Mean Plant Angle Presented as a Function of Maturity
Comparison to the literature (at silking) is included.

						Silking						
	5/22	6/5	6/12	6/19	6/26	7/10	7/16	7/23	7/30	8/6	8/11	9/3
Mean Plant Angle (leaves, stalk & fruit)	57°	55°	55°	55°	57.5°	58°	59°	59°	61°	60°	61°	60°
Whigham & Wooley						59.2° 79.7°						
Pepper, et al.						73.8° 63.7° 43.4°						
Winter & Ohlrogge						45°						

The percentage of leaves (and stalks) in the angular ranges between 10°-45° and 45°-90° shows how these components change with maturity (Table 5.2). A graphical representation of this changing plant-structure can be seen in Fig. 5.4, where the 10° (horizontal) and 90° (vertical) plant components are plotted versus maturity.

The 10° LAD components are compared to plant moisture in Fig. 5.5. This trend shows that plant vigor, as evidenced by plant moisture, is related to plant geometry in that as the plant dries, its ability to support the leaves decreases; hence the number of horizontal components decreases.

5.2.2 Azimuthal Orientation of Corn

The corn plant has a definite orientation with azimuth. This orientation is generally perpendicular to the row structure and, in the mature plant, may be attributable to the planting density where the struggle for light forces the plant leaves into the rows (Fig. 5.6). However, early plants (only a week or two after emergence) are seen to lack a preferred orientation relative to row direction, although they do have a bilateral structure. The 0° look angle, when compared with the 90° look angle, shows how strongly the plant is oriented in azimuth. The further apart these two plots are when the plant is vigorous, the greater the degree of orientation. Figures 5.7 through 5.9 show how the plant is oriented in azimuth as a function of time. It can be seen that as the plant ages and the number of vertical components in leaves increases, the 0° angle approaches 90° azimuth angle, which corresponds to the plant's

TABLE 5.2

The Percentage of Plants Occurring in the 10°-45° and 45°-90° Angular Ranges is Shown

Date	10° - 45°	45° - 90°
5/22	30.5%	67.00%
6/5	34.97%	61.8%
6/12	37.58%	59.5%
6/19	33.4%	63.7%
6/26	27.32%	70.3%
7/10	25.85%	72.00%
7/16	23.43%	74.7%
7/23	23.88%	74.00%
7/30	17.62%	81.00%
8/6	19.05%	79.6%
8/11	19.84%	79.00%
9/3	18.59%	80.3%

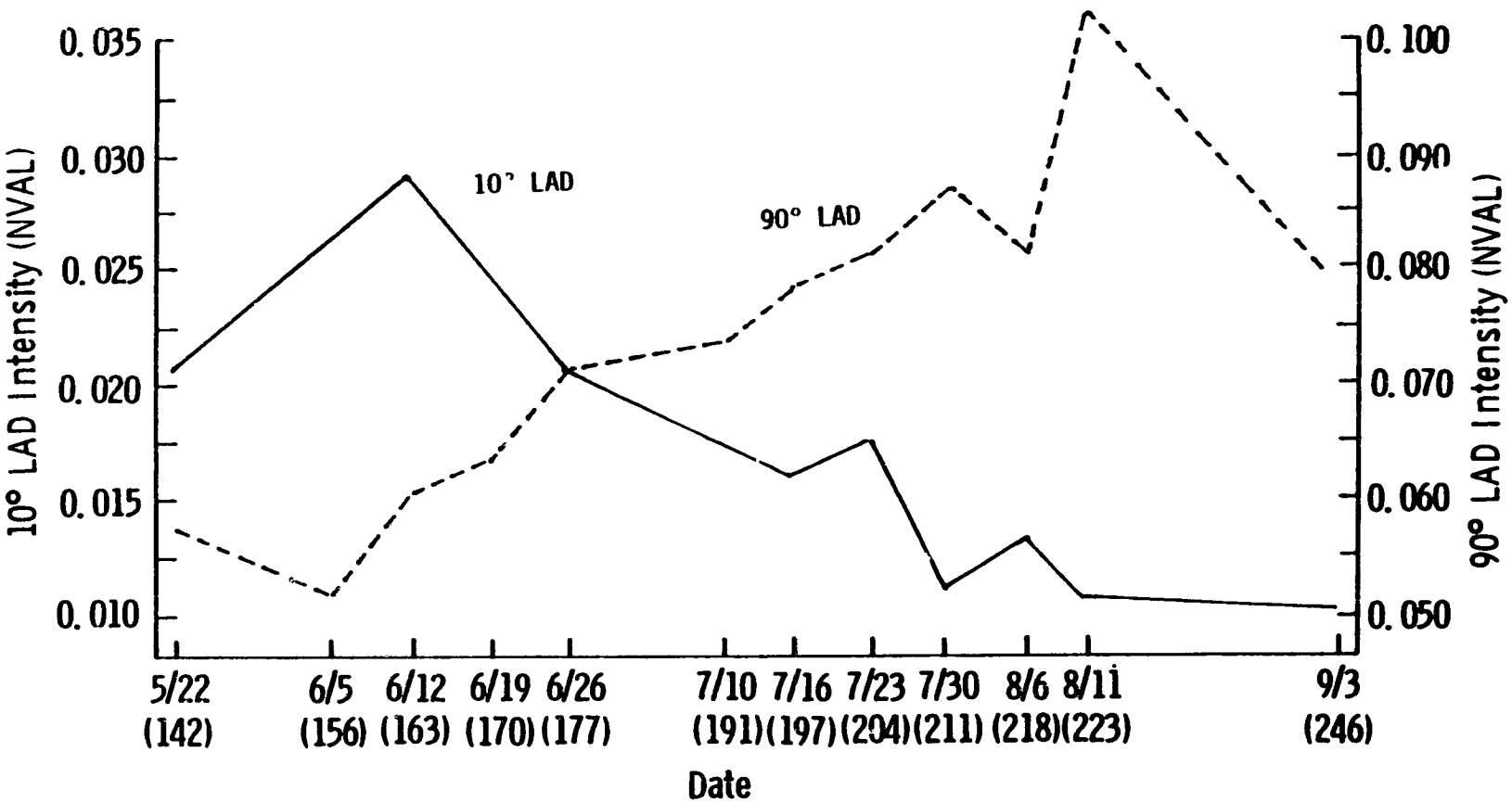

Figure 5.4. A plot of 10° LAD (horizontal) and 90° LAD (vertical) vs. maturity shows how the plant becomes more vertical as it matures. Notice how 8/6 tends to stop the process by increasing the 10° LAD and decreasing the 90° LAD.

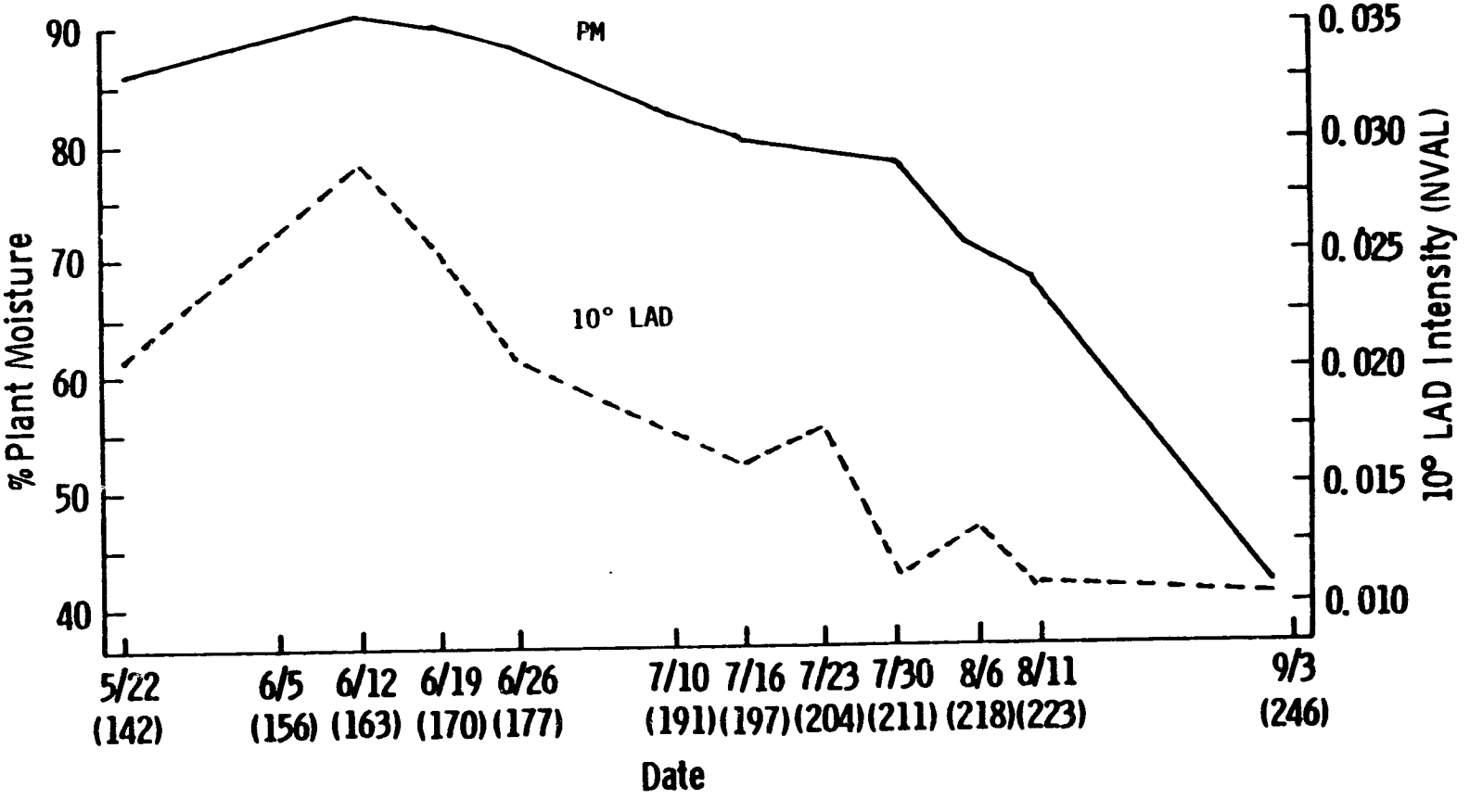

Figure 5.5. Graphically shows the dependence of horizontal leaf components on plant moisture. The dryer the plant, the less capable it is of supporting a horizontal structure.

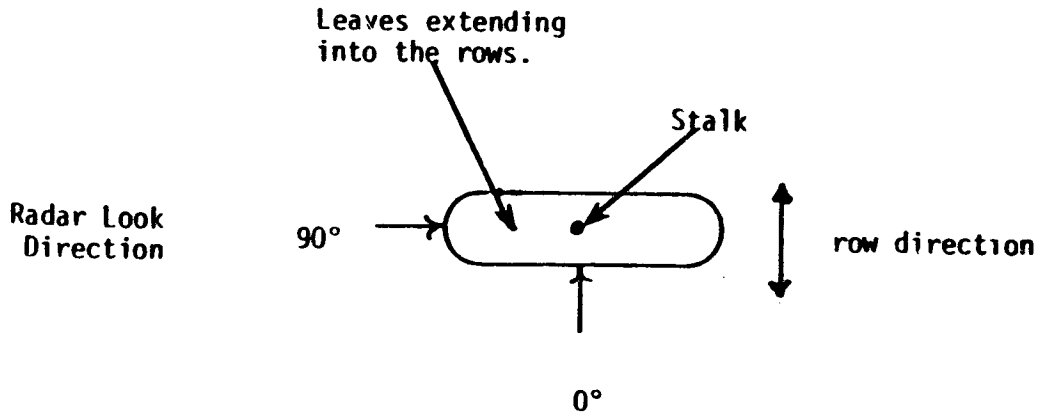

Figure 5.6. The corn plant has a definite azimuthal orientation fully dependent on row direction. The 0° look angle and 90° look angle are defined.

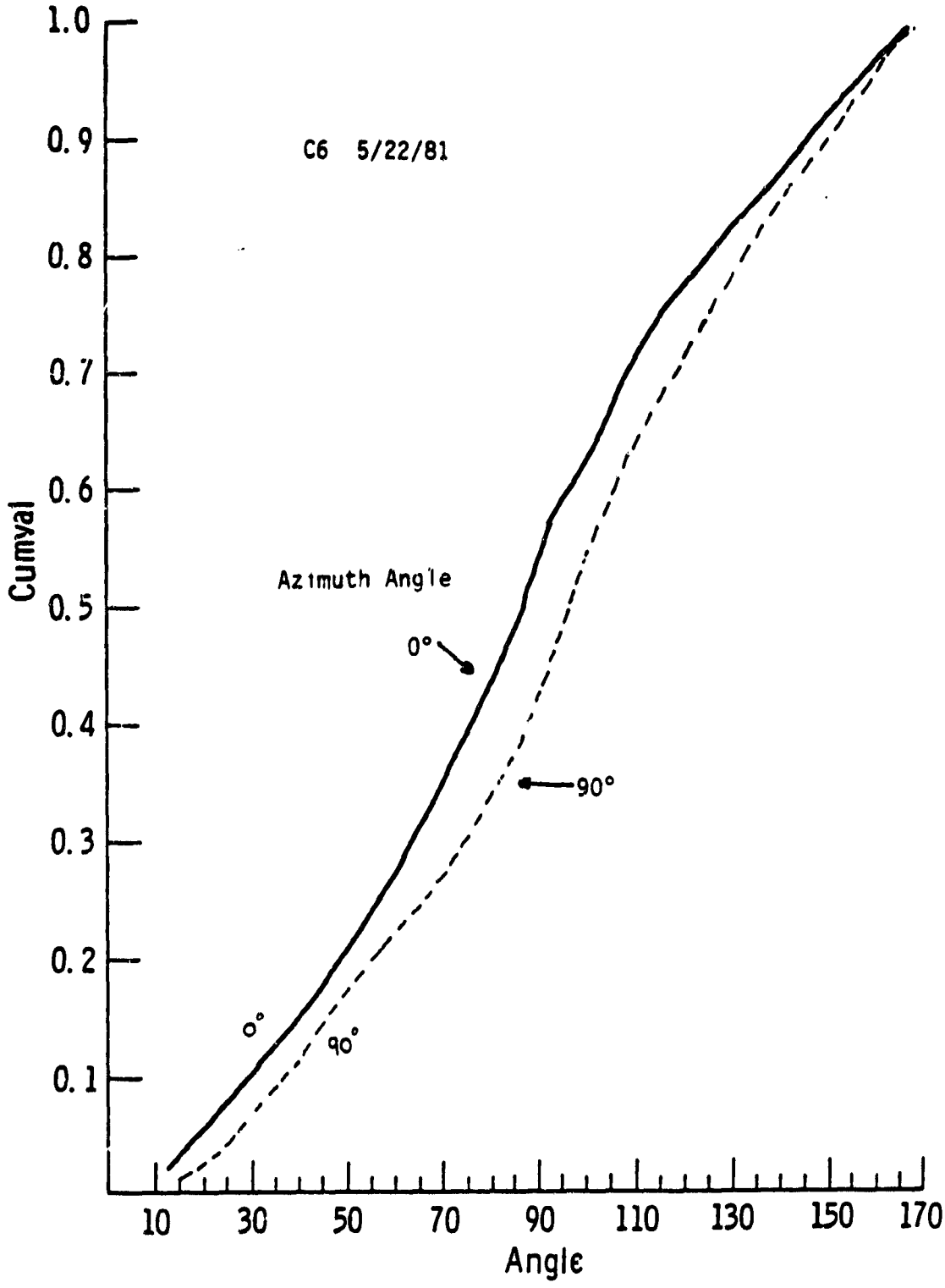

Figure 5.7. A young plant is somewhat oriented even though the other plants have not forced the orientation yet.

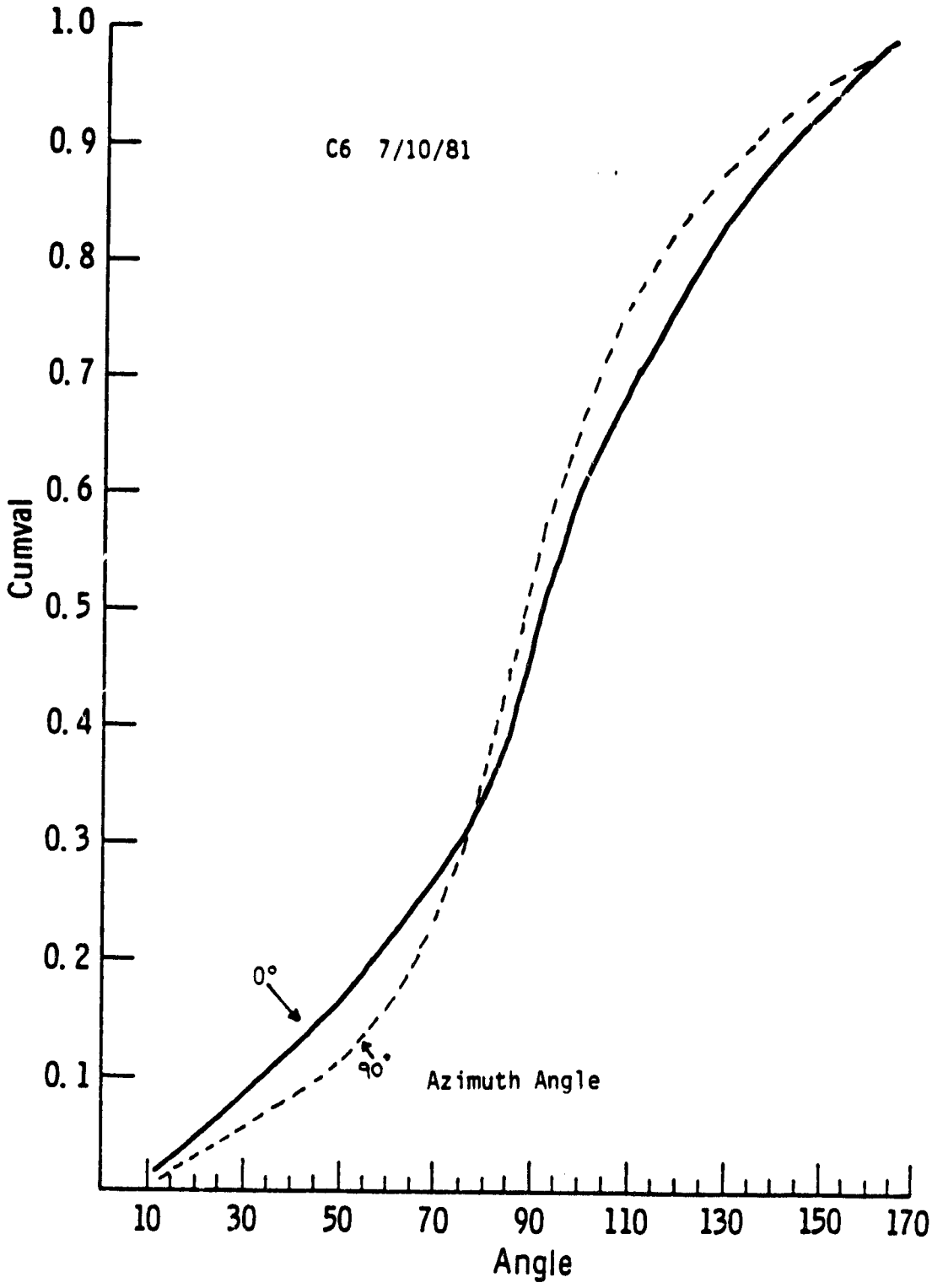

Figure 5.8. The orientation between 0° and 90° is shown here. The 90° component is more vertically structured (dotted line) than the 0° component and shows the azimuthal orientation of corn.

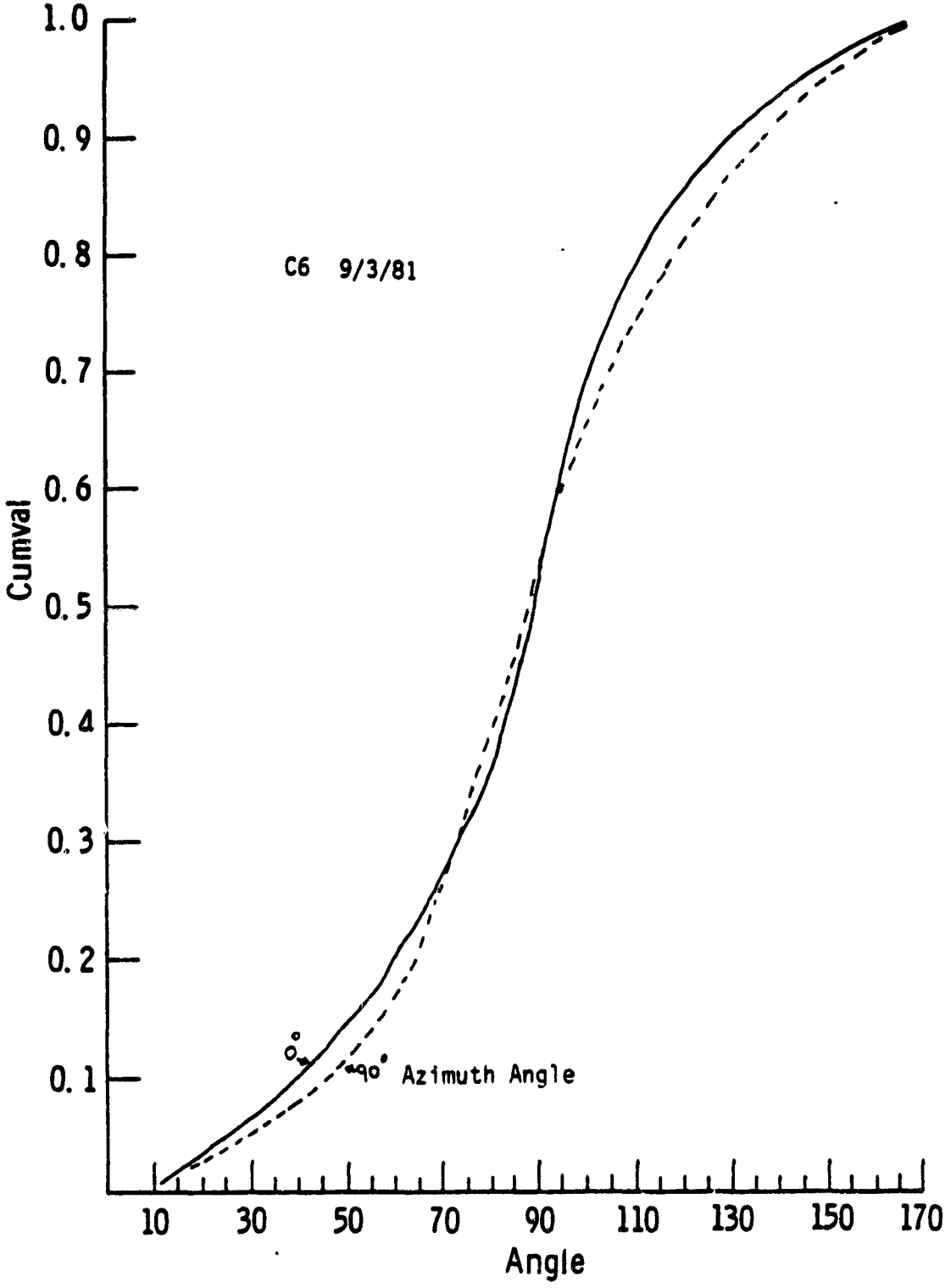

Figure 5.9. As the plant dies, the 0° component approaches the 90° component. This is an erectophile structure in both views.

becoming more erectophile with maturity. Similar results for C10 will not shown here, as they are included in the appendix.

5.2.3 LAD, Plant Moisture (PM), and Soil Moisture (SM)

The relationship between the 0° look angle, LAD, and plant moisture was presented in Section 5.2.1. Figure 5.10 shows the plant moisture and soil moisture as a function of time for Field C6. The rain events are shown and a relationship between soil moisture and these events can be seen. The plant moisture also seems to change, albeit slowly, due to physiological changes within the plant and is apparently not limited by the availability of soil moisture. Note especially the 6/5 to 6/19 area: the soil moisture dips at 6/5 but, due to the rain on 6/11, increases on 6/12. The plant moisture increases to a maximum on 6/12 and then starts its steady decrease to the level shown on 9/3. The period from 6/26 to 7/30 indicates that plant moisture is decreasing as the plant matures. The plant moisture seems to be related to plant maturity, and secondarily to soil moisture as a limiting factor. In addition, since this was a very wet crop season, crop vigor and turgor should not be soil-moisture limited. Similar data should be obtained for a crop season where moisture deficiencies might induce changes in plant geometry.

Another interesting comparison is that between soil moisture and the 10° LAD (Fig. 5.11). In particular, notice the 6/12, 6/19, 7/16, 7/23, and 8/6 data points. The horizontal data points could be construed to follow soil moisture. This might suggest a relationship between soil moisture and plant geometry, however, the relationship

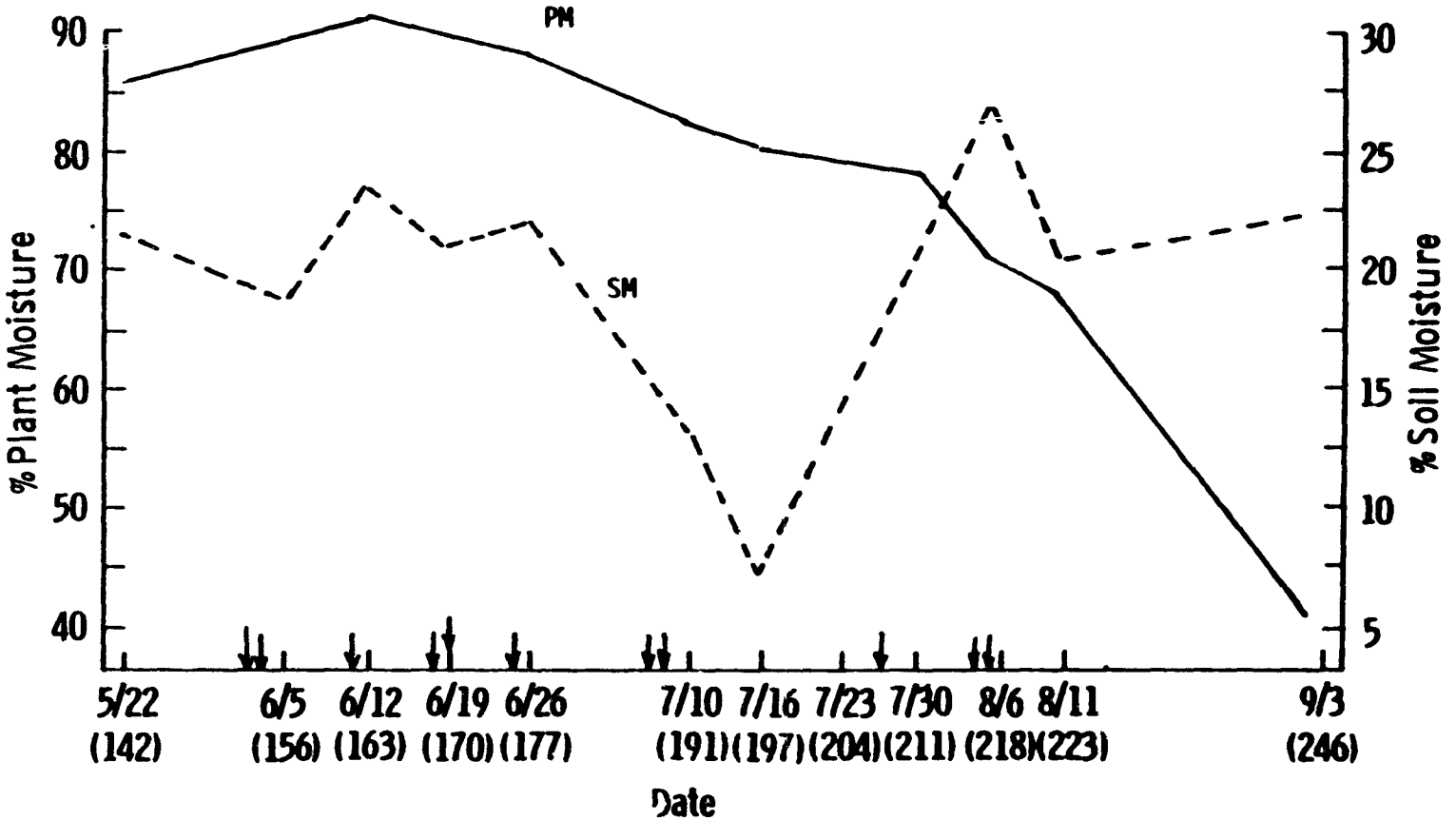

Figure 5.10. Plant moisture increases when plants are very young, but decreases with plant age (after 6/12). The arrows indicate rain events; increases in soil moisture can be seen to follow some of these events. In general, it was a very wet summer and corn-root depth may not have been as deep as usual.

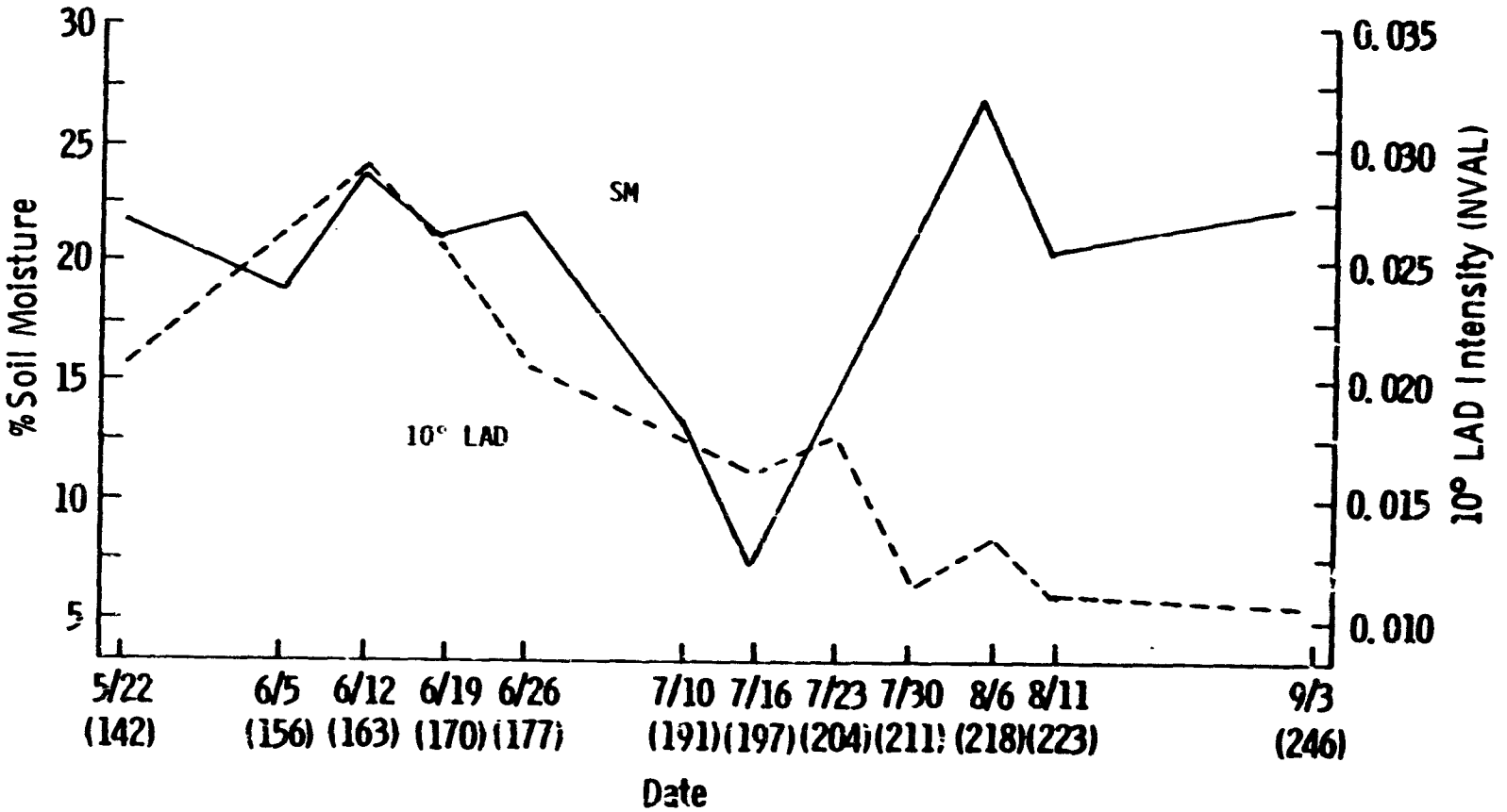

Figure 5.11. Recovery in the 10° LAD (horizontal) components can be seen as the soil moisture increases. This graph shows the dependence of plant geometry on soil moisture.

could be spurious and could be caused instead by small sample-size and intrafield variability in LAD.

5.3 Conclusions and Summary

This chapter has presented the results of the LAD experiment for the 1981 summer radar experiment. Included in these results were:

1. LAD versus maturity: It was shown that the corn plant changes structure with maturity from a more uniform leaf distribution to a strongly vertical structure.
2. The corn plant was shown to be azimuthally oriented throughout its growth period.
3. Possible relationships between soil moisture and plant geometry were shown to offer a potential for estimating subsoil water deficits.

These results both confirm previous work and point to new areas of research that should be investigated. The effect of soil moisture on LAD and its possible effect on σ^{o} is an exciting prospect for future work.

Suggestions for Further Research

1. Investigate further the soil moisture → LAD → σ^{o} relationship.
2. Improve the optical system using current technology. One suggestion for improvement might be the use of a single moving wedge that would be very narrow and would be

attached directly to an x-y plotter in order to continuously plot intensity versus angle for a full 360° rotation.

Other possible methods involve the use of a Visual Display Imager (VDI), thus allowing the computer to detect the angles. This would, however, require more time than would the optical determination method.

3. Improvements in the photographic technique might be made so that the photographs would exhibit higher contrast and would be less expensive to process. A possible solution would be to create a binary image directly on the negative. A liquid gate with the capability of holding a 35-mm negative roll is available. Processing of the plant photos could be accomplished by advancing the film through the liquid gate.

REFERENCES

[1] Blad, B. L. and D. G. Baker, "Orientation and Distribution of Leaves within Soybean Canopies," Agron. J., Vol. 61, Jan.-Feb. 1972.

[2] Brisco, B. and R. Protz, "Corn Field Identification Accuracy Using Airborne Radar Imagery," Canad. J. Rem. Sens., Vol. 6, No. 1, July 1980.

[3] Bush, T. F. and F. T. Ulaby, "Radar Return from a Continuous Vegetation Canopy," IEEE Trans. Antennas Propag., Vol. AP-24, No. 3, May 1976.

[4] Casasent, D., "Coherent Optical Pattern Recognition," IEEE Proc., Vol. 67, No. 5, May 1979.

[5] Casasent, D., "Spatial Light Modulators," IEEE Proc., Vol. 65, No. 1, January 1977.

[6] Casasent, D., "New Optical Transforms for Pattern Recognition," IEEE Proc., Vol. 65, No. 1, January 1977.

[7] Casasent, D., "Optical Data Processing for Engineers," Parts I, II, and III, EOSD, Feb., April, June, 1978.

[8] Duncan, W. G., "Leaf Angles, Leaf Area and Canopy Photosynthesis," Crop Sci., Vol. II, July-Aug. 1971.

[9] Egbert, D. D., J. R. McCauley, J. L. McNaughton and F. T. Ulaby, "Ground Pattern Analysis in the Great Plains," RSL Technical Report 2266-6, University of Kansas Center for Research, Lawrence, Kan., Aug. 1973.

[10] Fung, A. K. and F. T. Ulaby, "A Scatter Model for Leafy Vegetation," IEEE Trans. Geosci. Electr., Vol. GE-16, No. 4, Oct. 1978.

[11] Gaskill, J. D., "Optics for the Electronics Engineer," Parts I, II, and III, EOSD, Feb., April, and June 1977.

[12] Goodman, J. W., "Introduction to Fourier Optics," McGraw-Hill Book Co., 1968.

[13] Goodman, J. W., "Operations Achievable with Coherent Optical Information Processing Systems," IEEE Proc., Vol. 65, No. 1, Jan. 1977.

[14] Hecht, Z. A., Optics, Addison-Wesley Publishing Co., Reading, Massachusetts, 1974.

[15] Kimes, D. S., J. A. Smith and J. K. Berry, "Extension of the Optical Diffraction Analysis Technique for Estimating Forest Canopy Geometry," Aust. J. Botany, Vol. 27, pp. 575-588, 1979.

[16] Lang, A. R. G., "Note on Paper: 'Optical Diffraction Analysis for Estimating Foliage Angle Distribution in Grassland Canopies,' by J. A. Smith and J. K. Berry," Aust. J. Botany, Vol. 28, pp. 495-497, 1980.

[17] Lemeur, R., "A Method for Simulating the Direct Solar Radiation Regime in Sunflower, Jerusalem Artichoke, Corn and Soybean Canopies Using Actual Stand Structure Data," Agri. Meteorol., Vol. 12, pp. 229-247, 1973.

[18] Loomis, R. S. and W. A. Williams, "Productivity and the Morphology of Crop Stands: Patterns with Leaves," in Physiological Aspects of Crop Yield, American Society of Agronomy, pp. 27-47, Madison, Wis., 1969.

[19] Pepper, G. E., R. B. Pearce and J. J. Mock, "Leaf Orientation and Yield of Maize," Crop Sci., Vol. 17, Nov.-Dec. 1977.

[20] Purdue University, LARS Information Note 120776, "A Laser Technique for Characterizing the Geometry of Plant Canopies," West Lafeyette, Ind., January 1977.

[21] Shanmugam, K. S., Digital and Analog Communication Systems, John Wiley and Sons, Inc., New York, 1979.

[22] Smith, J. A. and J. K. Berry, "Optical Diffraction Analysis for Estimating Foliage Angle Distribution in Grassland Canopies," Aust. J. Botany, Vol. 27, pp. 123-133, 1979.

[23] Smith, J. A., R. E. Oliver and J. K. Berry, "A Comparison of Two Photographic Techniques for Estimating Foliage Angle Distribution," Aust. J. Botany, Vol. 25, pp. 545-553, 1977.

[24] Thompson, B. J., "Hybrid Processing Systems--An Assessment," IEEE Proc., Vol. 65, No. 1, January 1977.

[25] Ulaby, F. T., "Radar Response to Vegetation," IEEE Trans. Antennas Propag., Vol. AP-23, No. 1, January 1975.

[26] Ulaby, F. T., "Vegetation Clutter Model," IEEE Trans. Antennas Propag., Vol. AP-28, No. 4, July 1980.

[27] Ulaby, F. T., "Microwave Response of Vegetation," Adv. Space Res., 23rd Annual Conf. Com. Space Res. (COSPAR), Budapest, Hungary, Vol. 1, pp. 55-70, 1981.

[28] Ulaby, F. T. and T. F. Bush, "Monitoring Wheat Growth with Radar," Photogram. Eng. Rem. Sens., Vol. 42, No. 4, pp. 557-568, April 1976.

[29] Ulaby, F. T. and T. F. Bush, "Corn Growth as Monitored by Radar," IEEE Trans. Antennas Propag., Vol. AP-24, No. 6, pp. 819-828, November 1976.

[30] Ulaby, F. T., M. C. Dobson and G. A. Bradley, "Radar Reflectivity of Bare and Vegetation-Covered Soil," Adv. Space Res., 23rd Annual Conf. Com. Space Res. (COSPAR), Budapest, Hungary, Vol. 1, pp. 91-104, 1981.

[31] Vanderlugt, A., "Coherent Optical Processing," IEEE Proc., Vol. 62, No. 10, October 1974.

[32] Whigham, D. K. and D. G. Wolley, "Effect of Leaf Orientation, Leaf Area and Plant Densities on Corn Production," Agron. J., Vol. 66, July-Aug. 1974.

[33] Wilson, W. J., "Inclined Point Quadrants," New Phytol., Vol. 59, pp. 1-8, 1960.

[34] Winter, S. R. and A. J. Ohlrogge, "Leaf Angle, Leaf Area and Corn (Zea Mays L) Yield," Agron. J., Vol. 65, May-June 1973.

[35] Ulaby, F. T., R. K. Moore and A. K. Fung, Microwave Remote Sensing, Vol. I: Microwave Remote Sensing Fundamentals and Radiometry, Addison-Wesley/Benjamin-Cummings, Inc., Advanced Book Program, Reading, Massachusetts, Oct. 1981; Vols. II and III to be published in 1982.

APPENDIX A

LITERATURE REVIEW--LAD

LITERATURE REVIEW--LAD

The leaf angle distribution of corn (Zea Mays L) has been the subject of much attention. Previous applications, however, have dealt primarily with the effect of LAD on the photosynthetic process and crop yield, whereas the present research focuses on the effect of LAD on radar return. The methods of measuring LAD are various, and different crops generally require different methods of description. Corn has been measured mostly with a protractor-like device called a clinometer. Other methods are used and will be discussed as well.

Whigham and Wooley [32], Lemeur [17], and Winter and Ohlrogge [34], used the clinometer. They measured the LAD at the point where the leaf meets the stalk. Whigham and Wooley state that the mean leaf angle ranged between 59.2° and 79.7°, and noted that the leaves above the cob were more erect than those below it. These measurements were made at the time of corn silking. They concluded that the LAD is only one of many characteristics of the corn plant affecting crop yield.

Lemeur presents a model accounting for the penetration of light using LAD as one of its components. He does not describe the level of maturity of the crop at measurement but gives a September date, and compares his results to other distributions [18]; however, none states the plant growth stage. He also shows the azimuthal orientation of the corn plant as being perpendicular to the row (the present research observed a similar result). Blad and Baker [1], however, noticed no such tendency. Winter and Ohlrogge [34] again

used the clinometer but did not say how the angle was measured. They also do not state categorically the growth-stage at measurement but it is assumed to be the tassling stage. They did note, however, a mean orientation of 45°. To perform their experiment they physically changed the angles of the leaves above the ears (cob), and determined that the upright leaf orientation did not effectively increase crop yield.

Loomis and Williams [18] cited several works, none of which stated time-of-measurement. Therefore, all of the distributions differed. They state that "structural changes between juvenile and mature canopies are obvious for many species." This is true for corn, as this report shows.

Pepper, Pearce and Mock [19] appear to be the only researchers to have recognized the importance of the whole leaf; they developed the "leaf orientation value (LOV)" concept. This value is the ratio of the leaf-length to the flagging point (the point at which the leaf bends) to the total leaf-length multiplied by the angle. An average was then taken. Their results, for different corn types, show mean values of 73.8°, 63.7°, and 43.4°.

The use of point quadrants is also included in determining corn LAD (Wilson [33]). This method involves placing pointed sticks at a certain azimuth and elevation location and passing these sticks through the crop. The leaves that are stricken by the sticks are assumed to be at that orientation. This method is very time-consuming and accuracy is determined by the sharpness of the points on the sticks. Purdue updated this method [20] by using a laser directed at the crop. The laser, when collimated, has a very narrow beam, thereby increasing accuracy.

Smith et al. [22,23] used several methods in an attempt to provide (a) a less time-consuming method of predicting LAD, and (b) a more accurate measure. In 1977, they worked with orthogonal projections and the solutions of the Fredholm equation. Both methods involve photographic analysis. The orthogonal projection method manually fits straight-line segments to various leaf parts, using a grid marking the x-y coordinates. The angles are taken from these coordinates. The Fredholm integral equation relates gap frequency and look angle to LAD in a very complex manner. Smith et al. measured wheat with the two methods and were able to produce relatively close results (mean LADs of 68° and 66°, respectively). Their 1979 paper used optical diffraction analysis. The mean LAD was calculated to be 66°, however, their method of obtaining this mean, by convolving two orthogonal projections, was refuted by Lang [16] in 1980. Using the optical diffraction method, Kimes et al. [15] analyzed trees.

APPENDIX B

LITERATURE REVIEW--OPTICS

LITERATURE REVIEW--OPTICS

This report deals in part with the study of coherent optical techniques. Many papers have been written on this subject, dealing primarily with pattern recognition and data processing.

Goodman [12] provides the definitive work in his book on Fourier optics. Much of the present analysis was gleaned from his book, which covers all aspects of coherent optics from diffraction theory to holography. The chapters of main concern are Chapters 4, 5, and 7. Chapter 4 explains Fresnel and Fraunhofer diffraction and presents examples for different apertures. The Fraunhofer region was of primary importance in Chapter 4, as the distance from the image to the frequency plane is large enough in the optical system used to assume the Fraunhofer approximation. Chapter 5 covered lenses and their uses in obtaining a Fourier transform. The first section explains how the lens, using phase differences, bends the coherent beam. Mathematical descriptions for determining the Fourier transform with different image locations complete this valuable chapter. Of particular interest was the derivation of the case where the object (image) was placed in front of the lens. It was shown that this type of location eliminates the phase errors in the electric field at the transform plane. Consequently, it is this configuration that is used in the present experiment. Chapter 7 discusses filtering, which is not used in this experiment but is extremely important to researchers working in the pattern-recognition area. Photographic film-use was covered in this chapter and a very good explanation of the liquid gate is included.

Goodman's paper [13] covers transformations and filtering (linear and nonlinear). Nonlinear filtering is accomplished using grey tones to either (1) apply different angular orientations, in a grating, to different grey tones; or (2) develop binary images using pulse-width/area modulation to retain the grey tones. A filter in the transform plane can then be used to detect a particular grey tone for the output. Goodman states that this method is still under intensive research but may be valuable in communications by separating multiplicative noise from a signal.

Gaskill [11] wrote a three-part article that appeared in EOSD. Part 1 included basic lens theory and image formation. Part 2 reviewed basic Fourier theory and concluded with an account of Fourier transformation with a lens (similar to the information covered by Goodman).

Casasent [7] wrote a similar series for EOSD. He covers the basics of the Fourier transformation and its use in spatial filtering. He also introduces the theory of real-time image devices. These devices are placed in the image plane but have the ability to spatially modulate a coherent source in real time rather than having to wait for photographic development. Much still needs to be done in this area, and Hughes in California has recently developed a device that seems to work fairly well. His third article refers to specific applications. In it he mentions the use of the 32-wedge, 32-ring detector used in this research. Pattern recognition is discussed, as is the optical generation of ambiguity functions.

Vanderlugt [31] wrote about coherent optical processing. In his article he covered the basic transform relationships as well as

spatial filtering. Some good examples of spatial filtering were shown including word recognition and cloud mapping. He concludes by briefly discussing real-time filters.

Casasent [4] wrote an article on coherent optical pattern recognition, which covers the same basic material covered by Vanderlugt [31]. He expands the concept somewhat, however, through the use of a "hybrid optical/digital correlator," which uses a microprocessor to control data flow.

Hecht and Zajac [14] wrote a book on optics. Chapters of particular interest were on geometrical optics/paraxial theory (Chapter 5), diffraction (Chapter 10), Fourier optics (Chapter 11), and Chapter 14, which covers miscellaneous topics.

APPENDIX C

LITERATURE REVIEW--RADAR AND VEGETATION

LITERATURE REVIEW--RADAR AND VEGETATION

Radar response to crops has been an area of major research interest at the University of Kansas, and it is from this research that the need for an accurate method of determining the LAD of corn evolved.

Ulaby, along with Bush, Dobson, and Bradley [3,25-30] have studied this radar response over the past 10 years. In 1975, Ulaby [25] reported on work accomplished using a 4 - 8-GHz radar in 1972, on four crop-types: corn, milo, soybeans, and alfalfa. In this report, six variables, responsible for measured backscatter response, are mentioned: (1) plant moisture, (2) soil moisture, (3) crop type, (4) frequency, (5) incidence angle, and (6) polarization. He then presented his results as a function of these parameters. The results showed that a frequency greater than 7 GHz was desirable to distinguish corn. He also proposed a dual-frequency system with VV and cross-polarizations to accurately describe crops.

Two papers appeared in 1976, in which Ulaby and Bush [28,29] describe the use of the 8 - 18 GHz system to monitor wheat- and corn-growth. Graphs were again used, relating σ° to various parameters. In the paper on corn-monitoring, they mention that "one plant characteristic of particular importance in the study of radar backscatter from vegetation is the macro- and micro-geometry and structure of plant leaves, which are influenced by plant vigor and, in turn, influence σ°."

In 1980, Ulaby [26] developed a clutter model relating σ° to look angle and frequency. Other papers have been written by

Remote Sensing Laboratory personnel, however, these will not be discussed here as they may be easily obtained (see reference section, pp.58-60).

APPENDIX D

PROCEDURE FOR DATA ACQUISITION AND TI-58C PROGRAMS

Procedure for Taking Data:

1) Turn on laser and RSI, wait 1 hour.

2) Place film into liquid gate, dull side facing the laser, and straighten.

3) With lights off maximize ring #1 by adjusting horizonal and vertical motion screws on the 32-wedge, 32-ring holder. (Display on x 10 scale).

4) Deselect ring #1 and select wedge #1, select x 1000 scale and note value.

5) Deselect wedge #1, select #2 and note value, continue this until all 32 wedge intensities have been noted.

6) Flip down the laser's shutter and take wedge intensities again. This gives you ambient values that are subtracted from the intensities obtained in 4 and 5 above.

7) Repeat steps 2 through 6 as necessary.

Programs for Data - TI-58C

These programs will calculate:

1) RVAL = VAL - AMB (real value = value - ambient value)

2) Total wedge power = ΣRVAL

3) NVAL (normalized value)

4) CUMVAL (cumulative NVAL)

Initialize:

1) put 33 in registers 00 and 01

2) make t = 1

3) put 0 in registers 39 and 38

Words:

Enter value (VAL) on keyboard, press "B" and continue until all 32 entries have been made, check register 00 for 1 value.

Program:

LBL B	address
STO IND 00	stores VAL in address register indicated by register 00
OP 30	decreases register 00 by 1
R/S	stops until "B" is depressed for next value

Words:

Enter ambient value (AMB) and press "C" copy down RVAL, continue until all 32 values have been entered. Check register 01 for 1 and check register 39 and note ΣRVAL.

Program:

LBL C	address
+/- + RCL IND 01 =	subtracts AMB value from VAL
STO IND 01	stores result, NVAL, in register indicated by register 01
SUM 39	sums each NVAL at end holds ΣRVAL
OP 31 R/S	decreases register 01 by 1

Words:

Press "D" read NVAL.
Press "R/S" read CUMVAL and continue until finished.

Program:

```
LBL
D          address

RCL
00
x = t 100  check to see if register 00 is at 1, if it is, it
           goes to address location 100

RCL
IND
00
÷          divides RVAL by ΣRVAL to get NVAL
RCL
39
=

SUM
38         produces CUMVAL

R/S        waiting to press "R/S" read NVAL and note

RCL
38
OP         recalls CUMVAL and increases register 00 by 1
20

R/S        waiting to press "D"

100

OP
20
GTO        increases register 00 by 1 and goes back to "D" address
D
```

This completes the procedure for entering the data. The resulting NVAL and CUMVAL can be graphed after averaging with results from two other plants.

APPENDIX E

RSI CALIBRATION

RSI CALIBRATION

1. Select ring 30. Place microvoltmeter leads between test points 1 and 2 (ground). These test points are located on the back of the device. Vary balance pot #1 to get 15μv ± 5μv on the meter. (Any x scale).

2. Deselect 30 and set balance pot #2 to zero on the x1000 scale.

3. Keep gain pot turned fully clockwise.

APPENDIX F

PROCEDURE FOR OBTAINING LASER READY CORN PHOTOS

PROCEDURE FOR OBTAINING LASER-READY CORN PHOTOS

The 35-mm negative is contact-printed onto Kodalith film using a process camera with a setting of F-22 for approximately 12 seconds. Normally, no filters are needed. This step produces a Kodalith "positive" and eliminates much extraneous detail and background data.

If it is a poor negative, the background can be masked with opaquing pens or dark tape before the contact prints are made.

Developing is done in Kodalith developer for approximately two minutes. If unwanted detail or shadows are still apparent at this point, they may be removed by using Kodagraph eradicator. Over-light areas may be filled in with drawing ink. Extra-fine details may be retained by overlaying two matching positives to create a positive of the necessary density for reproduction into a clear negative.

An alternate method of preserving detail on poor negatives, or for enhancing contrast when needed, is to repeat the entire process once more, producing a total of three negatives and two positives of each photo. These extra steps will allow greater control of detailing and density.

It is very important to maintain correct cornstalk position on the 4" x 5" negative. The easiest way to position the positive correctly is to place a piece of glass on a 4" x 5" area of graph paper, center the positive, then tape it to the glass with transparent tape. A strip of masking tape on the glass can be used to position the 4" x 5" film over the positive.

APPENDIX G

GROWTH STAGES OF C6 and C10 AND RAIN DATES

Growth Stage: The following table shows growth stage development of C6 and C10 (see Appendix H).

	6/09	6/19	7/01	7/08	8/04	8/05	9/01
C6	24	24	33	-	43	-	51
C10	23	24	-	33	-	43	51

Weather: Rain dates are as follows: 5/18, 6/02/ 6/03, 6/11, 6/18, 6/25, 7/07, 7/08, 7/22, 7/27, 8/04, and 8/05, 1981.

APPENDIX H

CORN GROWTH STAGES

3.4.3.2 Corn Growth Stages

CODE	STAGE
	PLANT EMERGENCE
10	Undetermined; plant emergence substage not detectable.
11	Plant emergence; tip of coleoptile visible above soil surface.
12	One or two leaves fully emerged from coleoptile.
	VEGETATIVE GROWTH
20	Undetermined; vegetative substage not detectable.
21	Three-four leaves emerged.
22	Five-eight leaves fully emerged.
23	Nine-twelve leaves fully emerged.
24	Thirteen-sixteen leaves fully emerged; lower four-five leaves perhaps lost leaving eight-nine functional leaves; tassel developed but still enclosed within whorl; brace roots from lower nodes are now developing.
25	Seventeen-twenty leaves fully emerged.
26	More than twenty leaves fully emerged.
	HEADING AND FLOWERING
30	Undetermined; heading and flowering substage not detectable.
31	Tips of tassels visible from whorl of leaves.
32	Tassels fully emerging; all leaves fully emerged; some silks starting to emerge from tip of husks.
33	Silks nearly fully emerged; pollen shedding.
	RIPENING AND SEED DEVELOPMENT
40	Undetermined; ripening and seed development substage not detectable.
41	Kernels in blister stage; cob, husks, and ear shank approaching full size; about twelve days after silking.
42	Soft dough or just past "roasting ear" stage; about twenty-four days after silking.
43	Beginning dent stage; a few kernels showing dents about thirty-six days after silking.
44	Full dent stage; all kernels fully dented but not dry; husks on ear and leaves starting to senesce.
	MATURITY
50	Undetermined; maturity substage not detectable.
51	Physiological maturity; about sixty days after silking; black layer formed at base of most kernels; some of remaining leaves still green.
52	Physiological maturity; black layer formed; leaves dried up and bright yellow.
53	Post maturity; crop still standing with leaves, stalks, and ear husks turning dark color.
	HARVEST
60	Undetermined; harvest substage not detectable.
61	Crop harvested green before full maturity for use as silage.
62	Crop harvested for grain with corn picker; ear only removed and plants still partially standing.
63	Crop harvested for grain with combine; plants reduced to stubble and residue.
64	Ear and entire plant removed; very little residue on soil surface.

APPENDIX I

C6 DATA

C-2

DATE		50° LAD	50° RDR (VV)	50° RDR (VH)	PLANT MOISTURE	SOIL MOISTURE
5/22	142	.0266	-8.08 db	-16.33 db	86.48%	21.51%
6/5	156	.0288	-5.15 db	-12.40 db	89.82%	18.82%
6/12	163	.0260	-5.78 db	-11.73 db	91.48%	23.79%
6/19	170	.0298	-6.07 db	-12.82 db	90.58%	21.21%
6/26	177	.0276	-5.53 db	-11.28 db	88.90%	22.26%
7/10	191	.0262	-6.05 db	-13.32 db	82.67%	13.26%
7/16	197	.0206	-9.1 db	-15.75 db	80.04%	7.23%
7/23	204	.0272	-7.88 db		79.06%	13.62%
7/30	211	.0218	-7.42 db	-14.57 db	78.76%	20.76%
8/6	218	.0315	-7.1 db	-13.35 db	71.13%	27.05%
8/11	223	.0202	-8.32 db	-14.27 db	68.16%	20.74%
9/3	246	.0225	-5.08 db	-13.76 db	40.06%	22.74%

APPENDIX J

C6, NVAL VS. ANGLE, AS A FUNCTION OF MATURITY

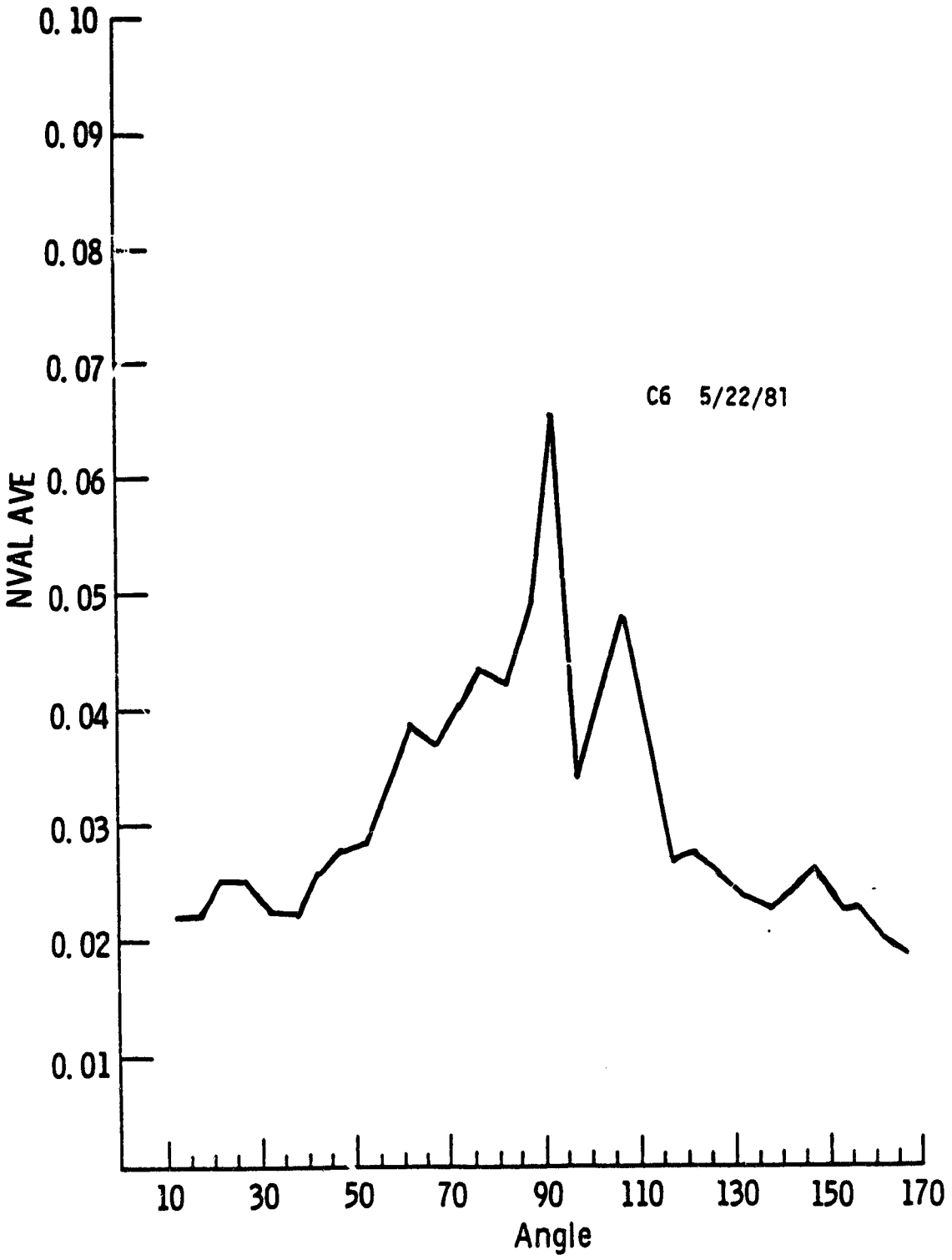
0.10
0.09
0.08
0.07
0.06
0.05
0.04
0.03
0.02
0.01
NVAL AVE
C6 5/22/81
10
30
50
70
90
110
130
150
170
Angle

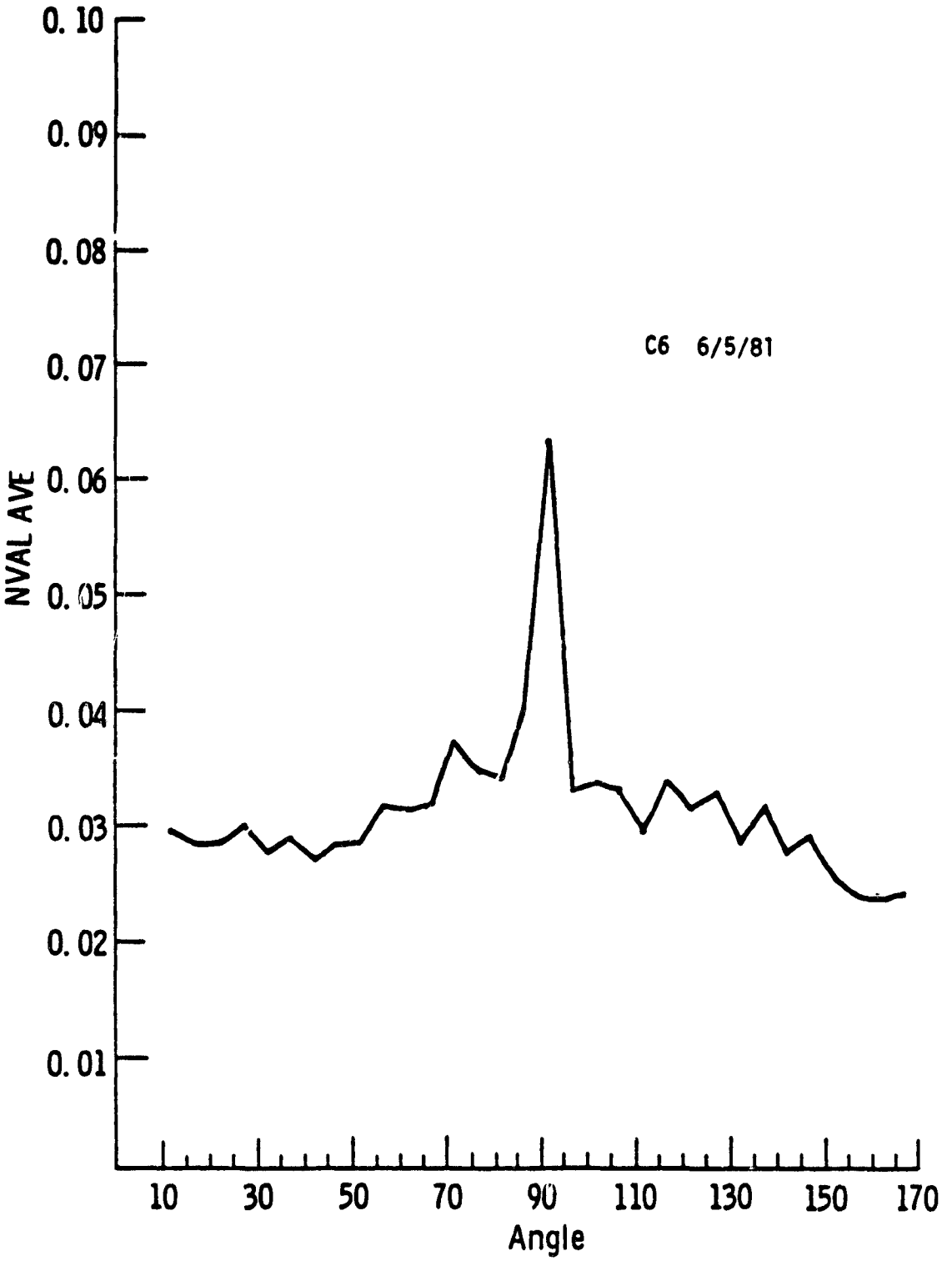
C6 6/5/81
NVAL AVE
0. 10
0. 09
0. 08
0. 07
0. 06
0. 05
0. 04
0. 03
0. 02
0. 01
10
30
50
70
90
110
130
150
170
Angle

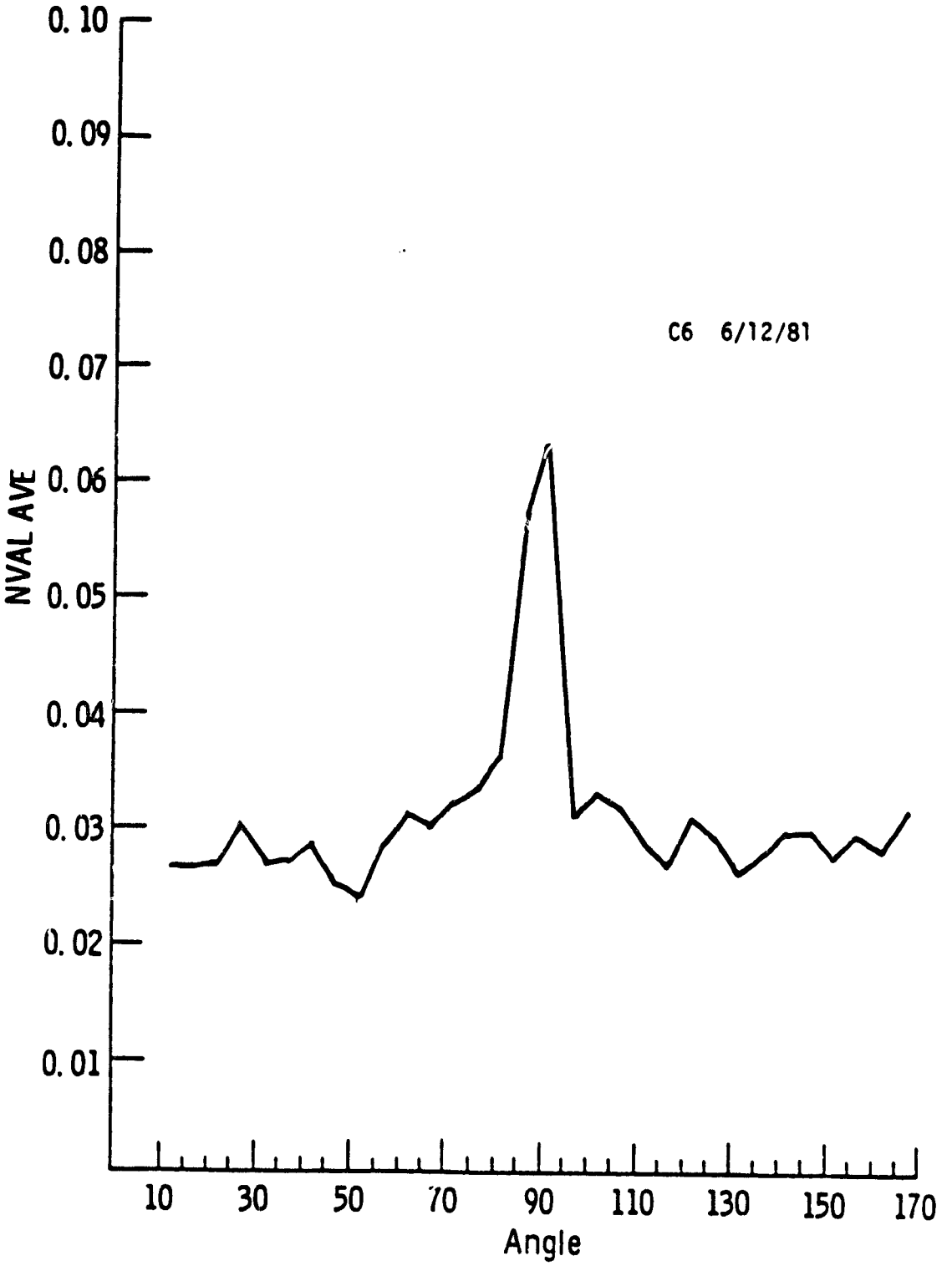
0. 10
0. 09
0. 08
0. 07
0. 06
0. 05
0. 04
0. 03
0. 02
0. 01
NVAL AVE
C6 6/12/81
10
30
50
70
90
110
130
150
170
Angle

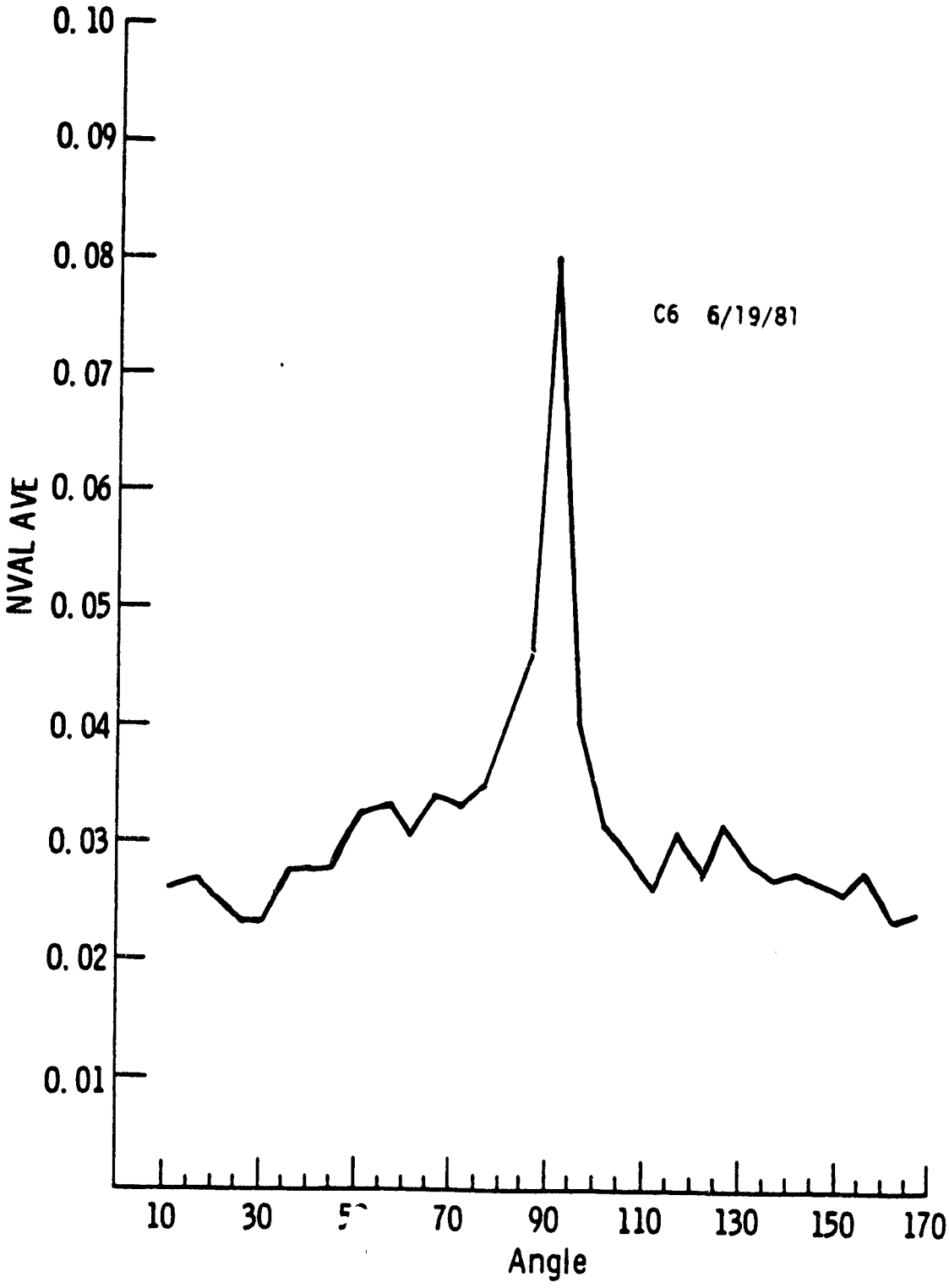
0. 10
0. 09
0. 08
0. 07
0. 06
0. 05
0. 04
0. 03
0. 02
0. 01
NVAL AVE
C6 6/19/81
10
30
70
90
110
130
150
170
Angle

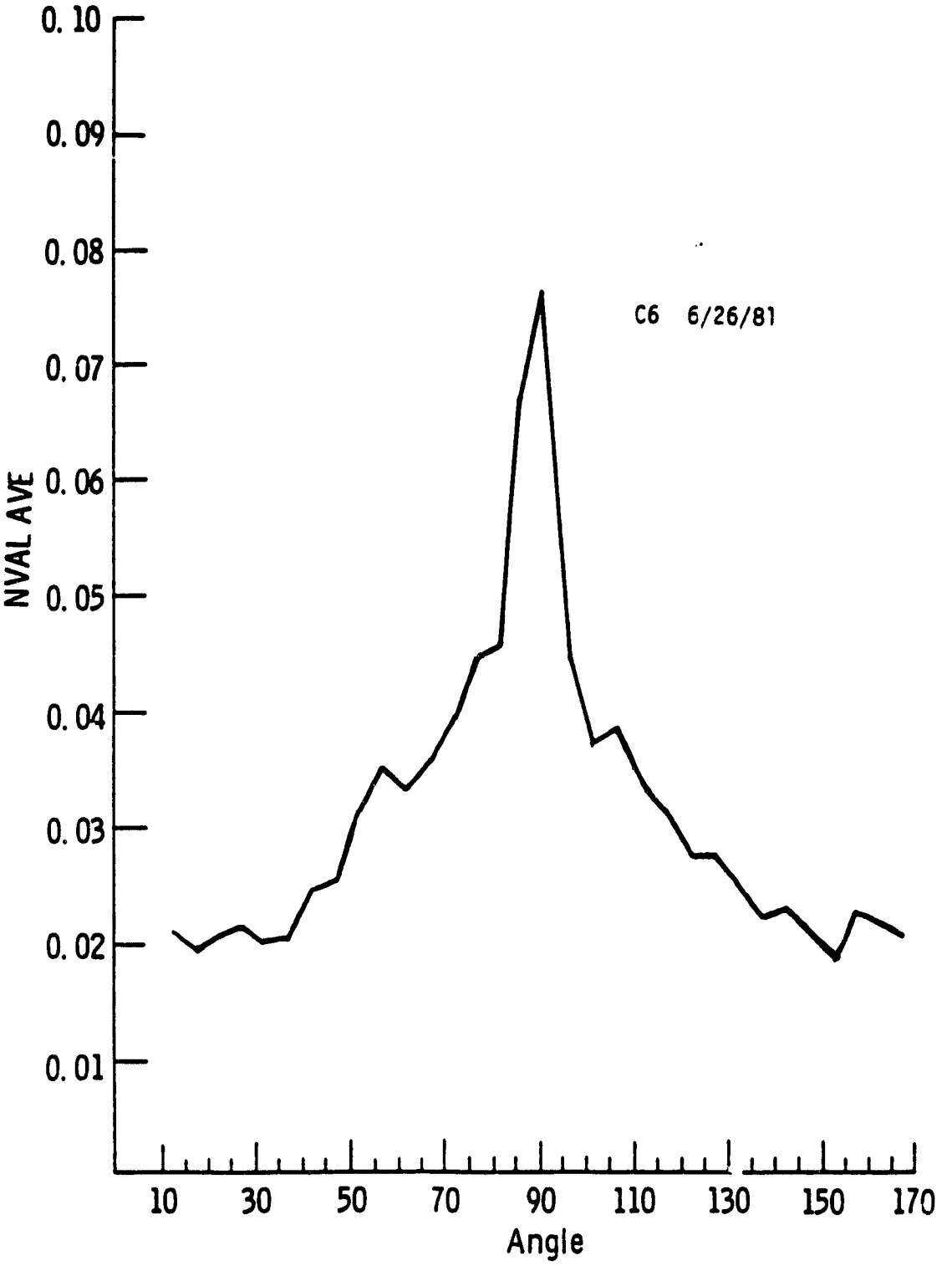
0.10
0.09
0.08
0.07
0.06
0.05
0.04
0.03
0.02
0.01
NVAL AVE
C6 6/26/81
10
30
50
70
90
110
130
150
170
Angle

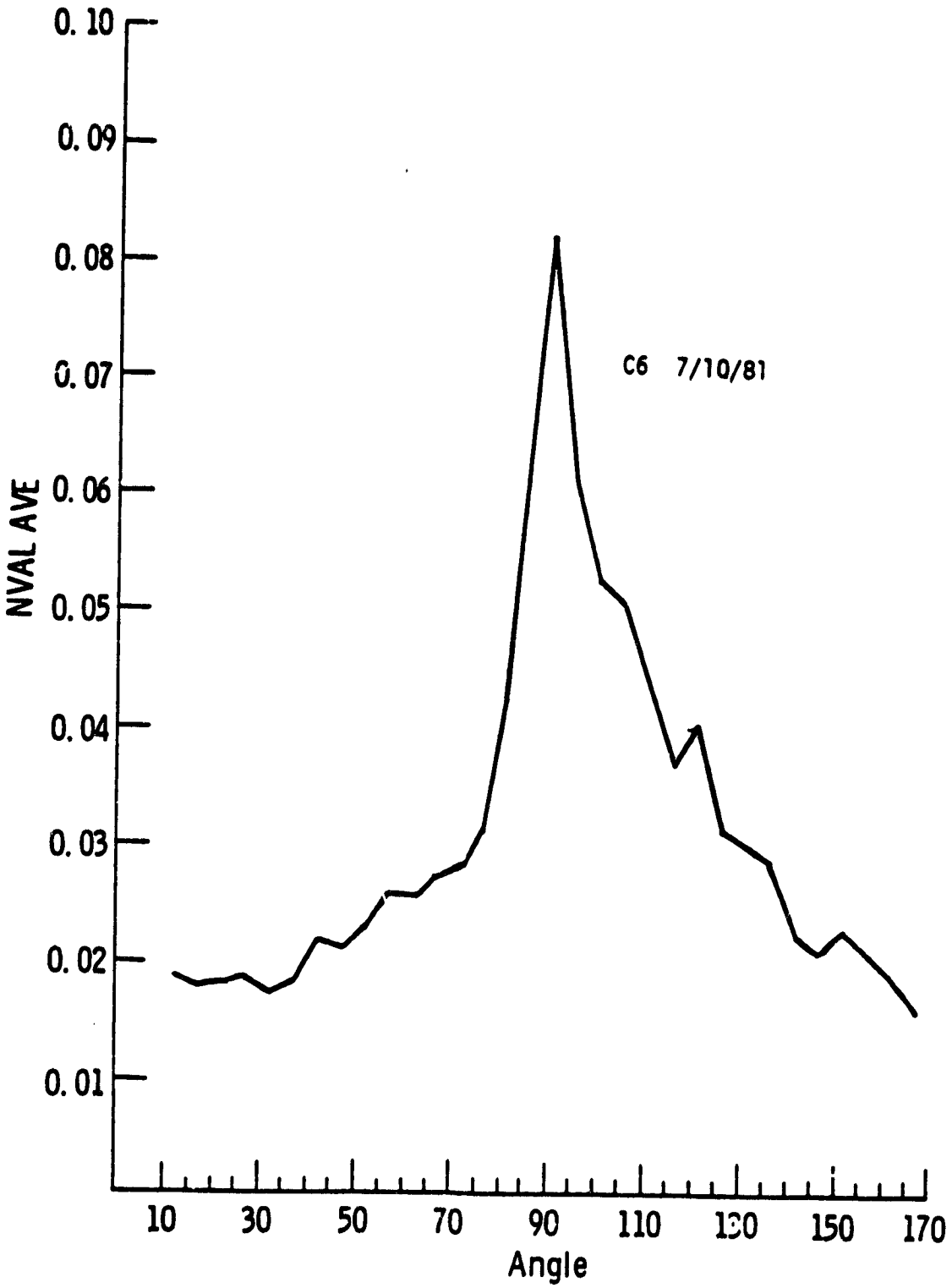
0.10
0.09
0.08
0.07
0.06
0.05
0.04
0.03
0.02
0.01
NVAL AVE
C6 7/10/81
10
30
50
70
90
110
130
150
170
Angle

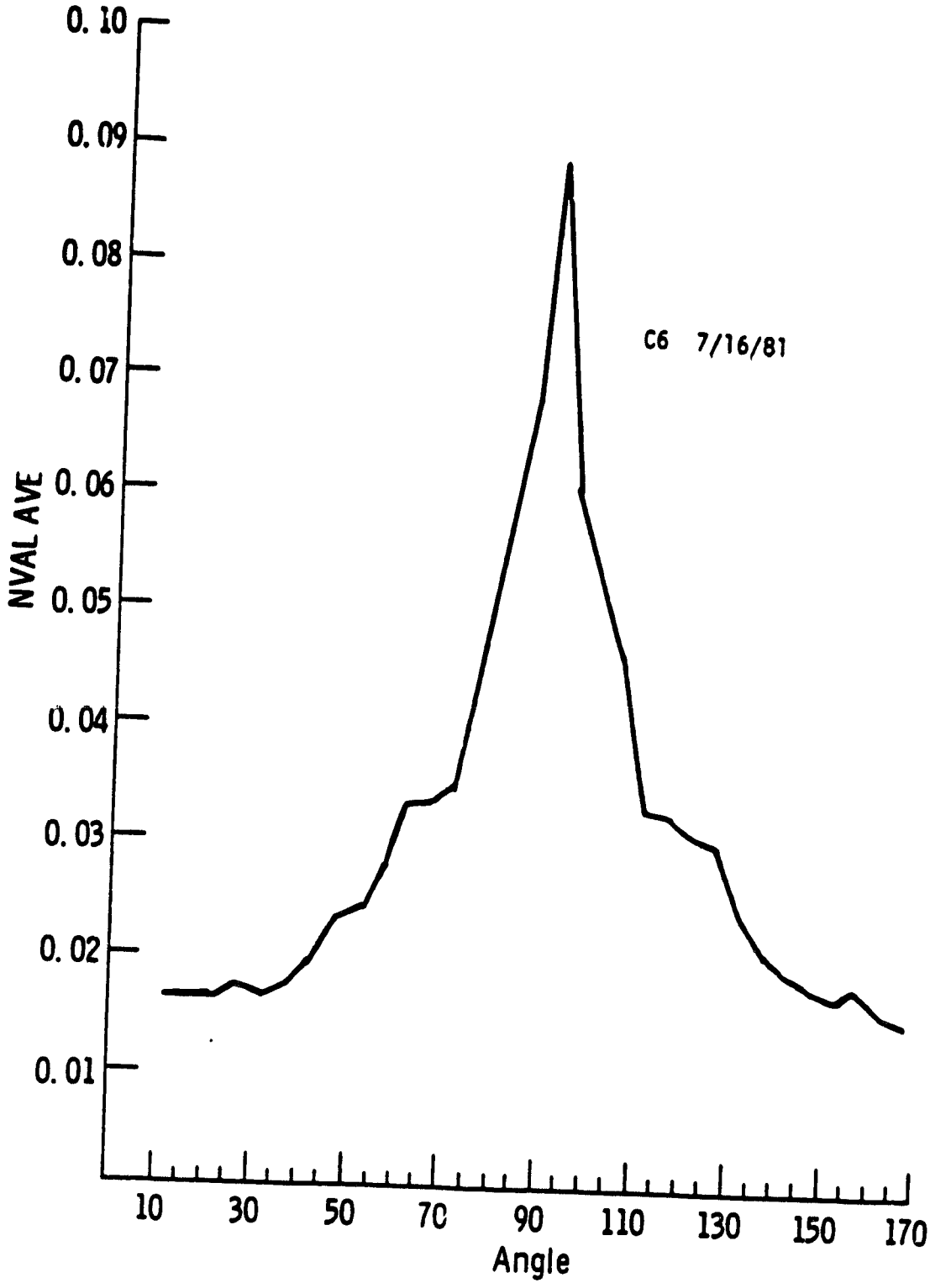
0. 10
0. 09
0. 08
0. 07
0. 06
0. 05
0. 04
0. 03
0. 02
0. 01
NVAL AVE
C6 7/16/81
10
30
50
70
90
110
130
150
170
Angle

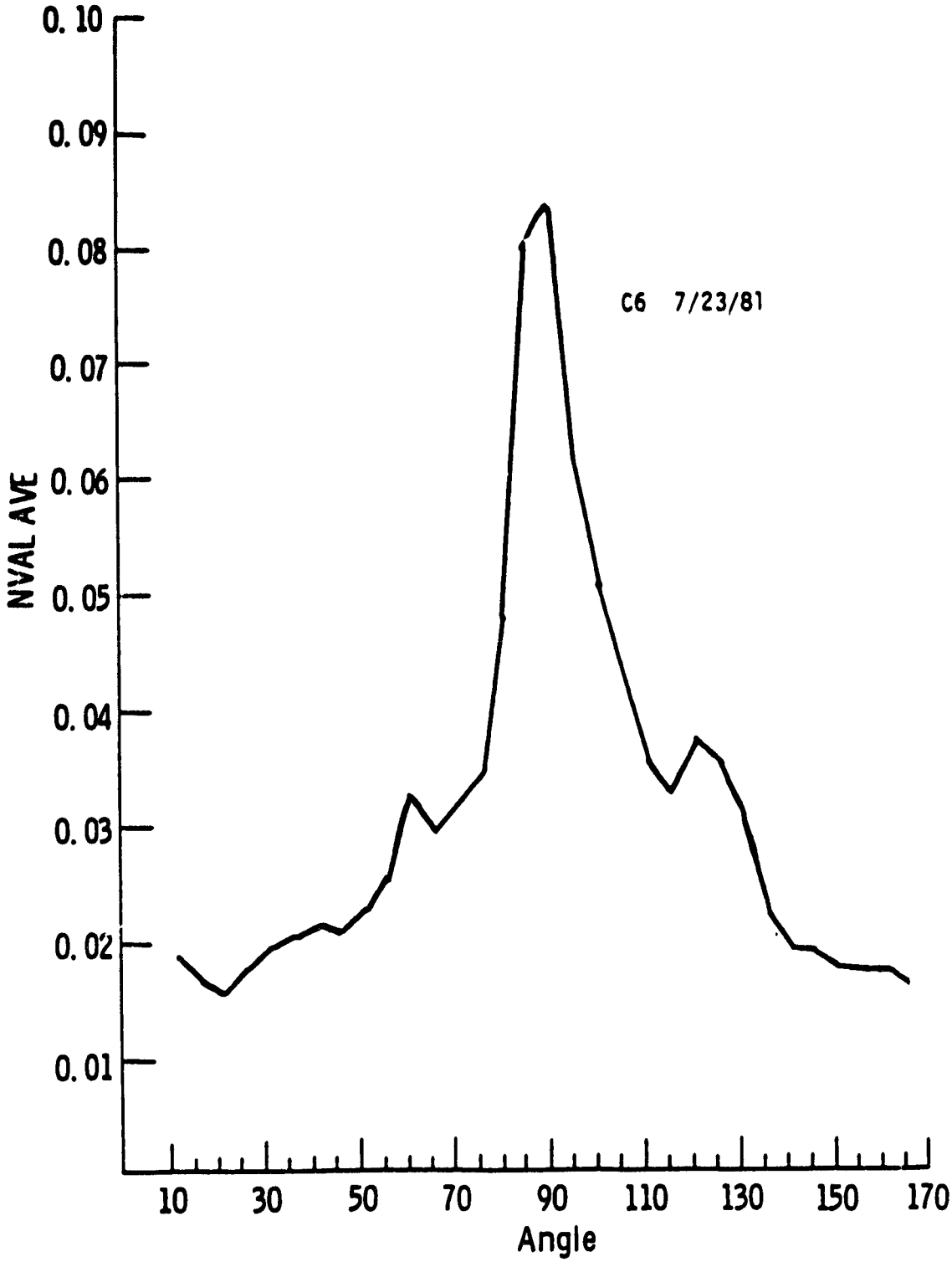
0. 10
0. 09
0. 08
0. 07
0. 06
0. 05
0. 04
0. 03
0. 02
0. 01
NVAL AVE
C6 7/23/81
10
30
50
70
90
110
130
150
170
Angle

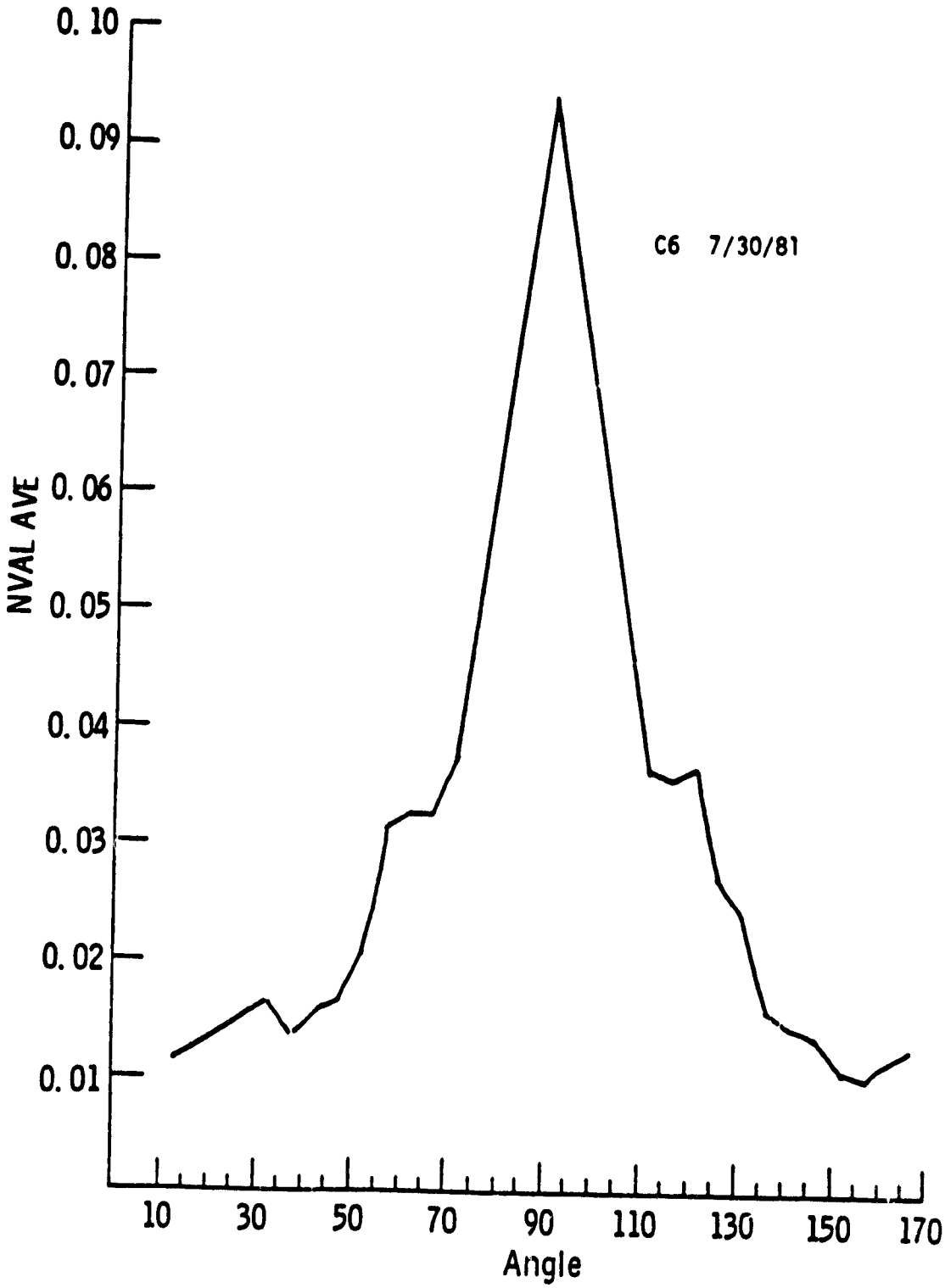
0. 10
0. 09
0. 08
0. 07
0. 06
0. 05
0. 04
0. 03
0. 02
0. 01
NVAL AVE
C6 7/30/81
10
30
50
70
90
110
130
150
170
Angle

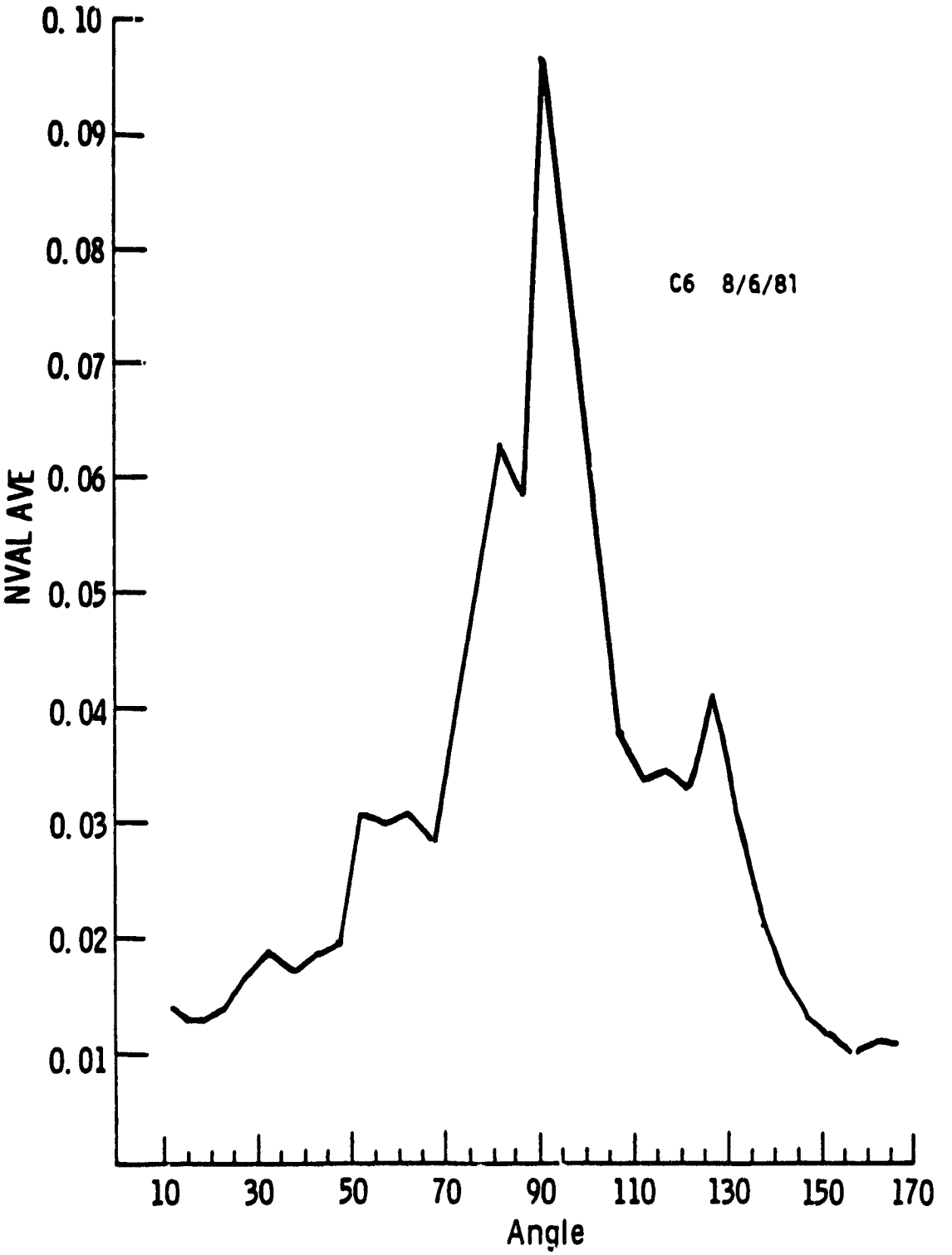
0. 10
0. 09
0. 08
0. 07
0. 06
0. 05
0. 04
0. 03
0. 02
0. 01
NVAL AVE
C6 8/6/81
10
30
50
70
90
110
130
150
170
Angle

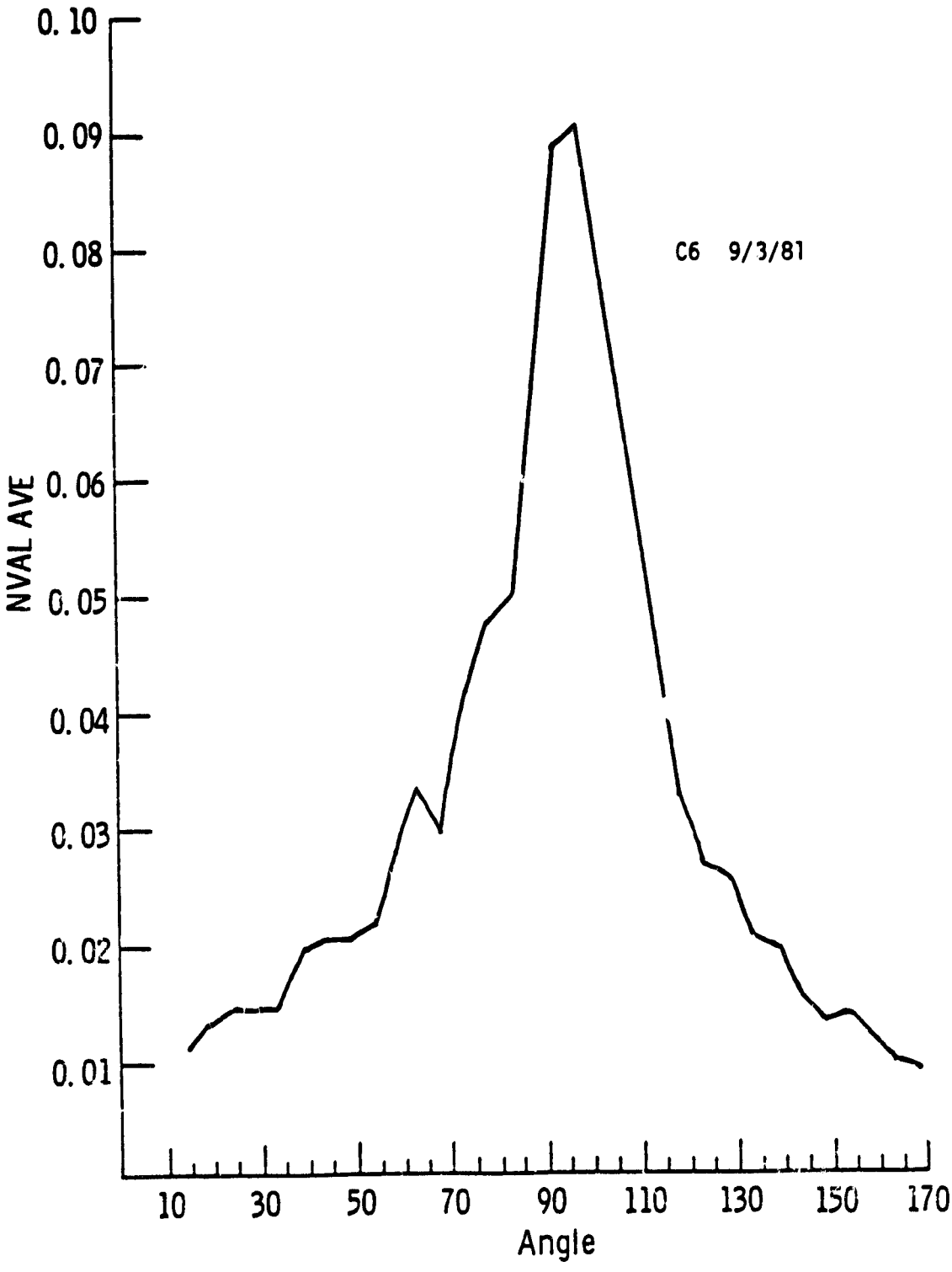
0. 10
0. 09
0. 08
0. 07
0. 06
0. 05
0. 04
0. 03
0. 02
0. 01
NVAL AVE
C6 9/3/81
10
30
50
70
90
110
130
150
170
Angle

APPENDIX K

C6, CUMVAL VS. ANGLE, AS A FUNCTION OF MATURITY

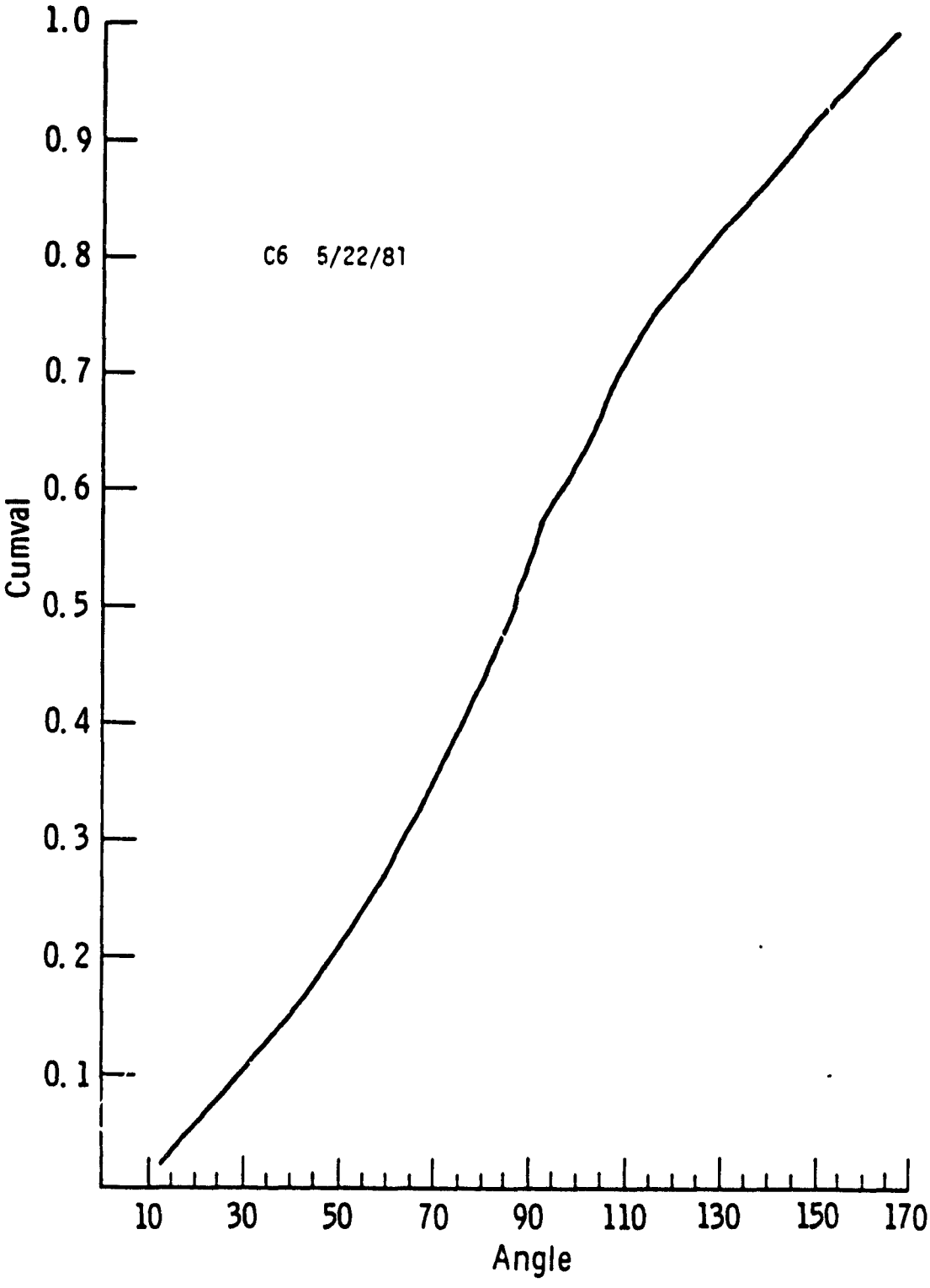
1.0
0.9
0.8
0.7
0.6
0.5
0.4
0.3
0.2
0.1
Cumval
C6 5/22/81
10
30
50
70
90
110
130
150
170
Angle

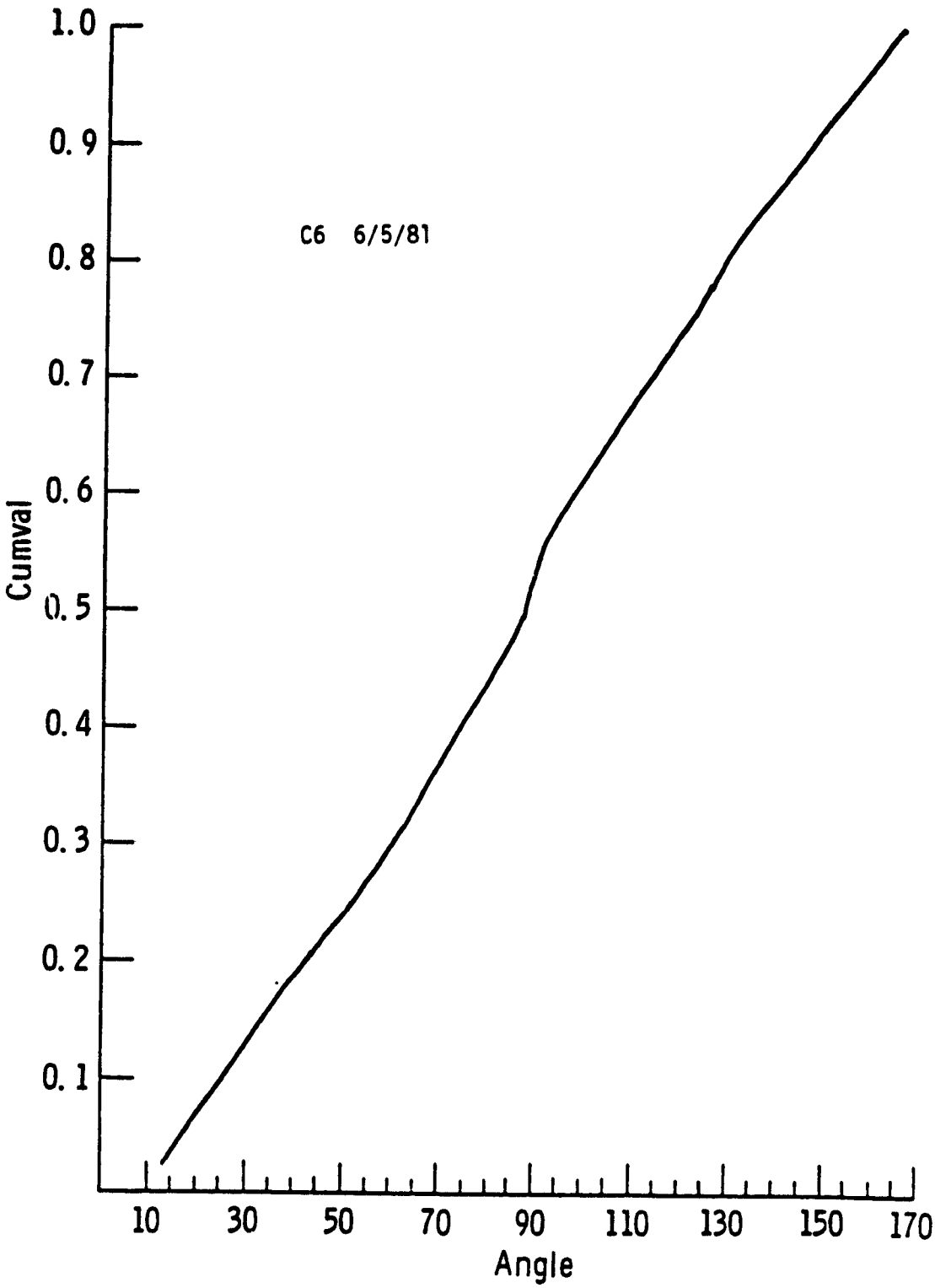
1.0
0.9
0.8
0.7
0.6
0.5
0.4
0.3
0.2
0.1
Cumval
C6 6/5/81
10
30
50
70
90
110
130
150
170
Angle

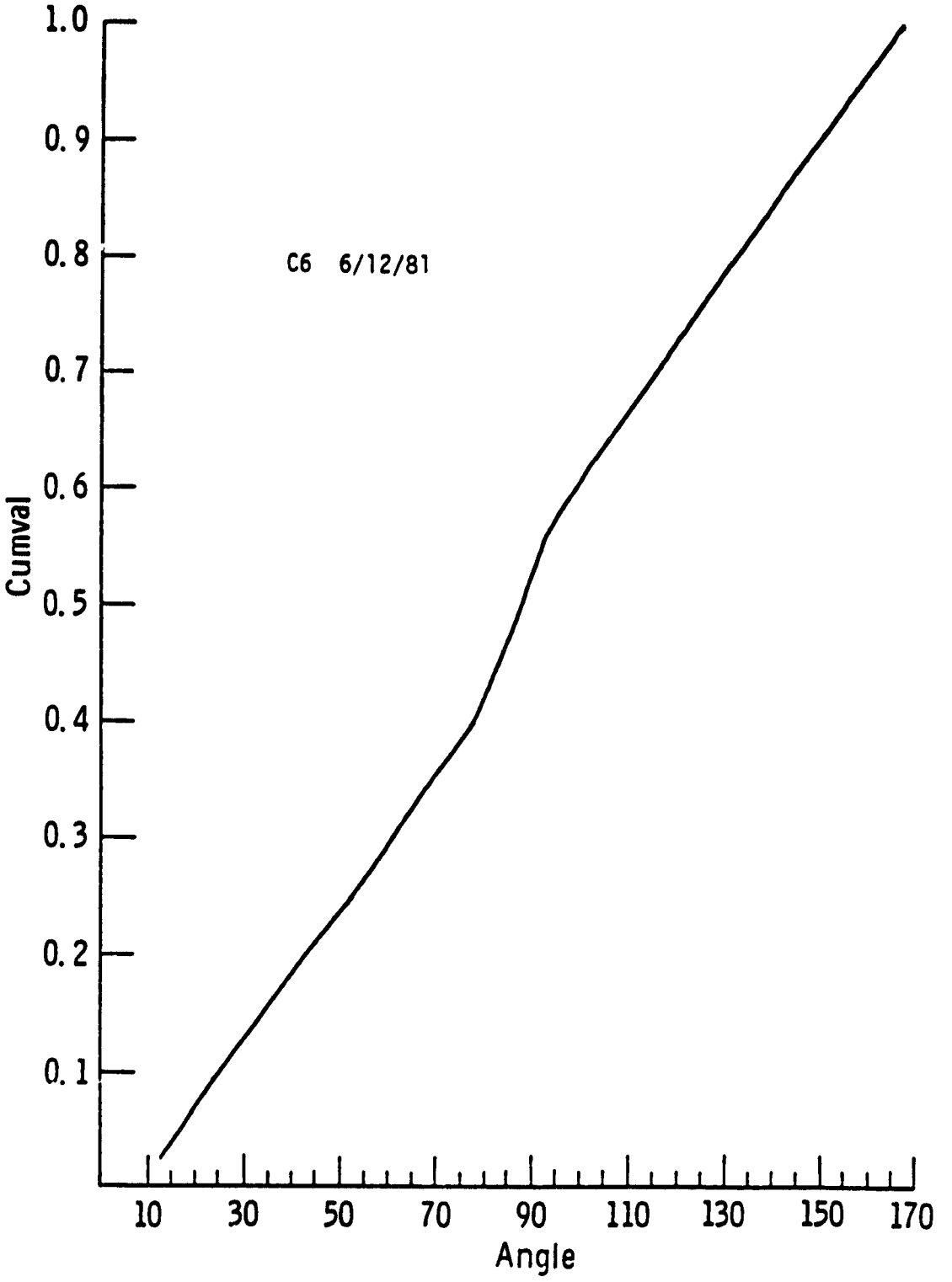
1.0
0.9
0.8
0.7
0.6
0.5
0.4
0.3
0.2
0.1
Cumval
C6 6/12/81
10
30
50
70
90
110
130
150
170
Angle

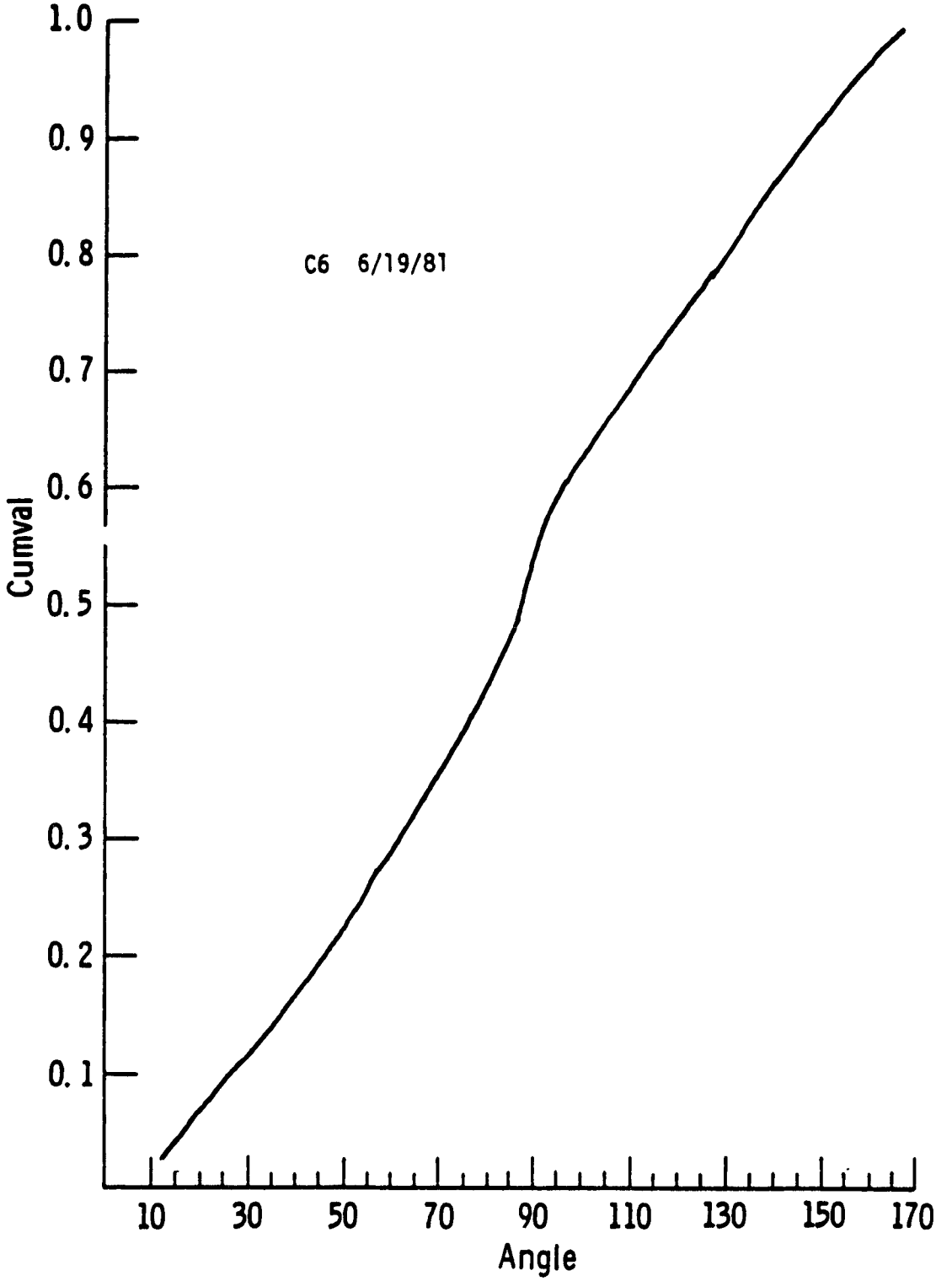
1.0
0.9
0.8
0.7
0.6
0.5
0.4
0.3
0.2
0.1
Cumval
C6 6/19/81
10
30
50
70
90
110
130
150
170
Angle

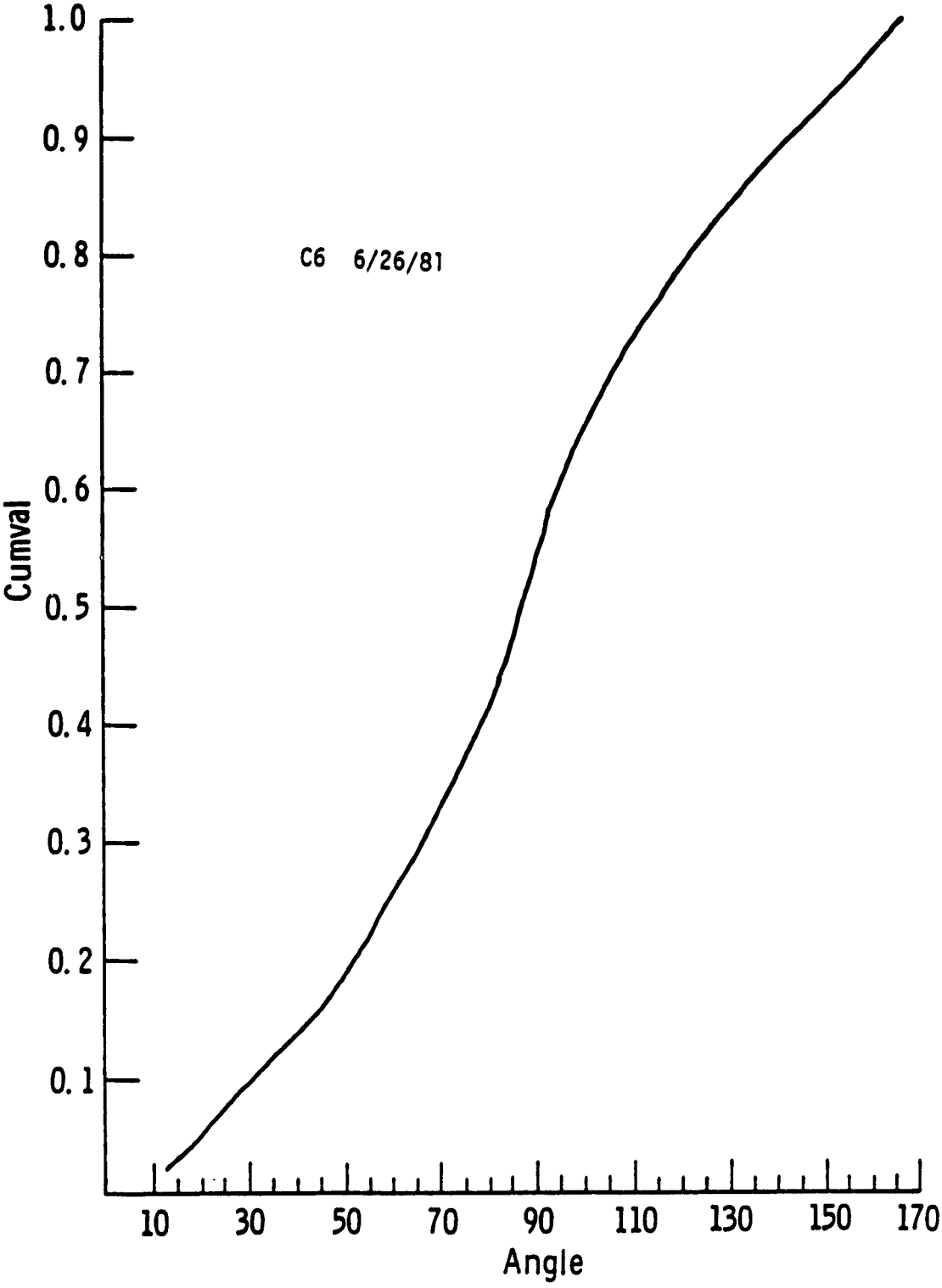
1.0
0.9
0.8
0.7
0.6
0.5
0.4
0.3
0.2
0.1
Cumval
C6 6/26/81
10
30
50
70
90
110
130
150
170
Angle

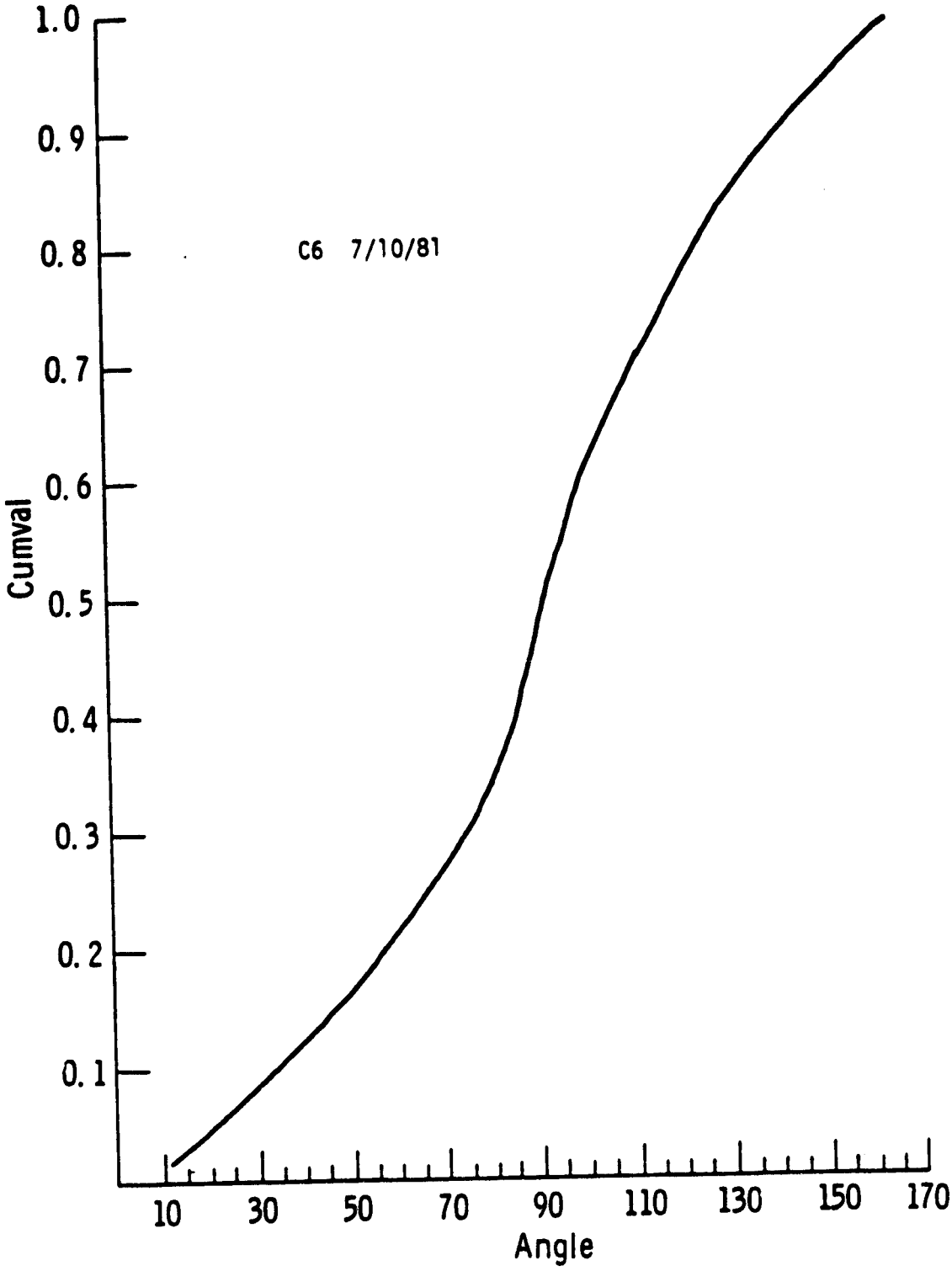
1.0
0.9
0.8
0.7
0.6
0.5
0.4
0.3
0.2
0.1
Cumval
C6 7/10/81
10
30
50
70
90
110
130
150
170
Angle

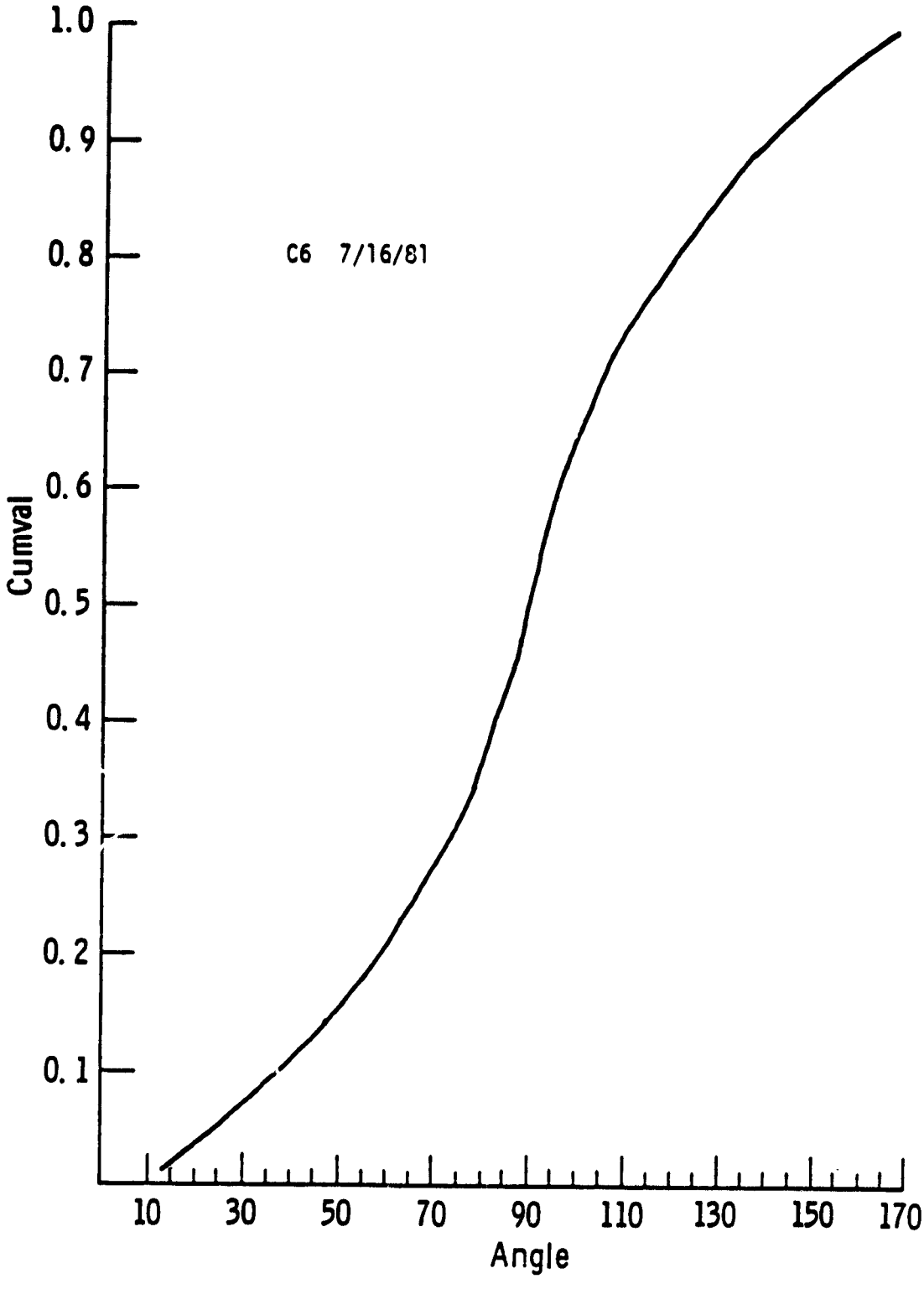
C6 7/16/81
Cumval
1.0
0.9
0.8
0.7
0.6
0.5
0.4
0.3
0.2
0.1
10
30
50
70
90
110
130
150
170
Angle

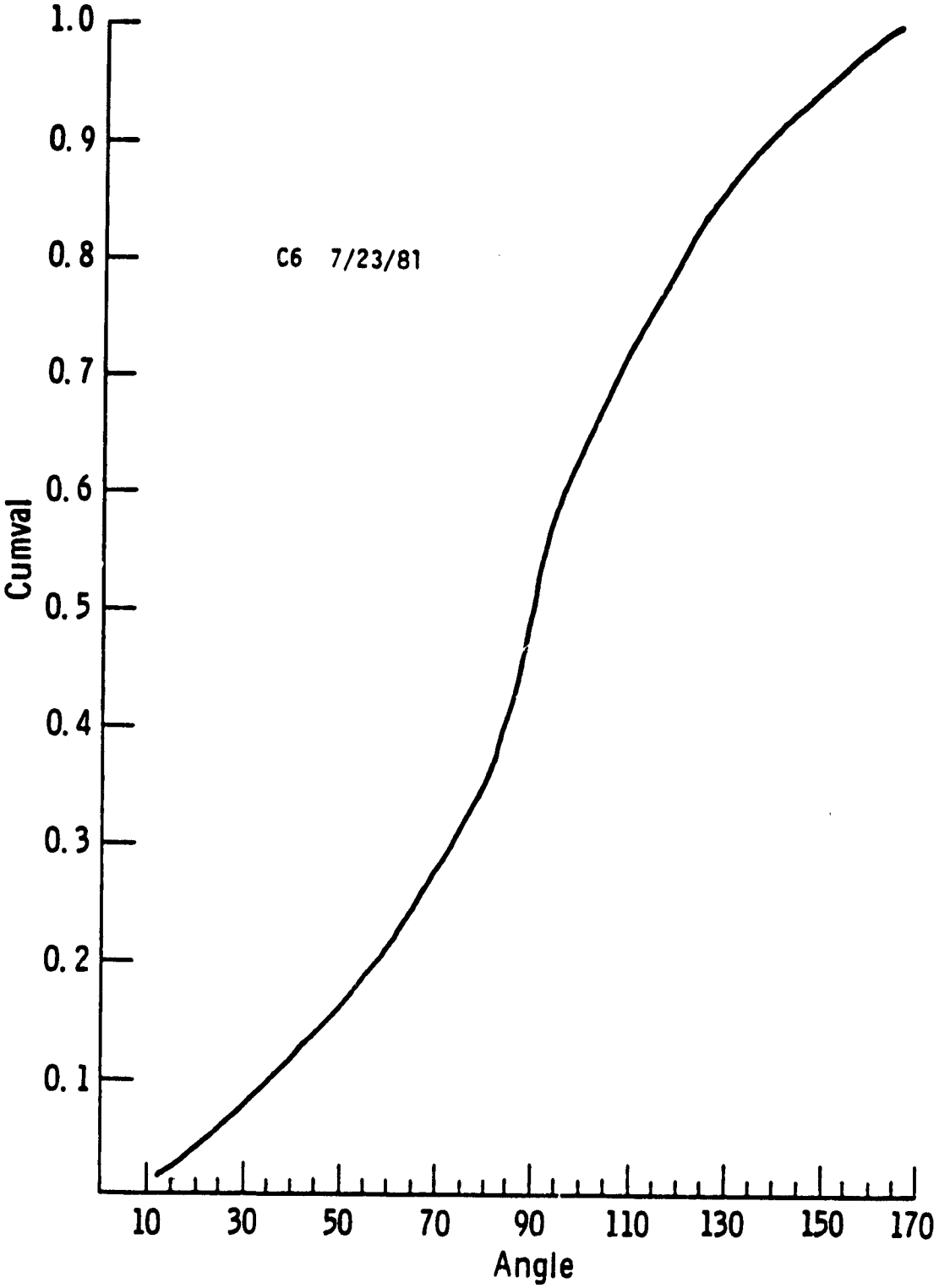
1.0
0.9
0.8
0.7
0.6
0.5
0.4
0.3
0.2
0.1
Cumval
C6 7/23/81
10
30
50
70
90
110
130
150
170
Angle

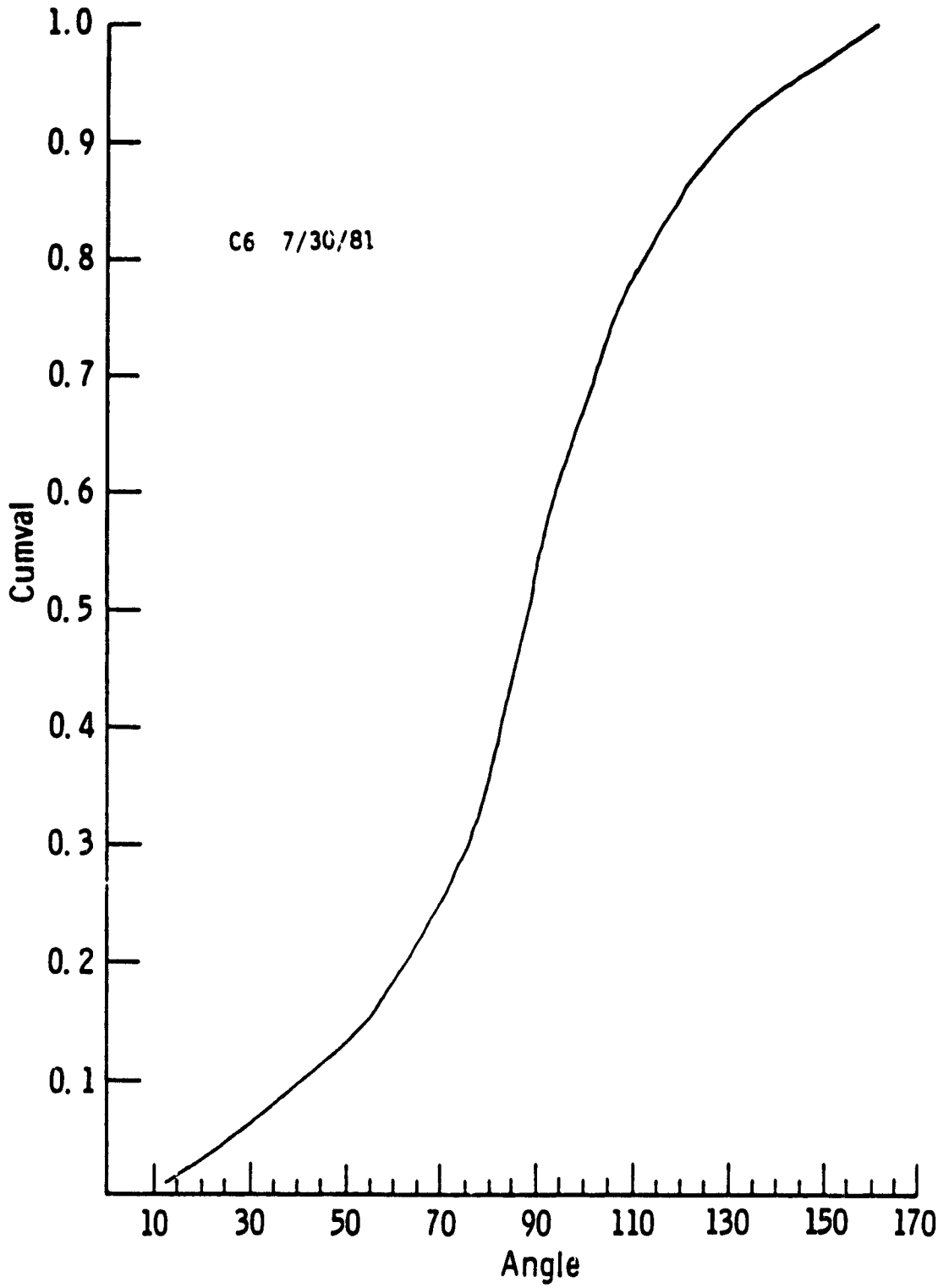
1.0
0.9
0.8
0.7
0.6
0.5
0.4
0.3
0.2
0.1
Cumval
C6 7/30/81
10
30
50
70
90
110
130
150
170
Angle

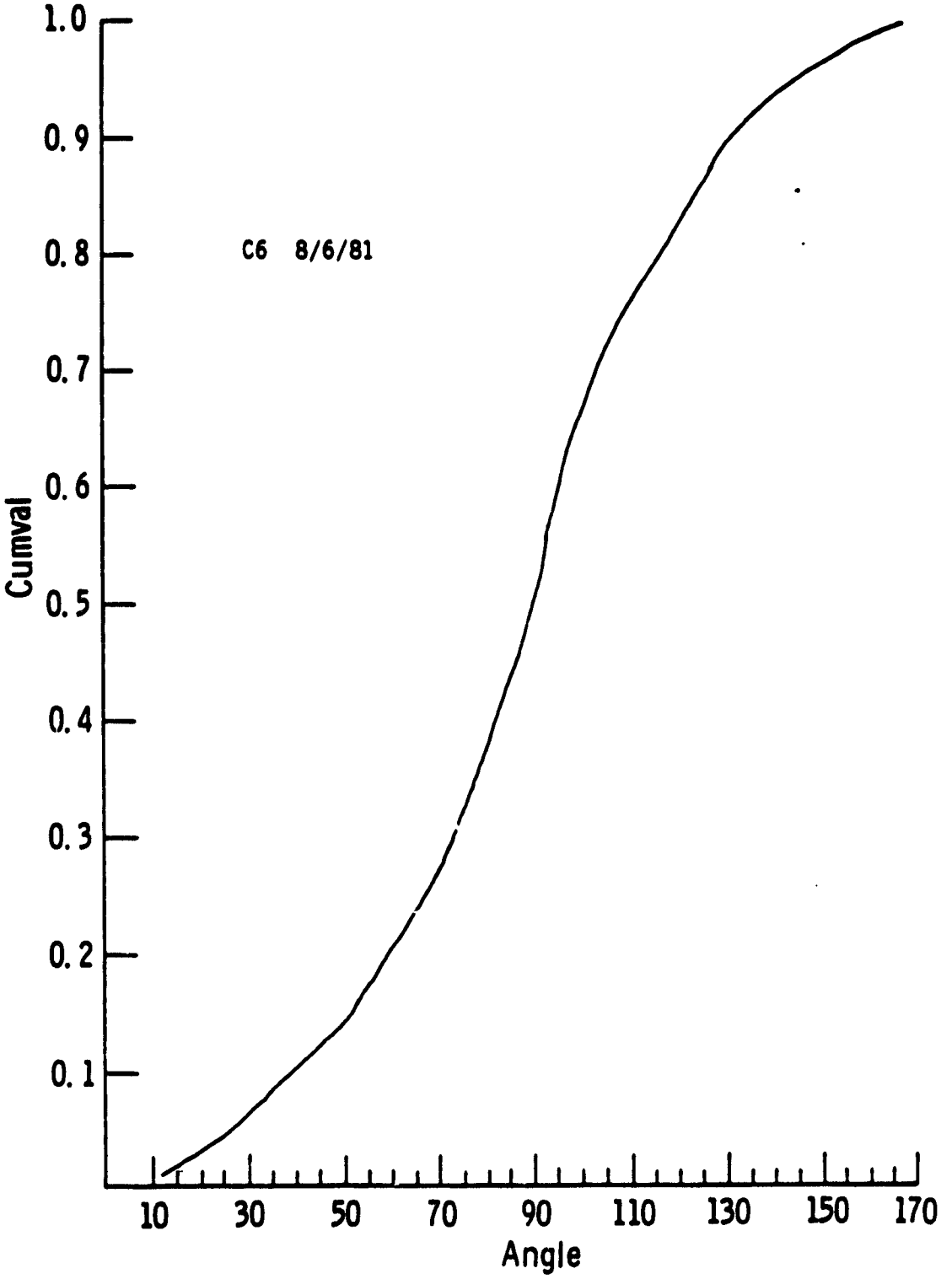
1.0
0.9
0.8
0.7
0.6
0.5
0.4
0.3
0.2
0.1
Cumval
C6 8/6/81
10
30
50
70
90
110
130
150
170
Angle

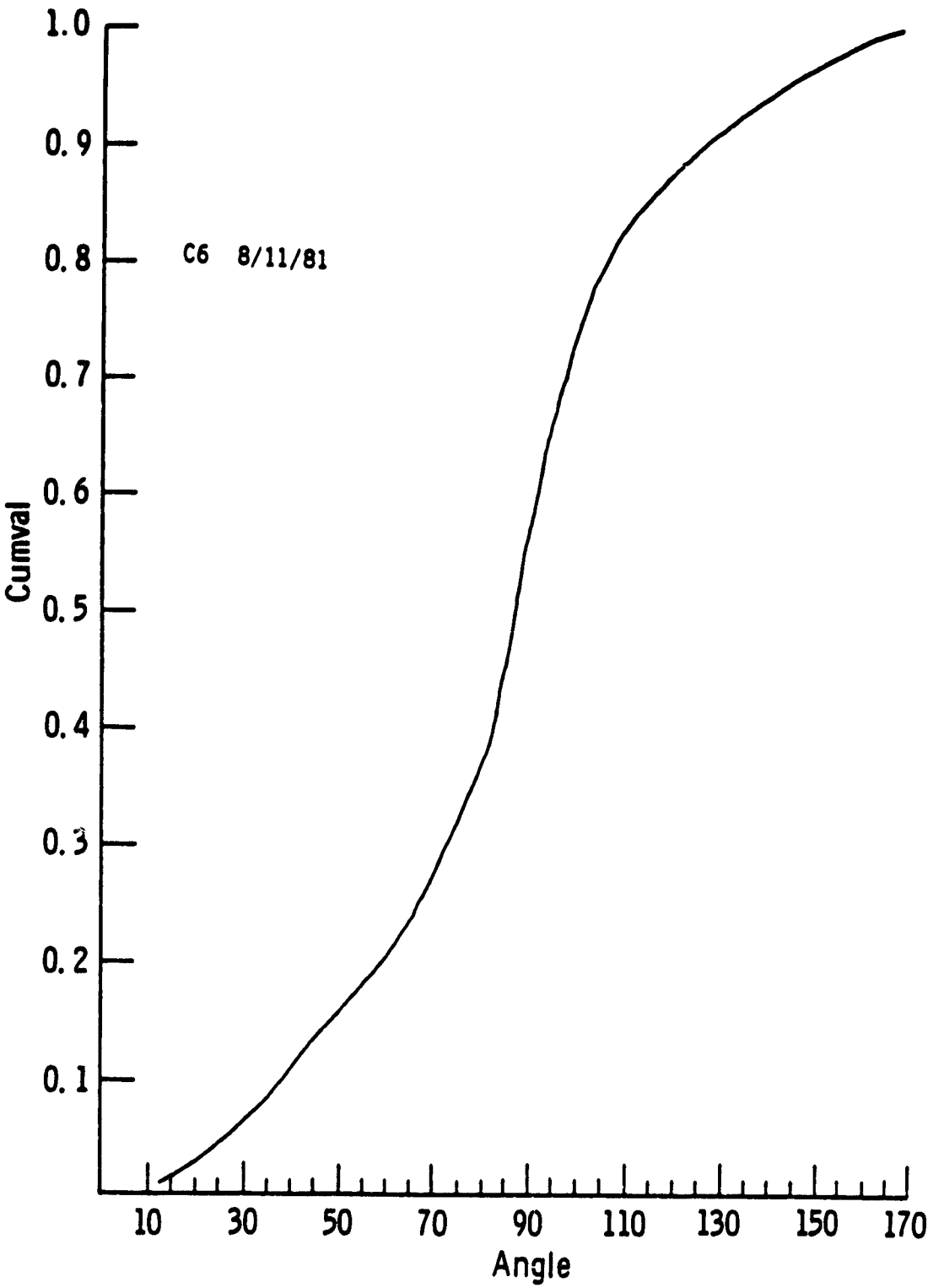
1.0
0.9
0.8
0.7
0.6
0.5
0.4
0.3
0.2
0.1
Cumval
C6 8/11/81
10
30
50
70
90
110
130
150
170
Angle

APPENDIX L

10° LAD AND 90° LAD VS. MATURITY FOR C10

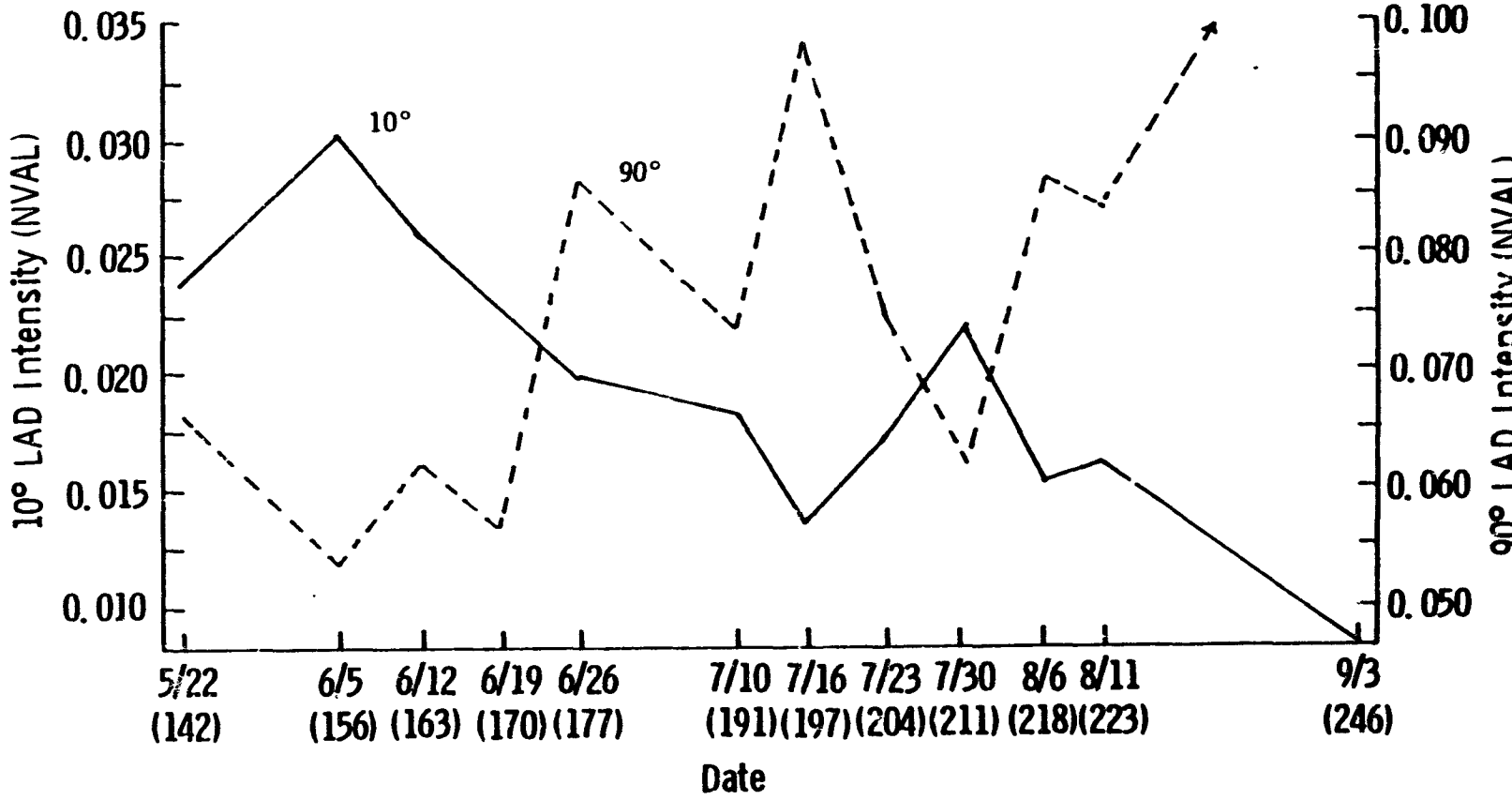
0.035
0.030
0.025
0.020
0.015
0.010
10° LAD Intensity (NVAL)
10°
90°
0.100
0.090
0.080
0.070
0.060
0.050
90° LAD Intensity (NVAL)
5/22 (142)
6/5 (156)
6/12 (163)
6/19 (170)
6/26 (177)
7/10 (191)
7/16 (197)
7/23 (204)
7/30 (211)
8/6 (218)
8/11 (223)
9/3 (246)
Date

APPENDIX M

PLANT AND SOIL MOISTURE VS. MATURITY FOR C10

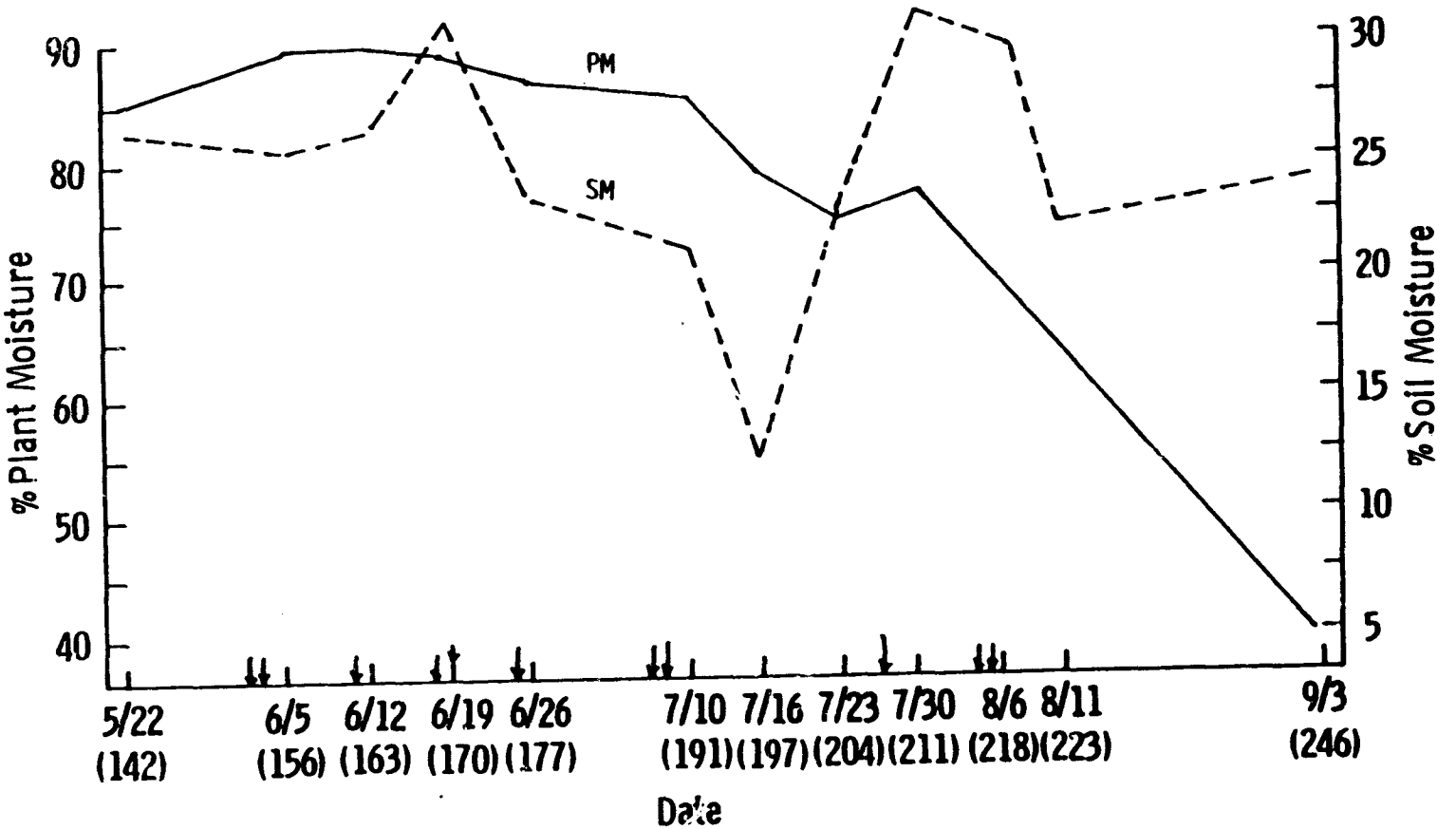
90
80
70
60
50
40
% Plant Moisture
PM
SM
30
25
20
15
10
5
% Soil Moisture
5/22 (142)
6/5 (156)
6/12 (163)
6/19 (170)
6/26 (177)
7/10 (191)
7/16 (197)
7/23 (204)
7/30 (211)
8/6 (218)
8/11 (223)
9/3 (246)
Date

APPENDIX N

C10, NVAL VS. ANGLE, AS A FUNCTION OF MATURITY

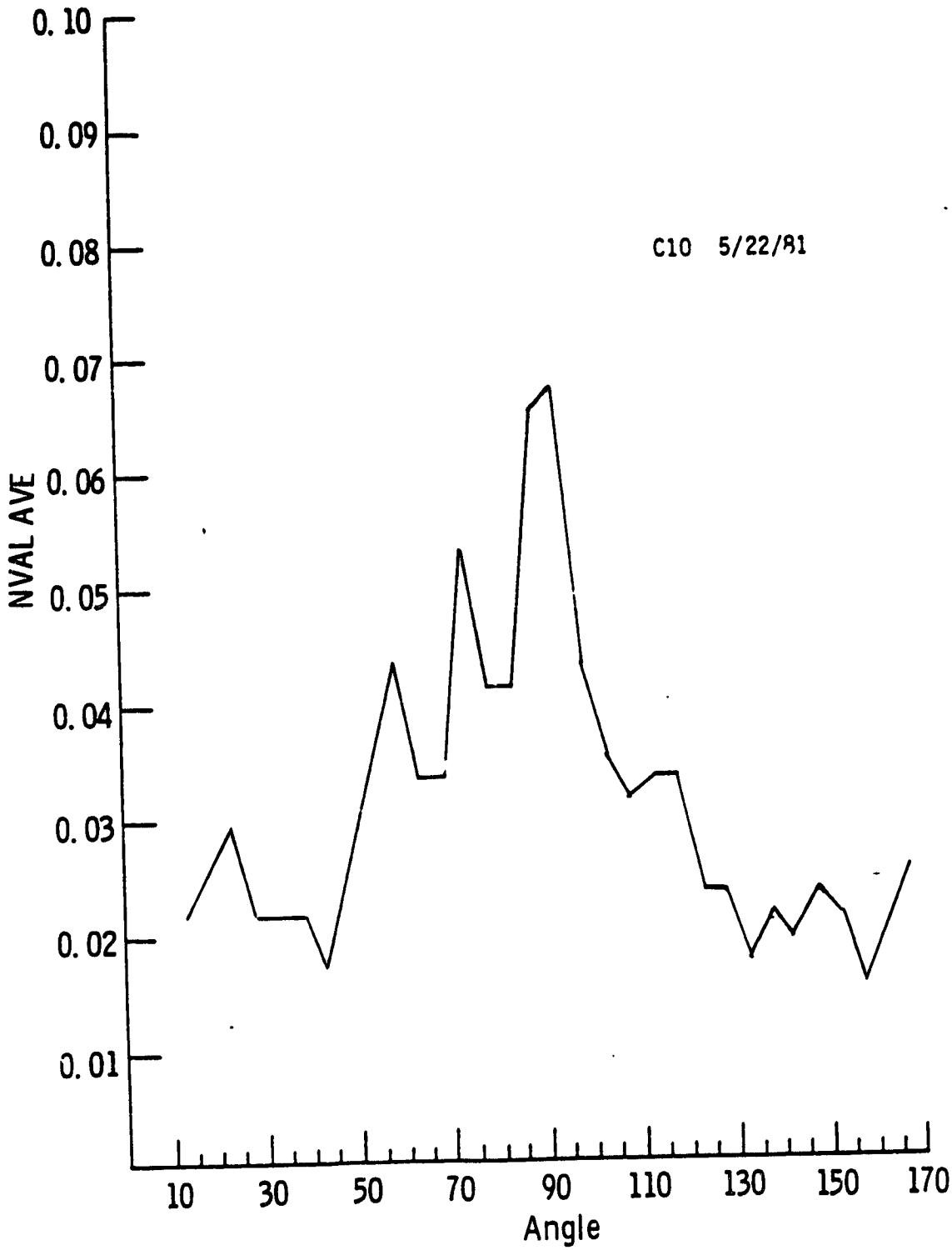
C10 5/22/81
NVAL AVE
0.10
0.09
0.08
0.07
0.06
0.05
0.04
0.03
0.02
0.01
10
30
50
70
90
110
130
150
170
Angle

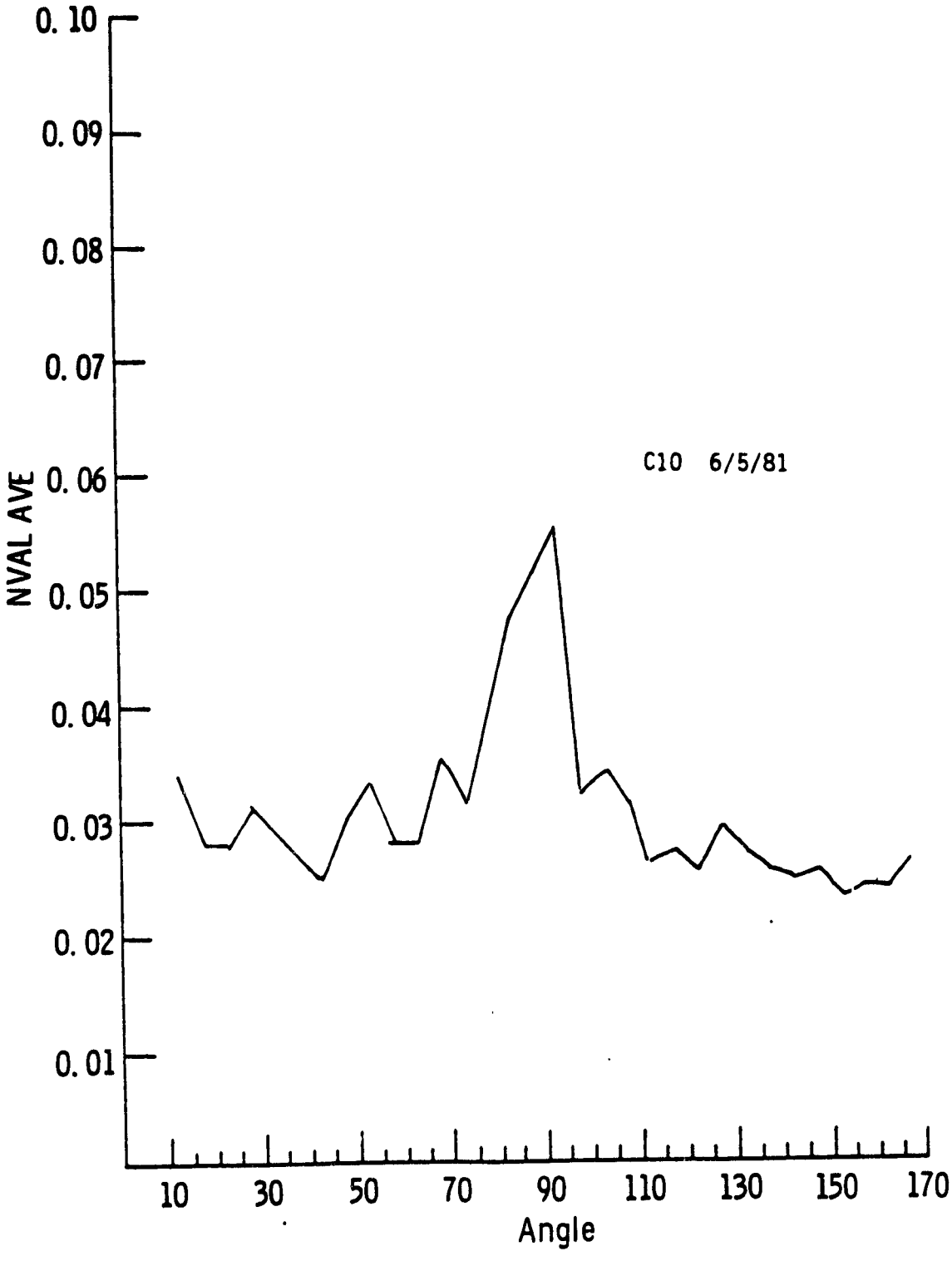
0. 10
0. 09
0. 08
0. 07
0. 06
0. 05
0. 04
0. 03
0. 02
0. 01
NVAL AVE
C10 6/5/81
10
30
50
70
90
110
130
150
170
Angle

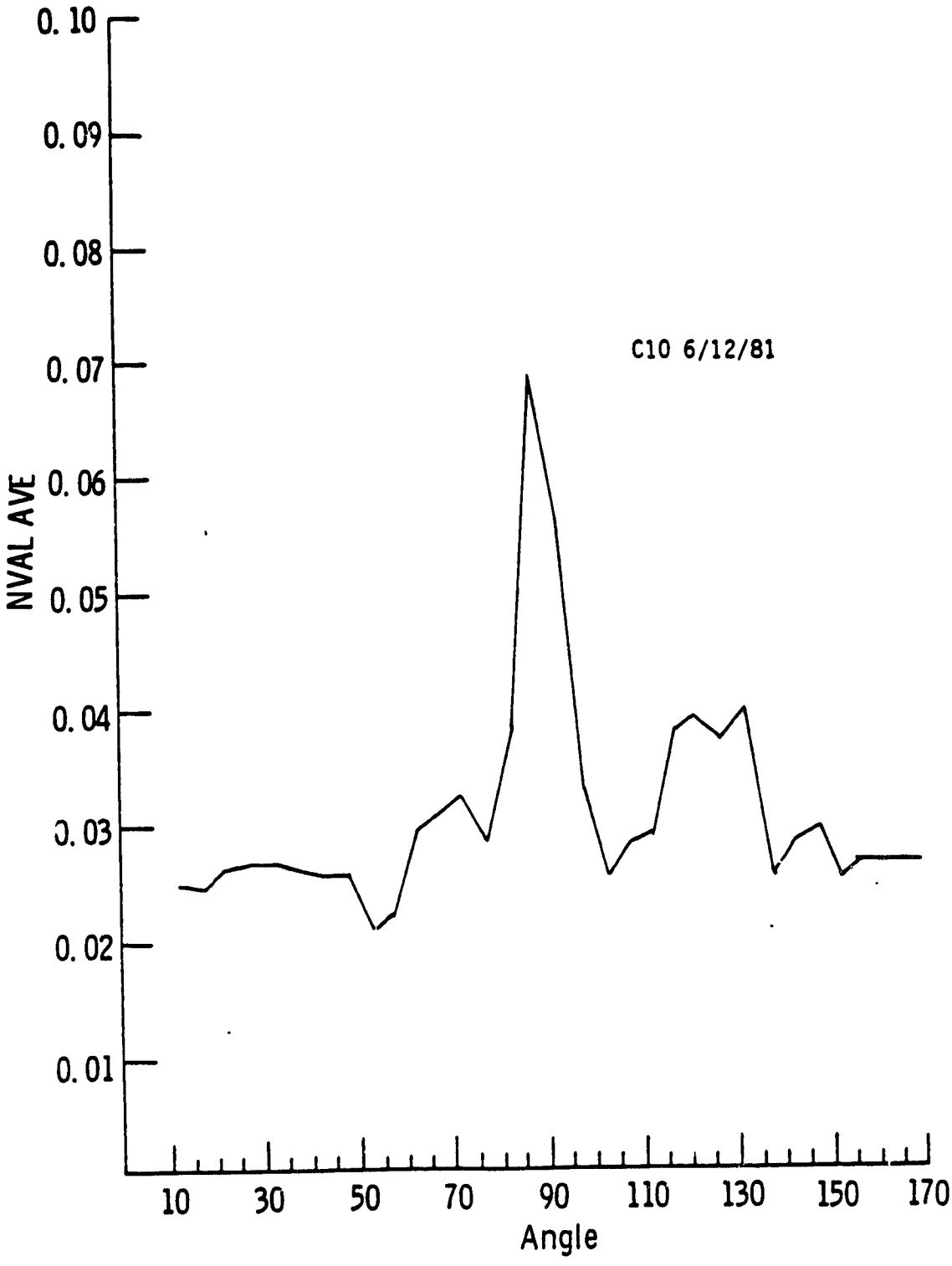
0.10
0.09
0.08
0.07
0.06
0.05
0.04
0.03
0.02
0.01
NVAL AVE
C10 6/12/81
10
30
50
70
90
110
130
150
170
Angle

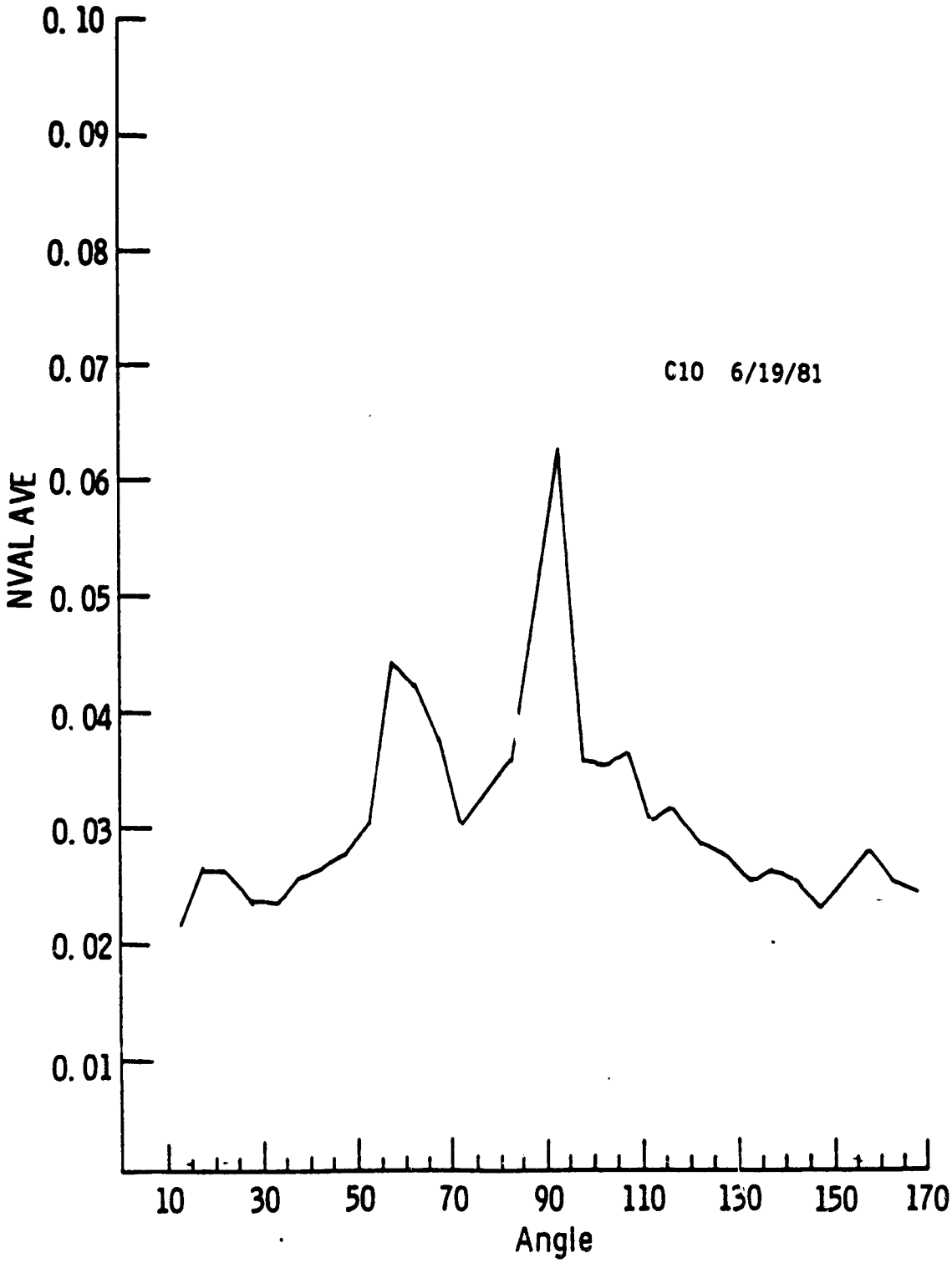
0. 10
0. 09
0. 08
0. 07
0. 06
0. 05
0. 04
0. 03
0. 02
0. 01
NVAL AVE
C10 6/19/81
10
30
50
70
90
110
130
150
170
Angle

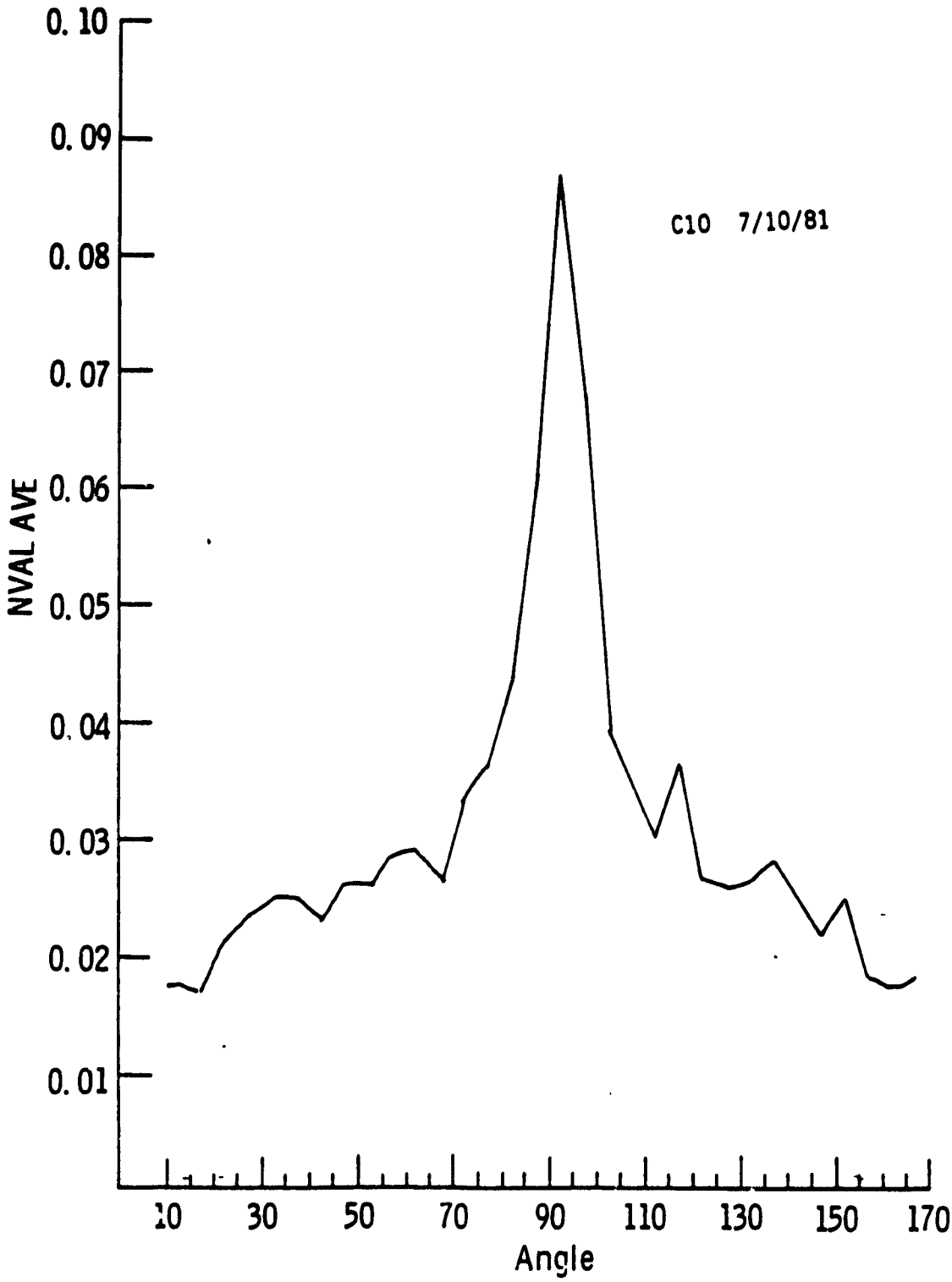
0.10
0.09
0.08
0.07
0.06
0.05
0.04
0.03
0.02
0.01
NVAL AVE
C10 7/10/81
10
30
50
70
90
110
130
150
170
Angle

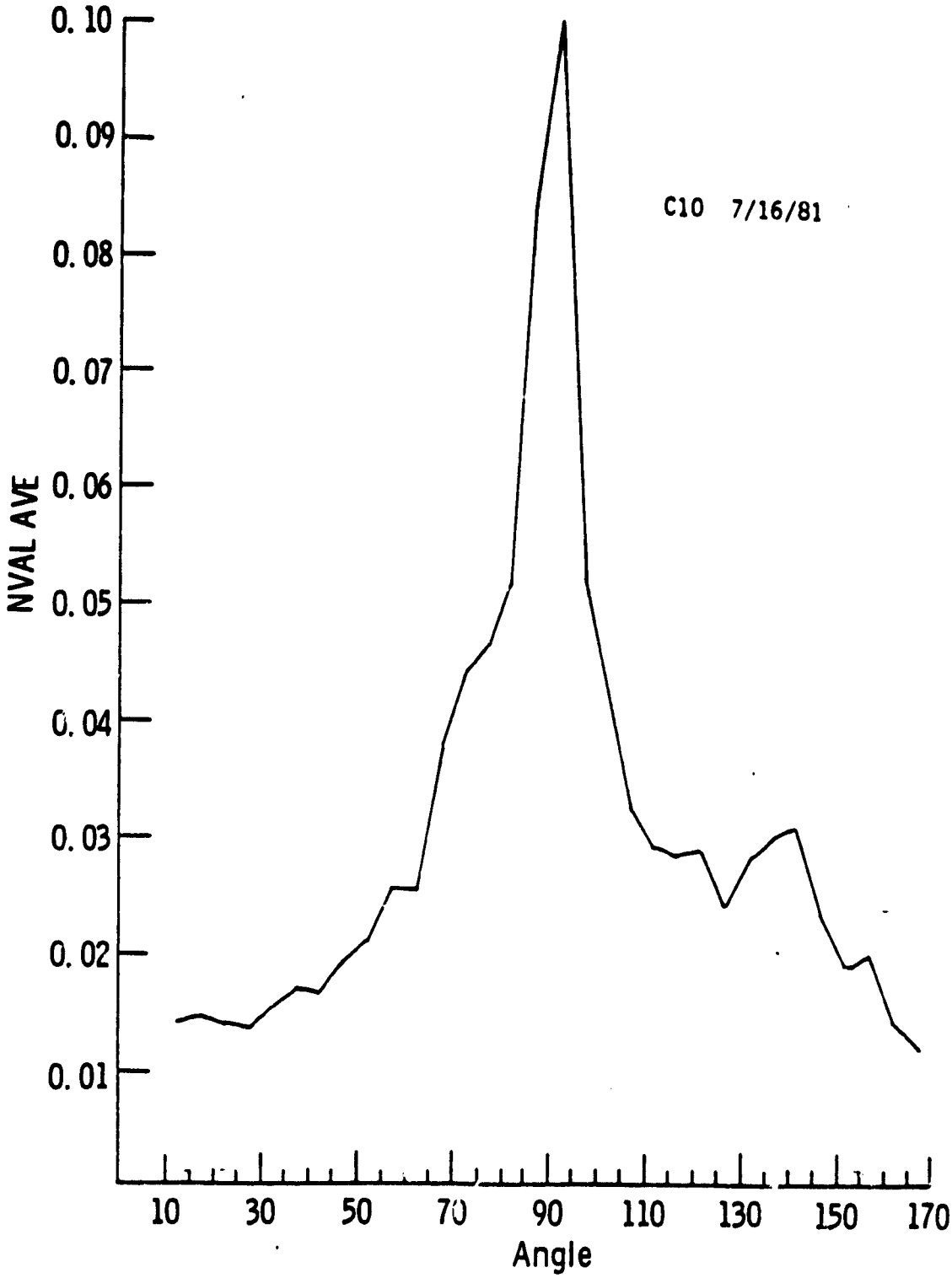
0.10
0.09
0.08
0.07
0.06
0.05
0.04
0.03
0.02
0.01
NVAL AVE
C10 7/16/81
10
30
50
70
90
110
130
150
170
Angle

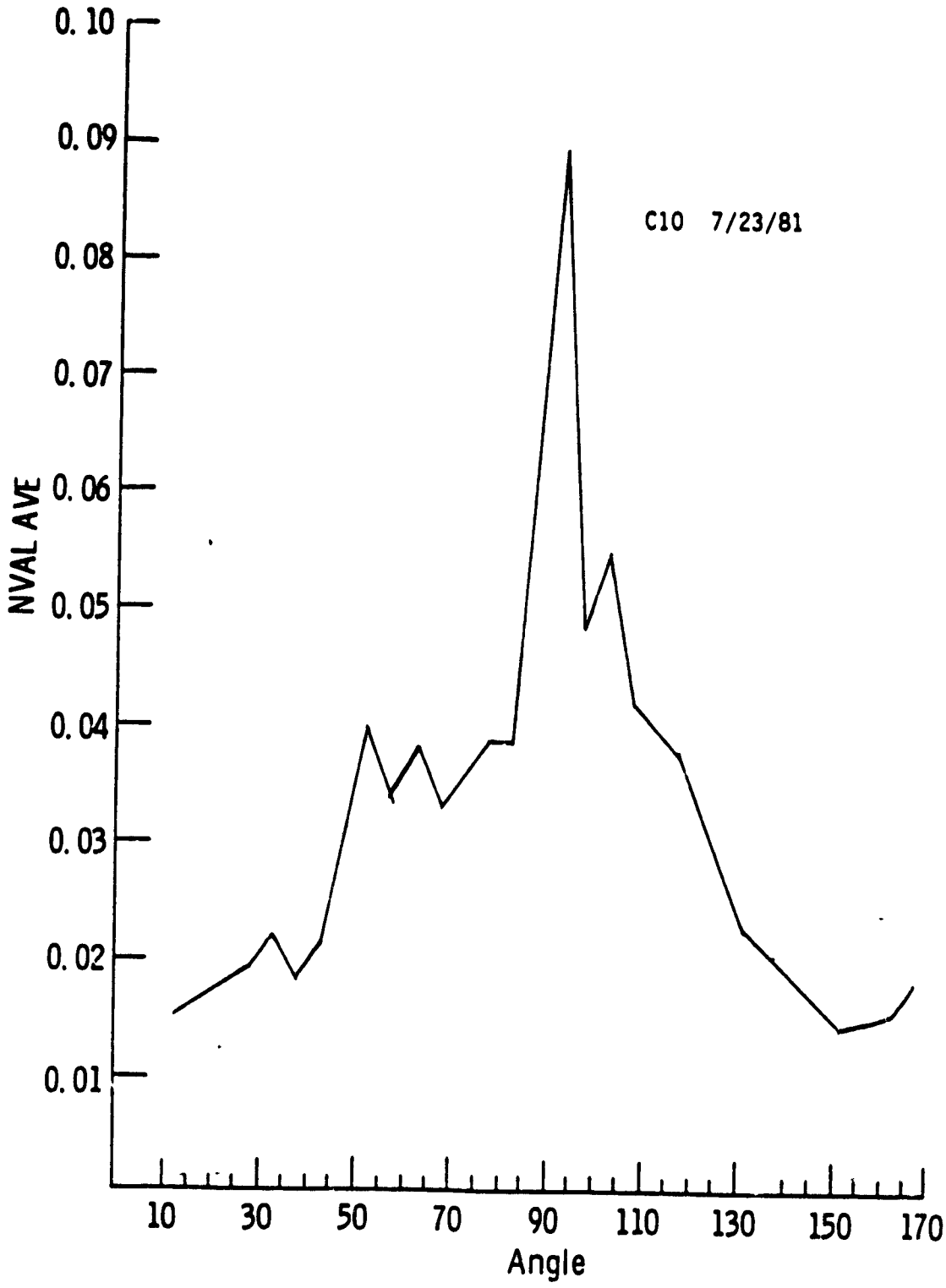
0. 10
0. 09
0. 08
0. 07
0. 06
0. 05
0. 04
0. 03
0. 02
0. 01
NVAL AVE
C10 7/23/81
10
30
50
70
90
110
130
150
170
Angle

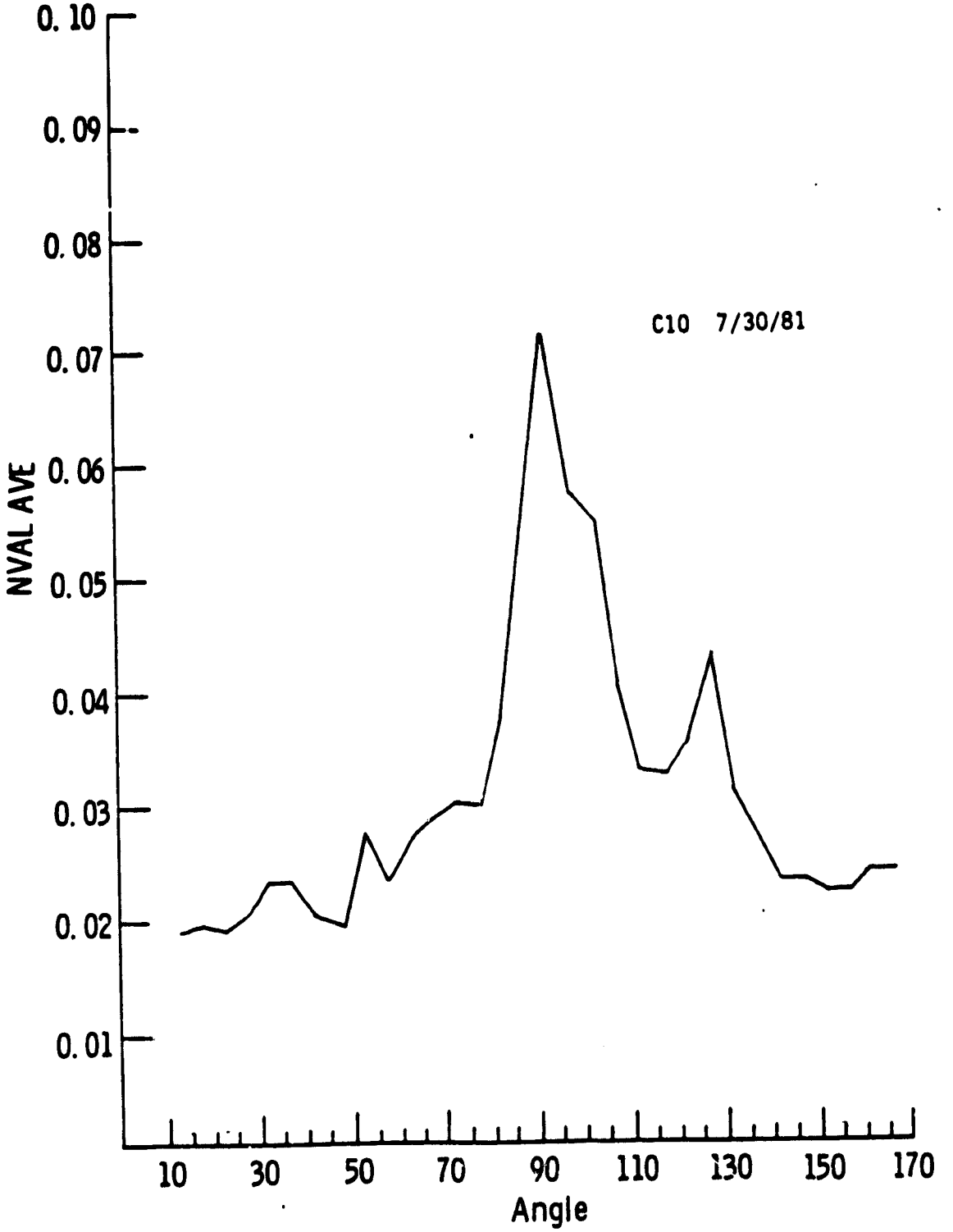
0.10
0.09
0.08
0.07
0.06
0.05
0.04
0.03
0.02
0.01
NVAL AVE
C10 7/30/81
10
30
50
70
90
110
130
150
170
Angle

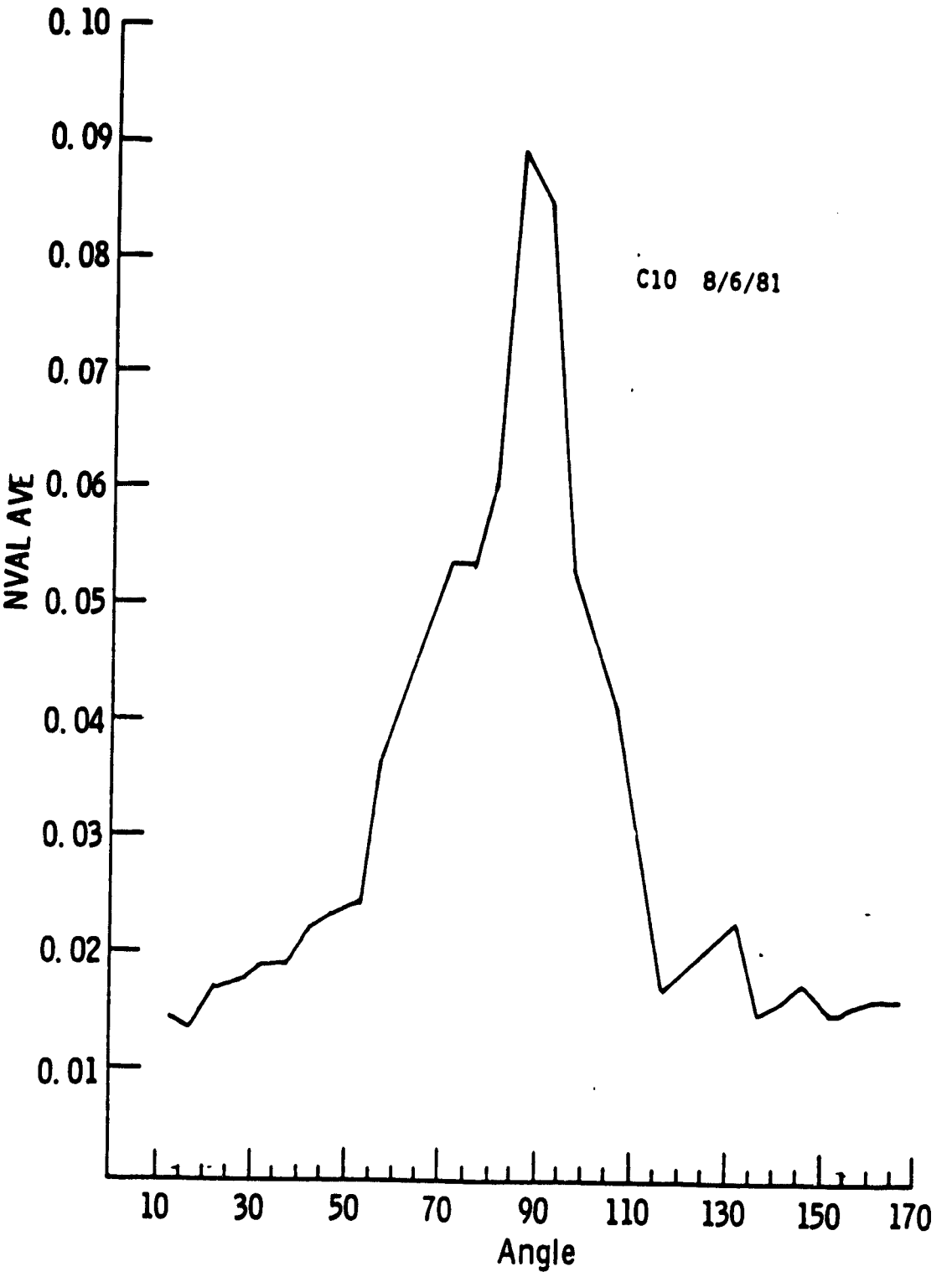
0. 10
0. 09
0. 08
0. 07
0. 06
0. 05
0. 04
0. 03
0. 02
0. 01
NVAL AVE
C10 8/6/81
10
30
50
70
90
110
130
150
170
Angle

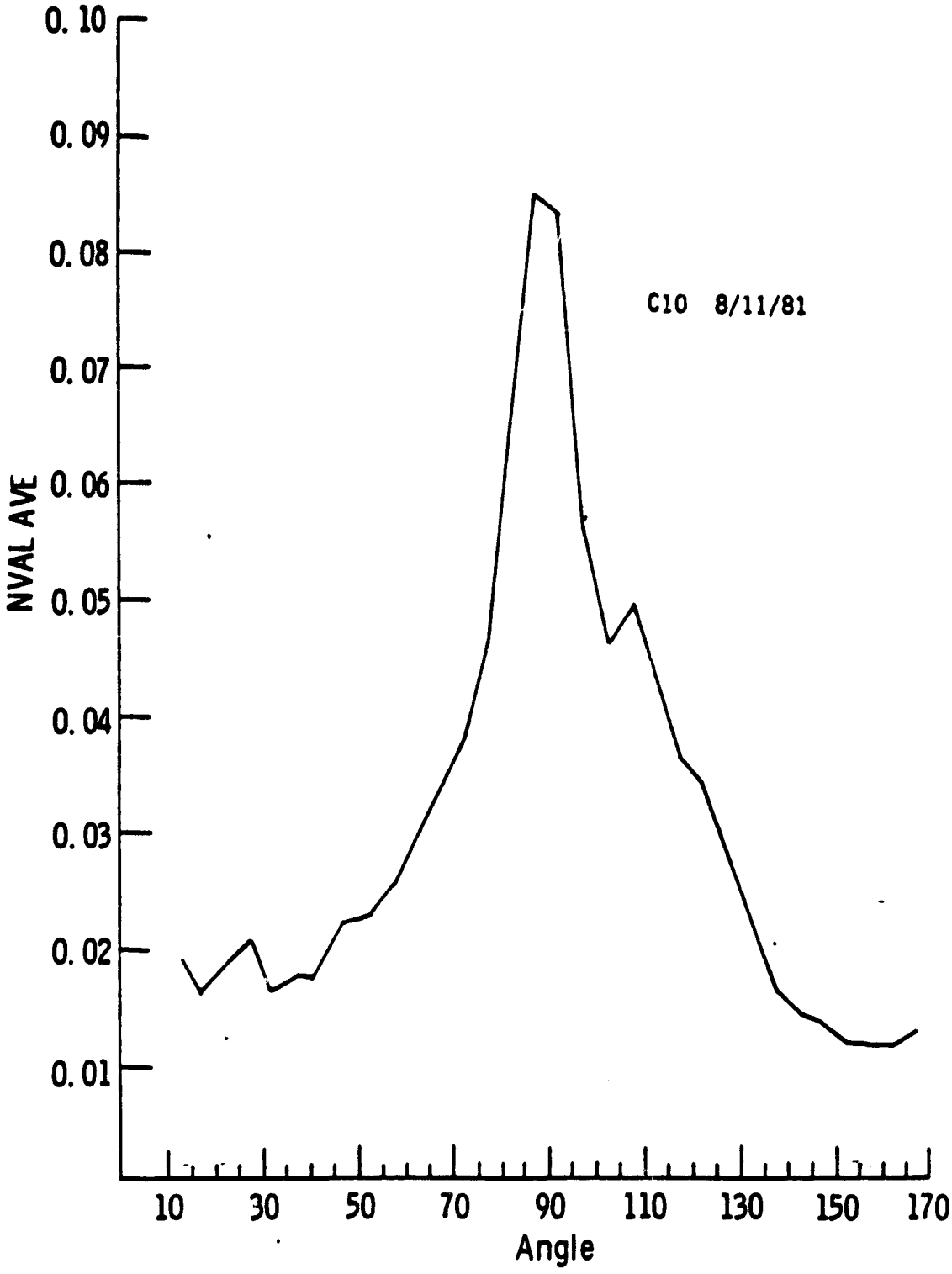
0. 10
0. 09
0. 08
0. 07
0. 06
0. 05
0. 04
0. 03
0. 02
0. 01
NVAL AVE
C10 8/11/81
10
30
50
70
90
110
130
150
170
Angle

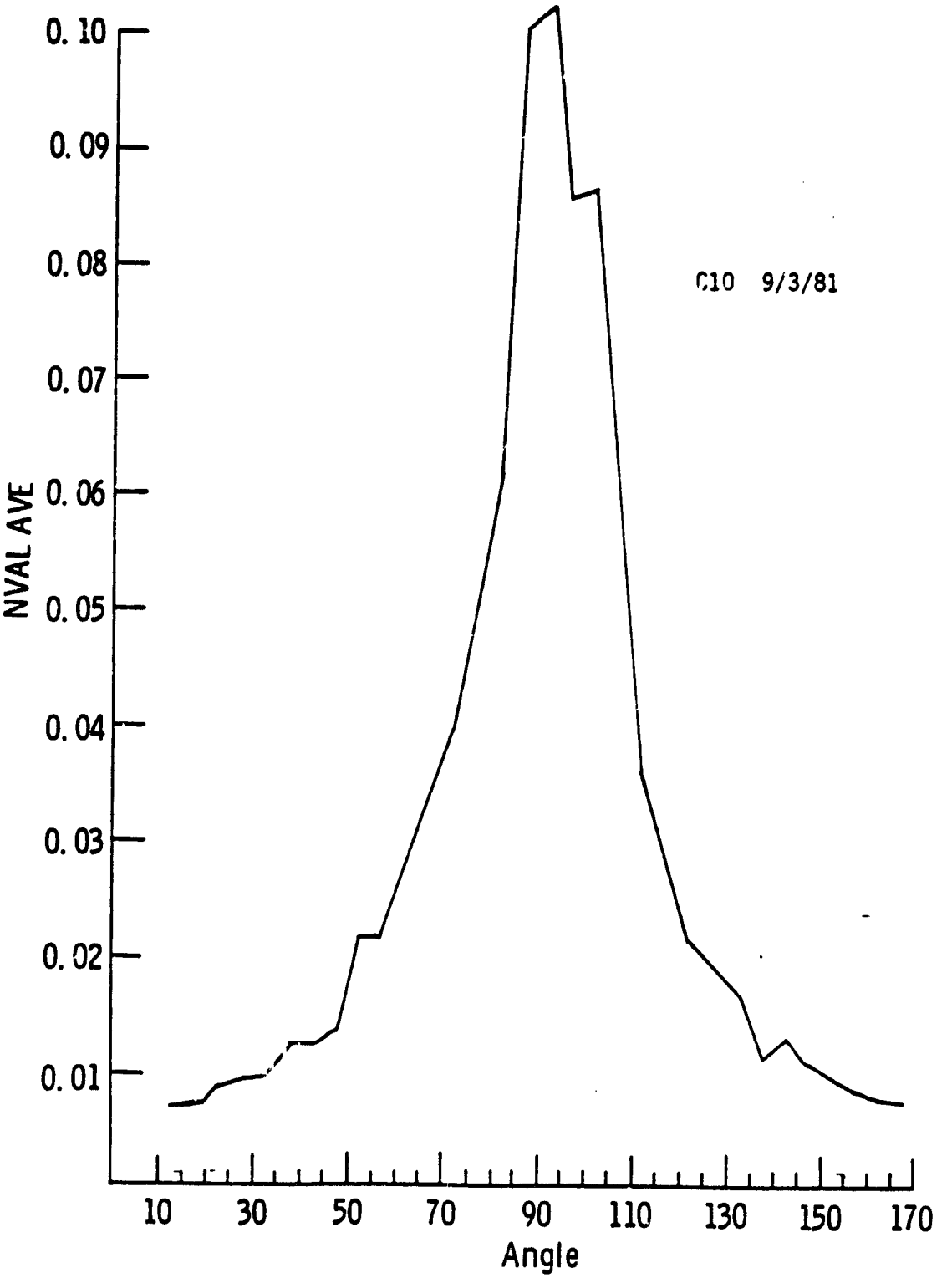
0.10
0.09
0.08
0.07
0.06
0.05
0.04
0.03
0.02
0.01
NVAL AVE
C10 9/3/81
10
30
50
70
90
110
130
150
170
Angle

APPENDIX O

C10, CUMVAL VS. ANGLE, AS A FUNCTION OF MATURITY

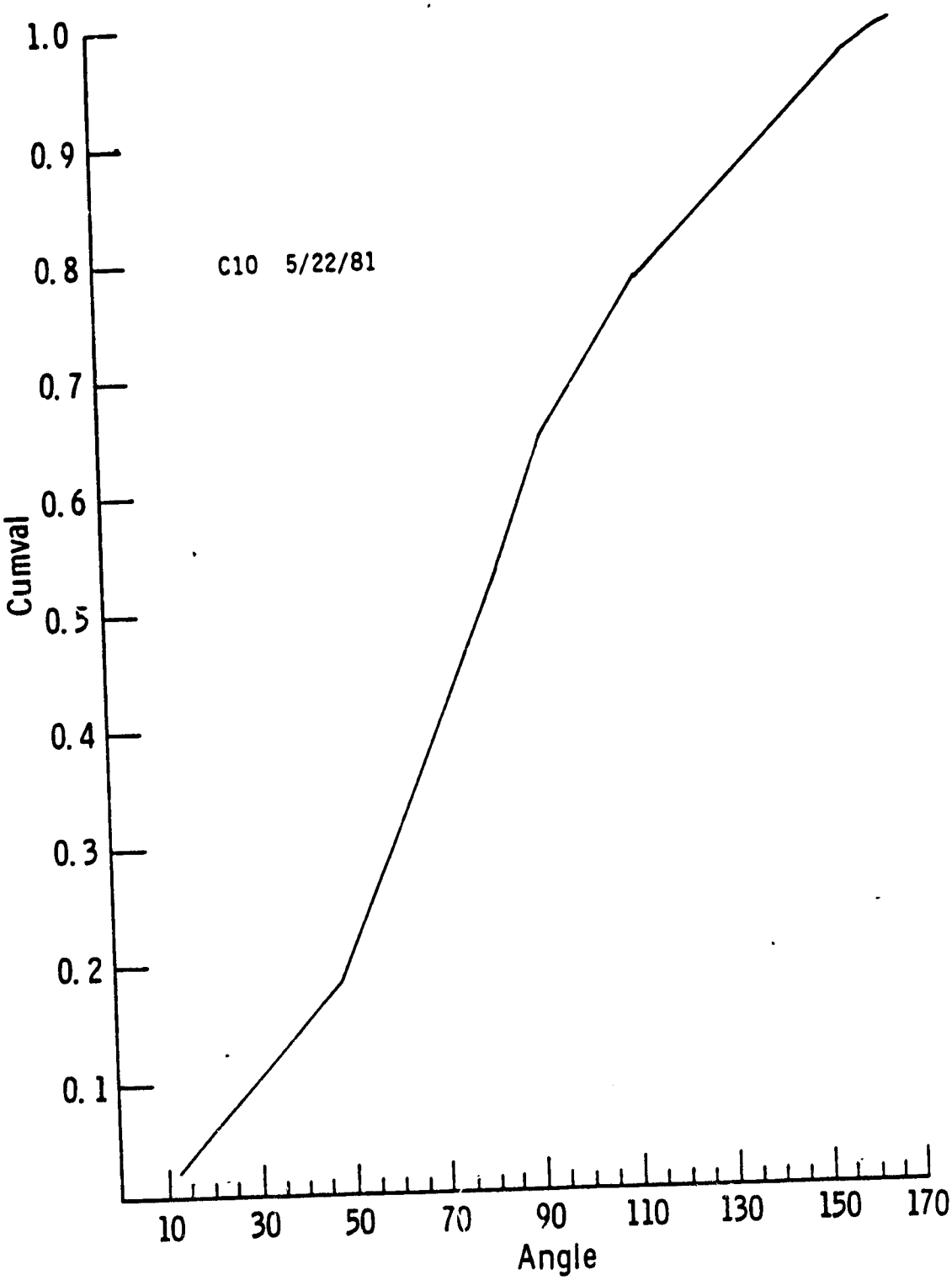
1.0
0.9
0.8
0.7
0.6
0.5
0.4
0.3
0.2
0.1
Cumval
C10 5/22/81
10
30
50
70
90
110
130
150
170
Angle

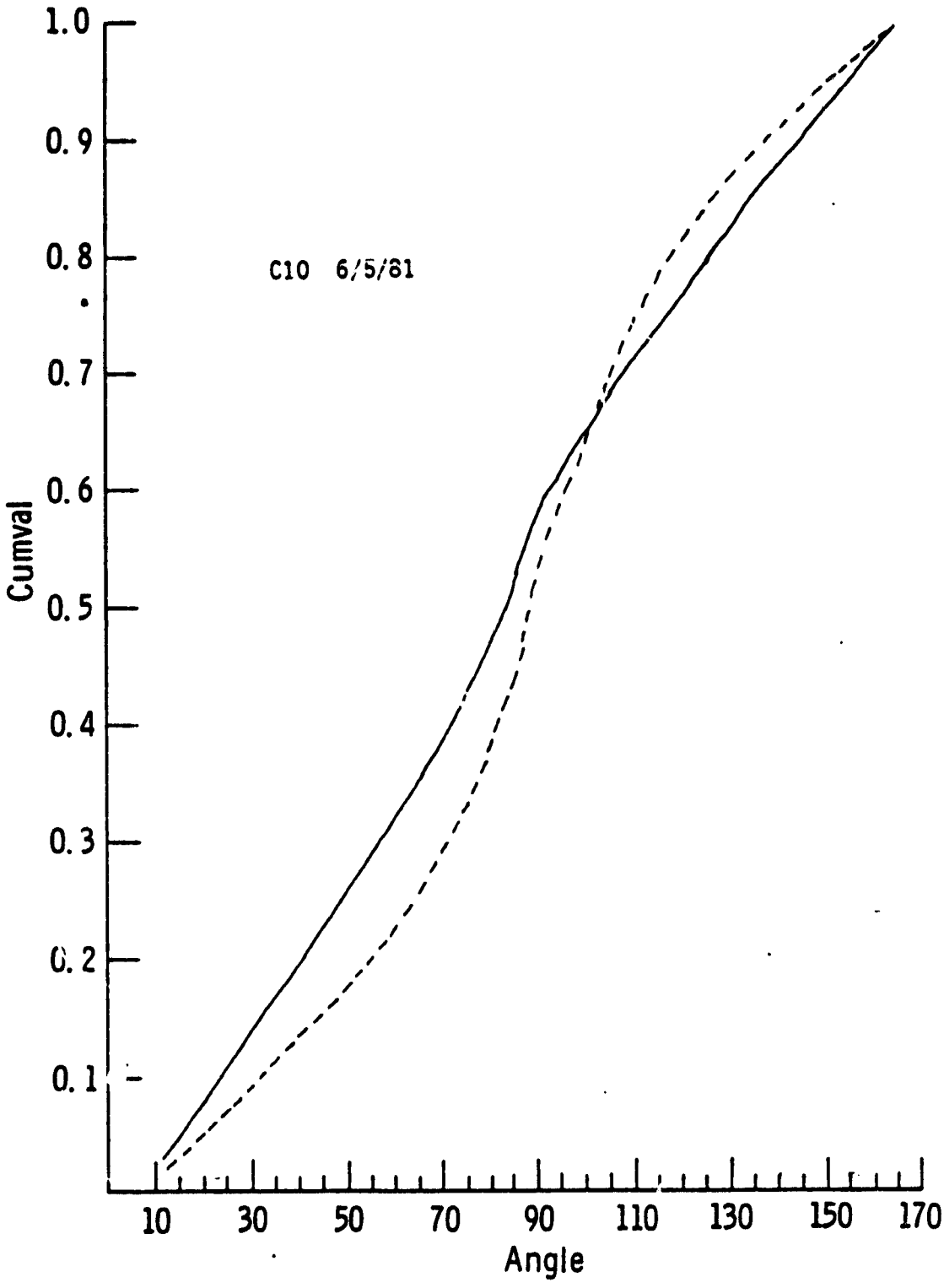
1.0
0.9
0.8
0.7
0.6
0.5
0.4
0.3
0.2
0.1
Cumval
C10 6/5/81
10
30
50
70
90
110
130
150
170
Angle

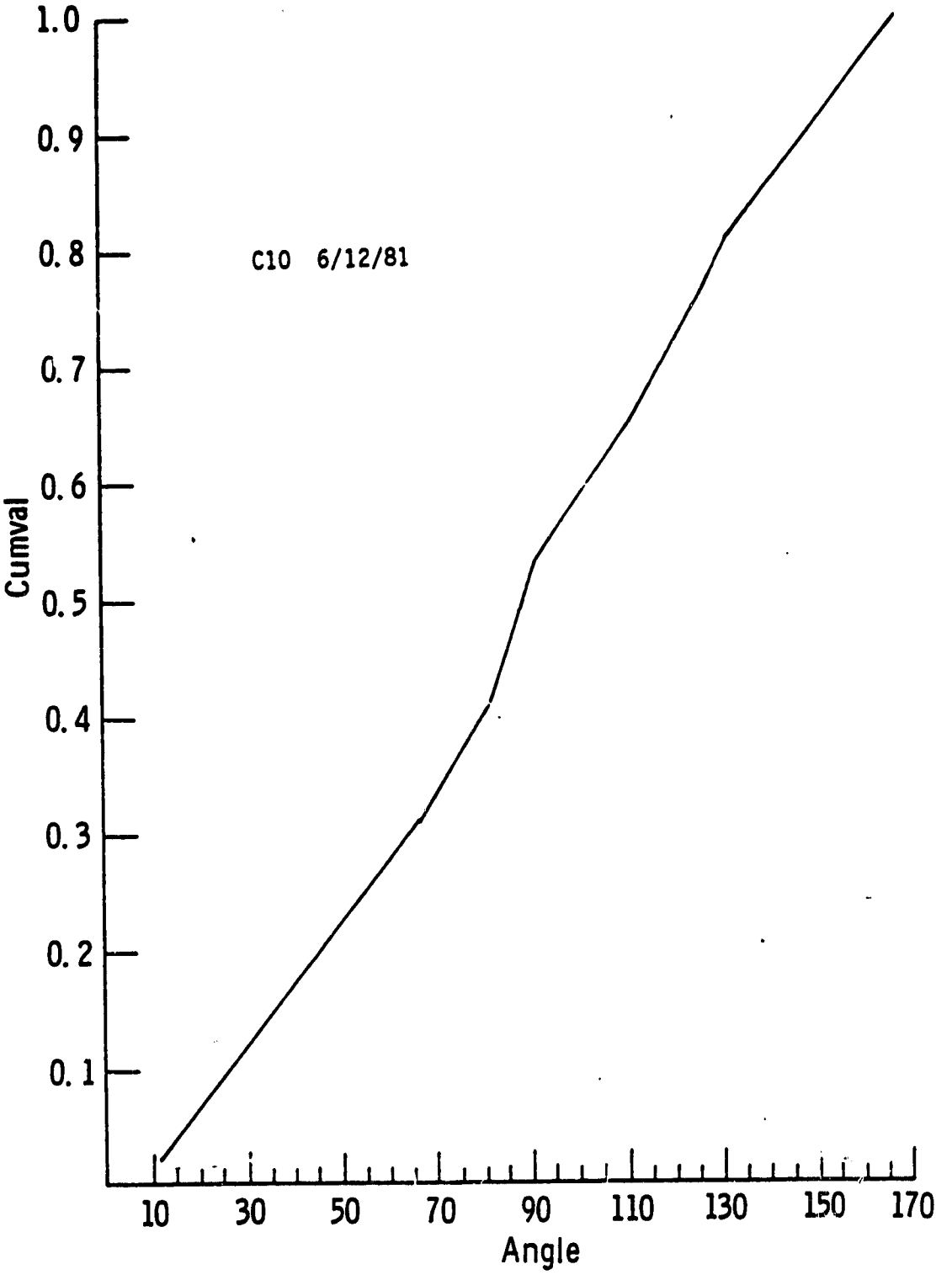
1.0
0.9
0.8
0.7
0.6
0.5
0.4
0.3
0.2
0.1
Cumval
C10 6/12/81
10
30
50
70
90
110
130
150
170
Angle

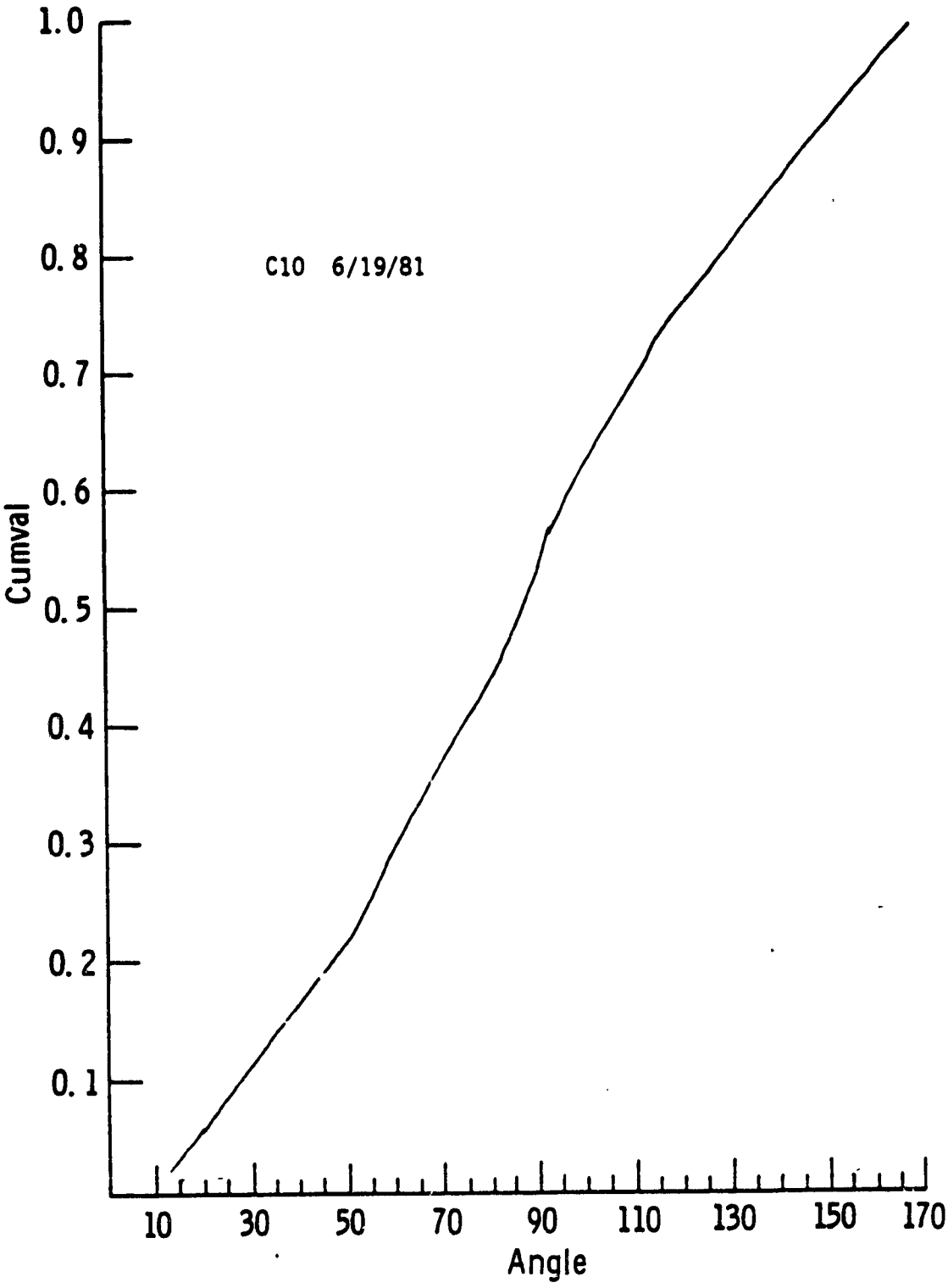
1.0
0.9
0.8
0.7
0.6
0.5
0.4
0.3
0.2
0.1
Cumval
C10 6/19/81
10
30
50
70
90
110
130
150
170
Angle

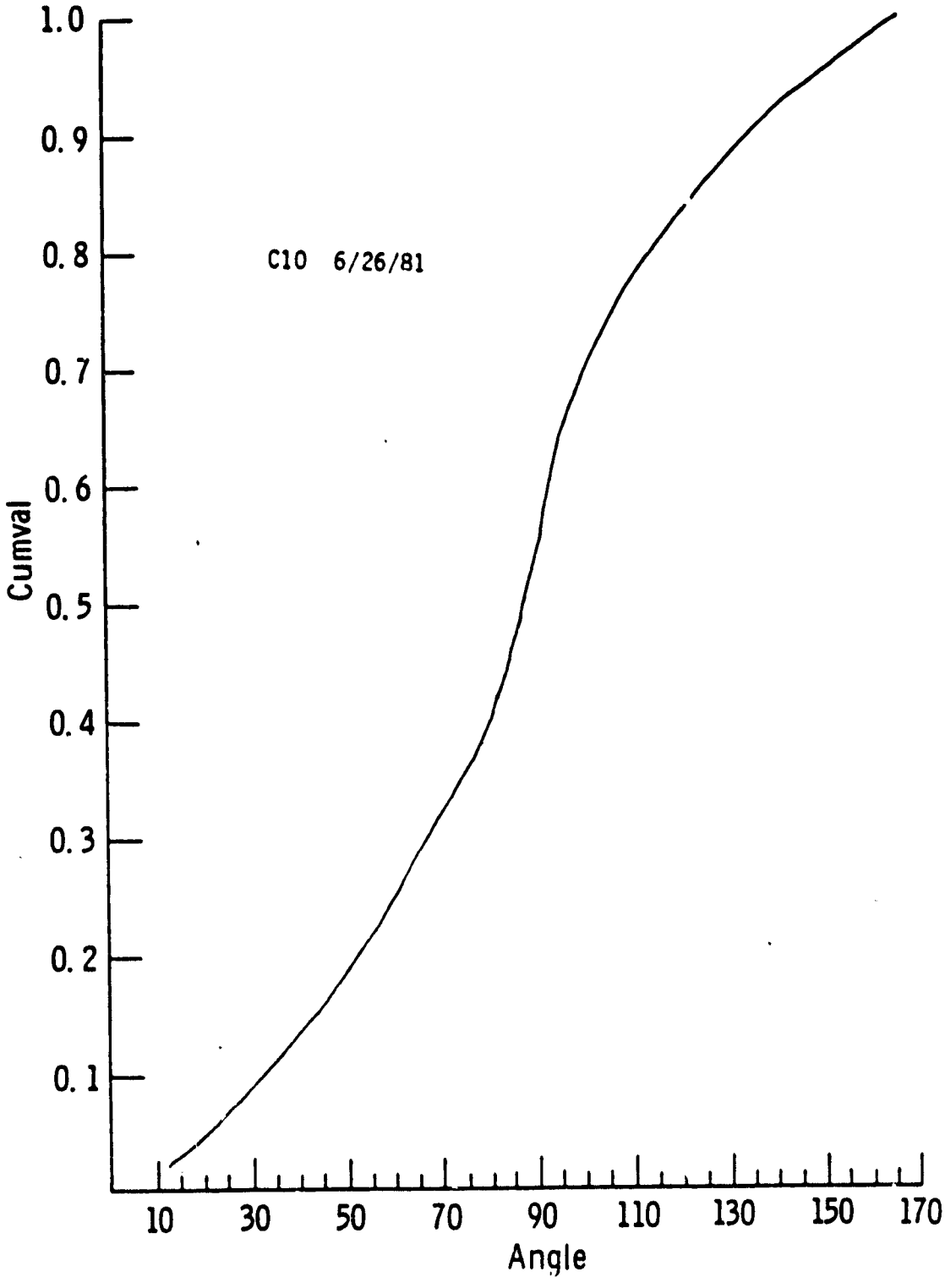
1.0
0.9
0.8
0.7
0.6
0.5
0.4
0.3
0.2
0.1
Cumval
C10 6/26/81
10
30
50
70
90
110
130
150
170
Angle

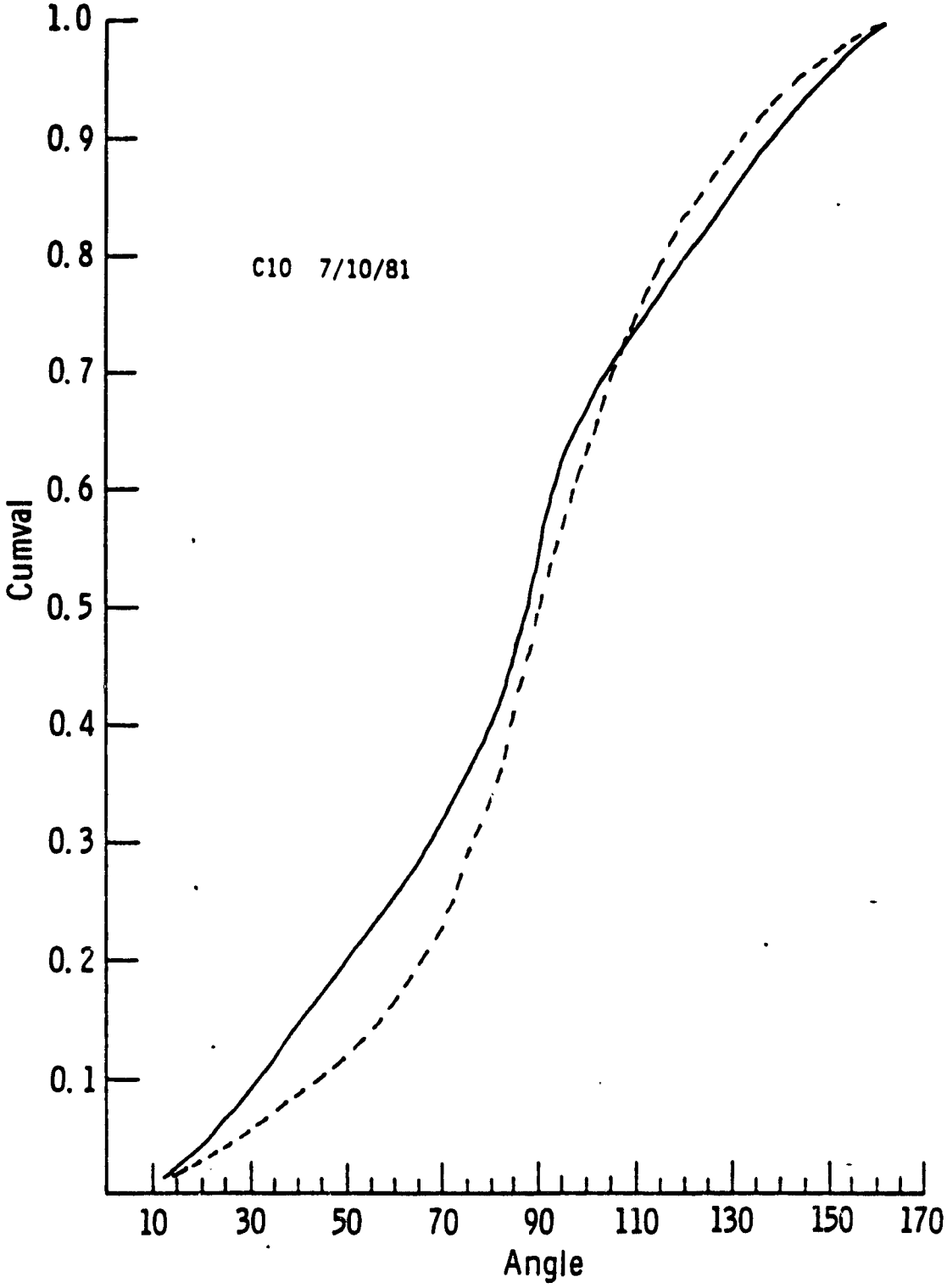
C10 7/10/81
Cumval
1.0
0.9
0.8
0.7
0.6
0.5
0.4
0.3
0.2
0.1
10
30
50
70
90
110
130
150
170
Angle

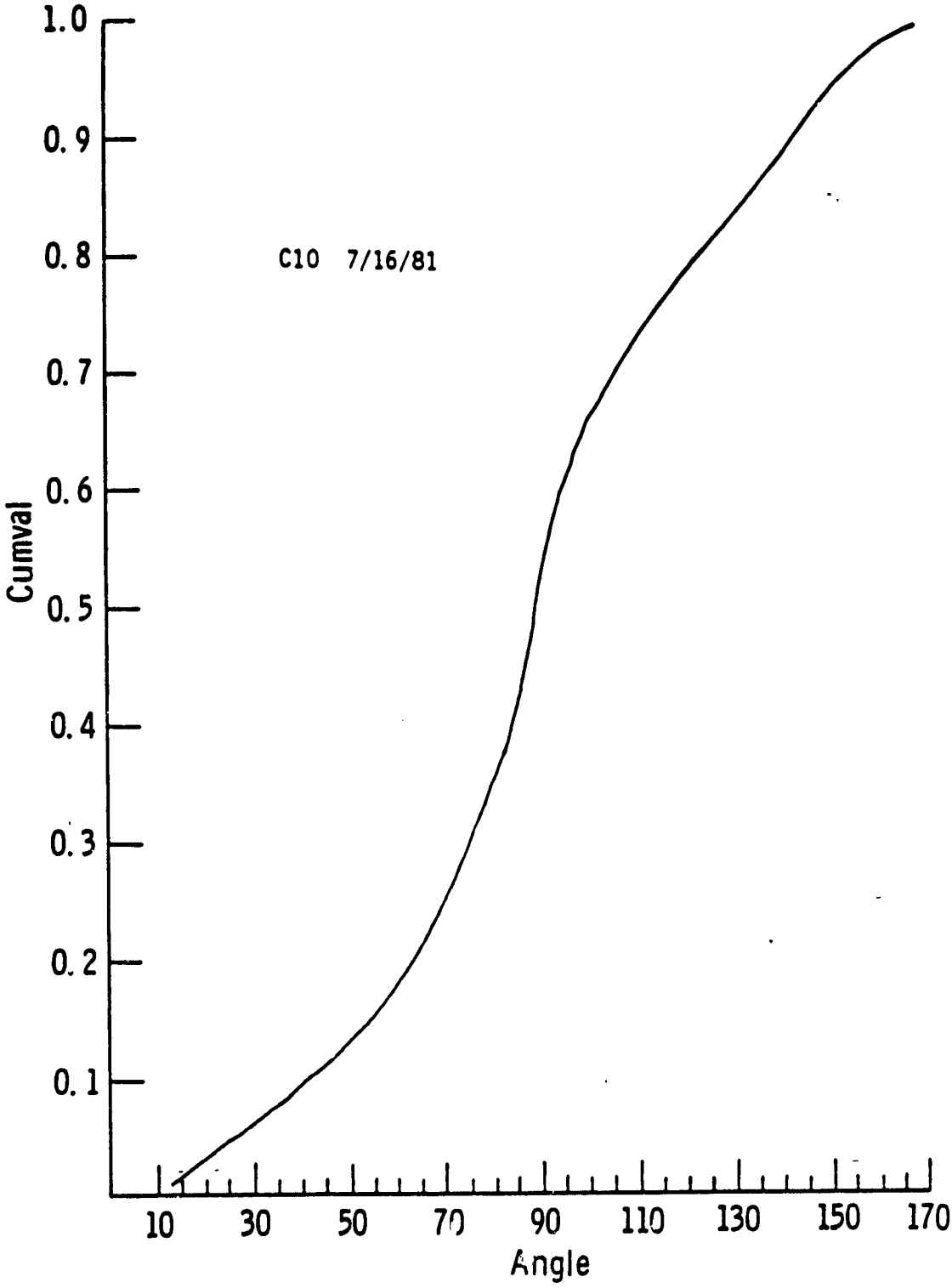
1.0
0.9
0.8
0.7
0.6
0.5
0.4
0.3
0.2
0.1
Cumval
C10 7/16/81
10
30
50
70
90
110
130
150
170
Angle

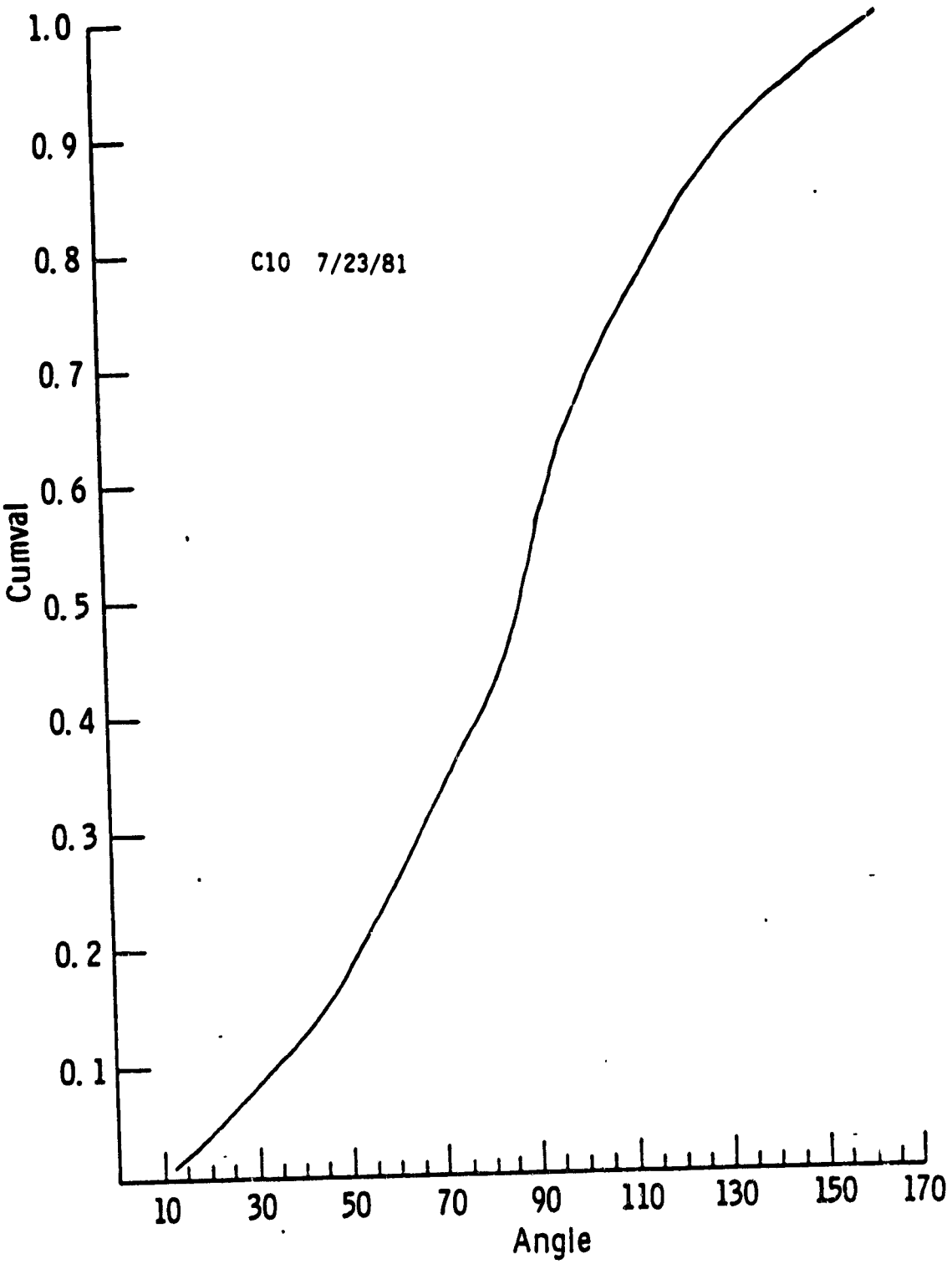
1.0
0.9
0.8
0.7
0.6
0.5
0.4
0.3
0.2
0.1
Cumval
C10 7/23/81
10
30
50
70
90
110
130
150
170
Angle

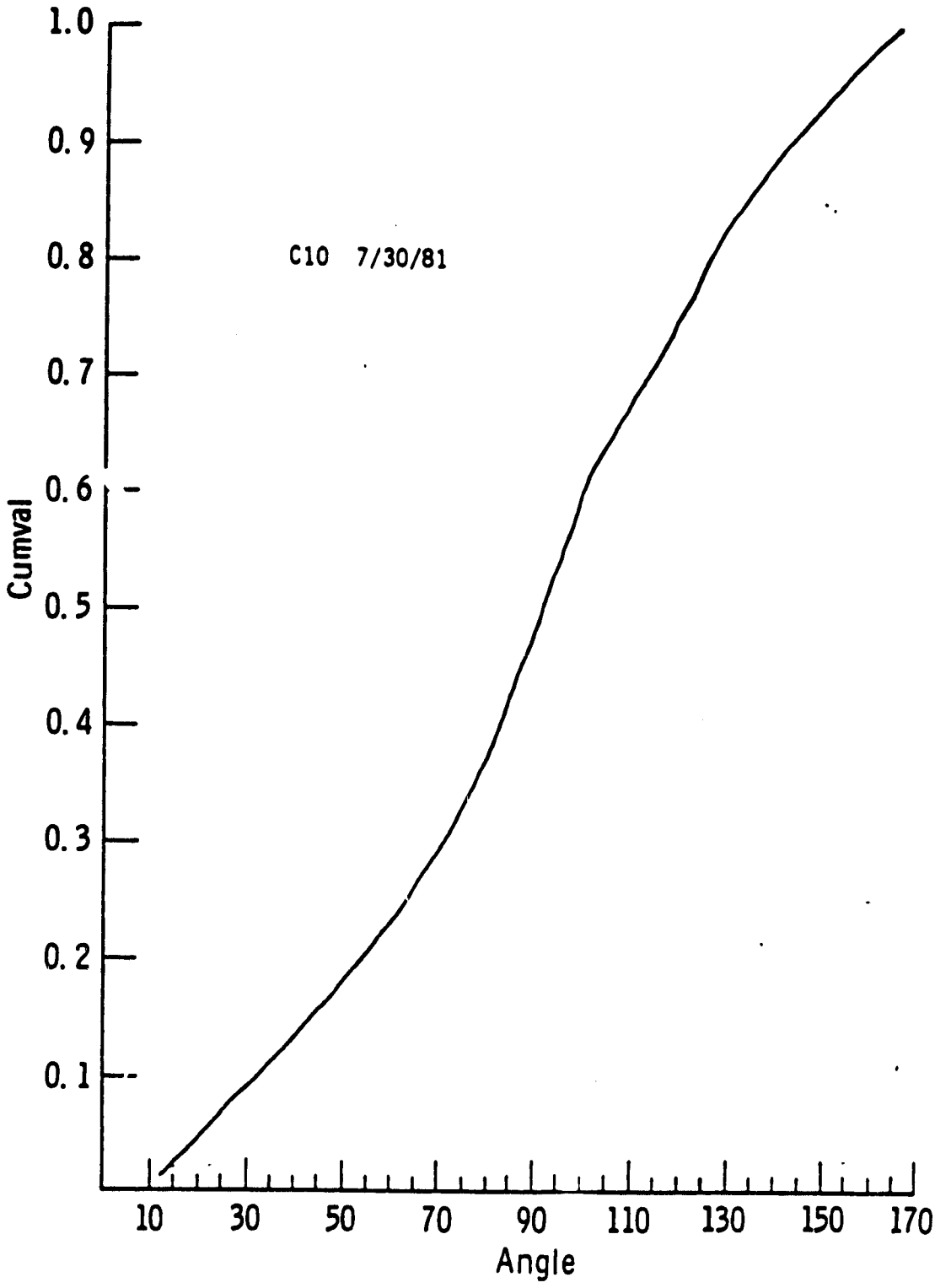
1.0
0.9
0.8
0.7
0.6
0.5
0.4
0.3
0.2
0.1
Cumval
C10 7/30/81
10
30
50
70
90
110
130
150
170
Angle

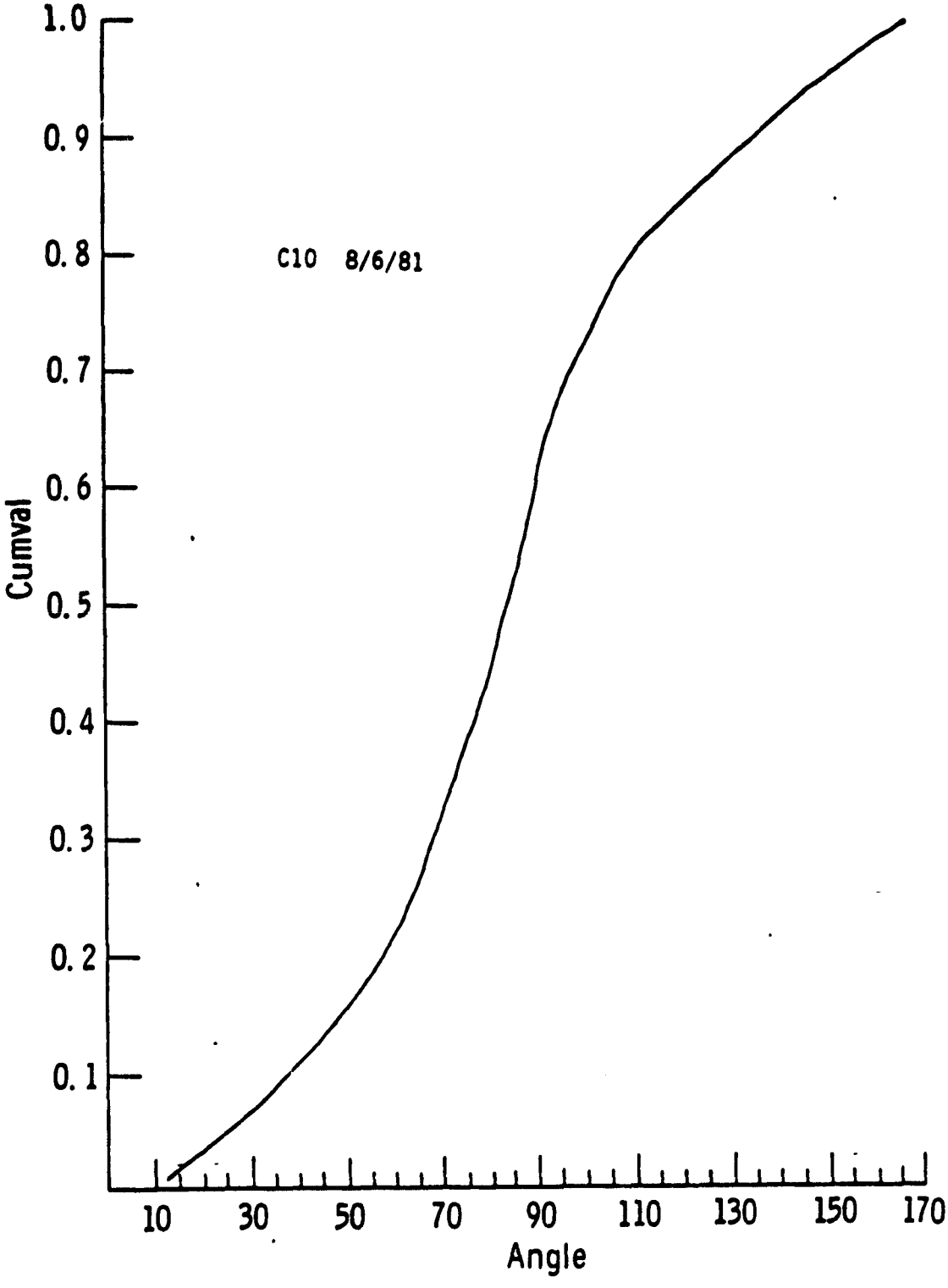
1.0
0.9
0.8
0.7
0.6
0.5
0.4
0.3
0.2
0.1
Cumval
C10 8/6/81
10
30
50
70
90
110
130
150
170
Angle

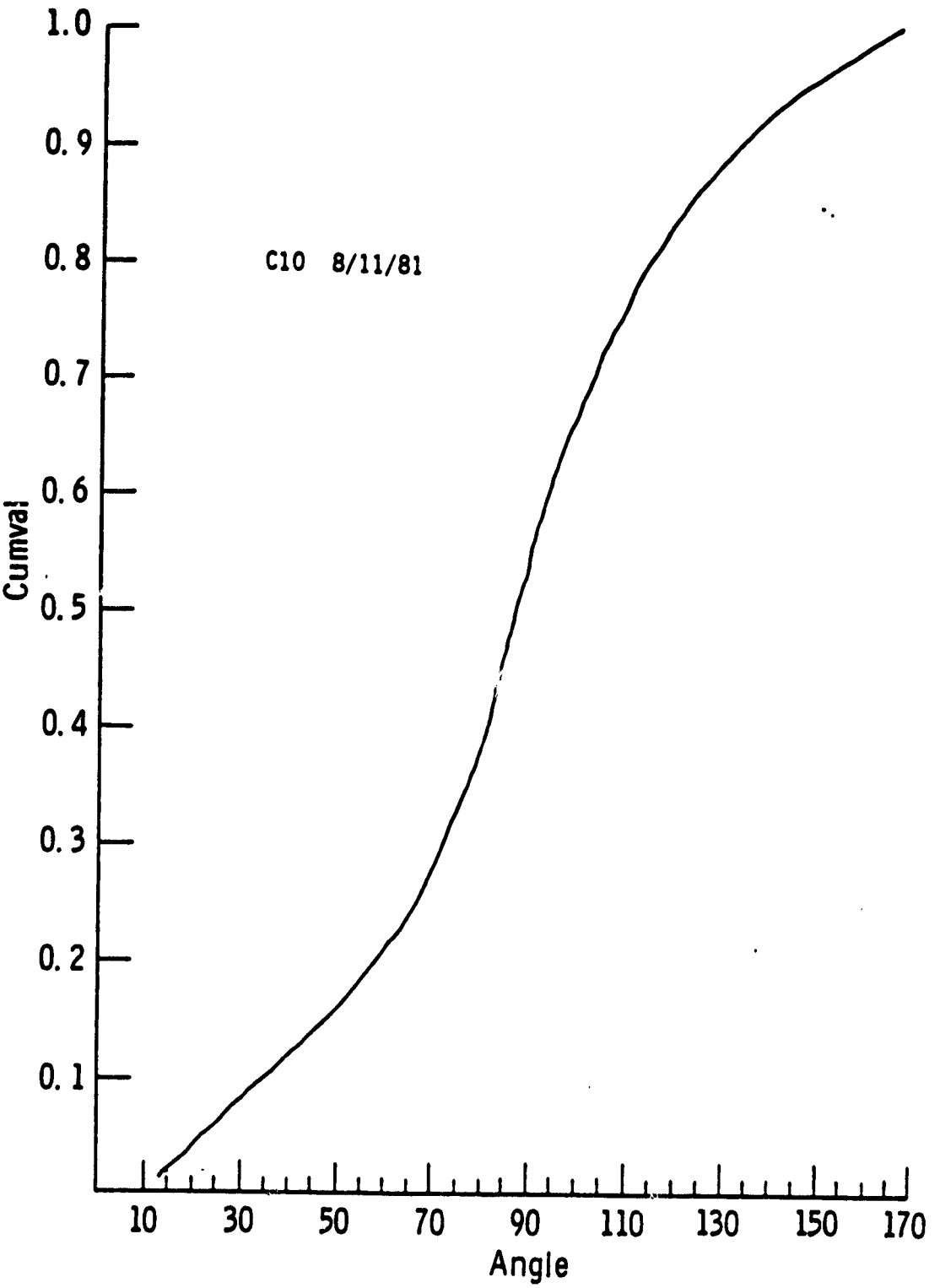
1.0
0.9
0.8
0.7
0.6
0.5
0.4
0.3
0.2
0.1
Cumval
C10 8/11/81
10
30
50
70
90
110
130
150
170
Angle

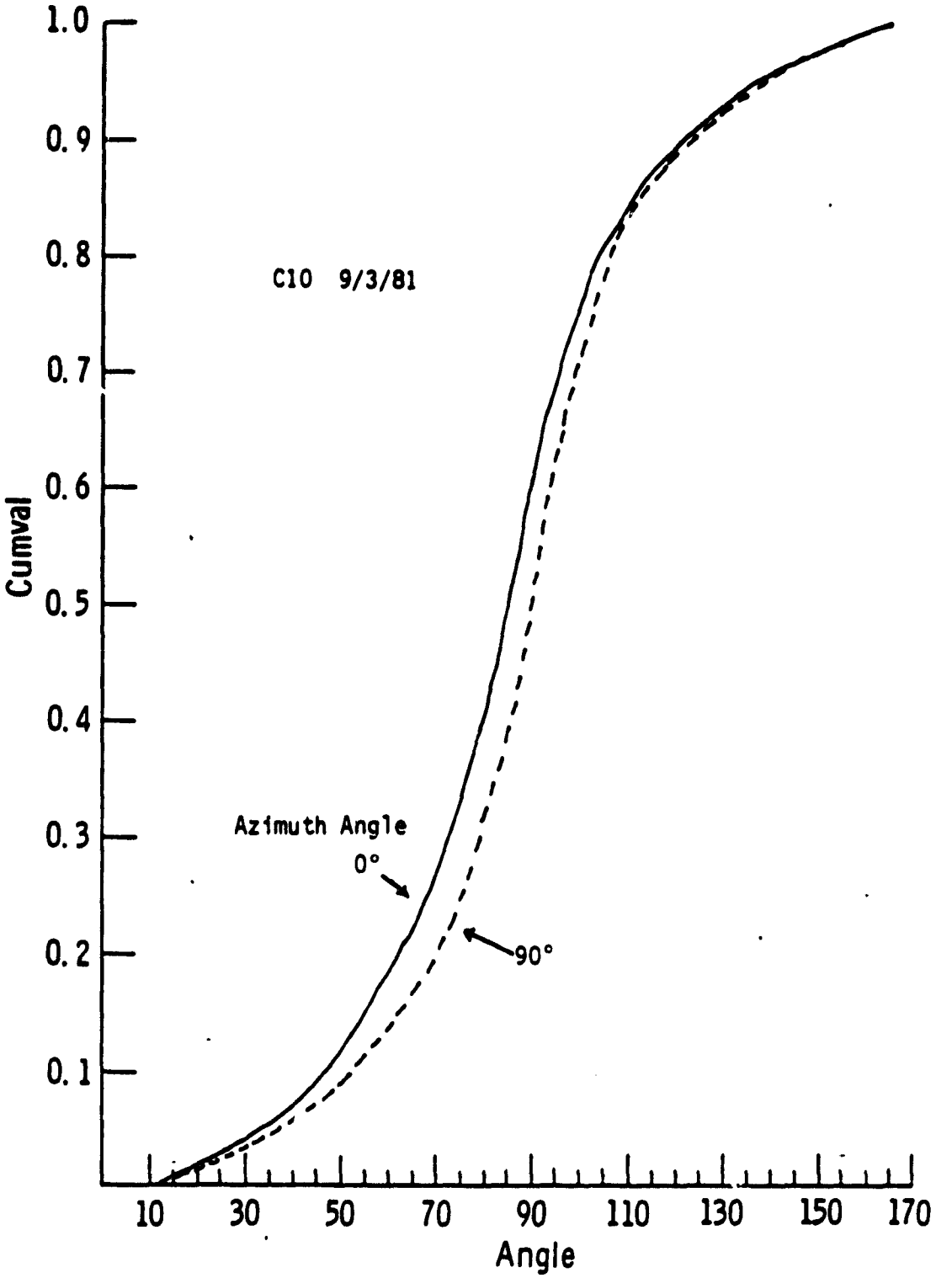

* U.S. GOVERNMENT PRINTING OFFICE 1982—569-011/48